HALLMARKS OF T CELL DYSFUNCTION ARE ESTABLISHED WITHIN HOURS AFTER TUMOR ANTIGEN ENCOUNTER

By

Michael William Rudloff

Dissertation
Submitted to the Faculty of the
Graduate School of Vanderbilt University
in partial fulfillment of the requirements
for the degree of

DOCTOR OF PHILOSOPHY

in

Molecular Pathology and Immunology
May 18, 2023
Nashville, Tennessee

Approved:
Luc Van Kaer, Ph.D.
Heather Pua, M.D., Ph.D.
Justin Balko, Pharm.D., Ph.D.
Emily Hodges, Ph.D.
Jeff Rathmell, Ph.D.
Mary Philip, M.D., Ph.D.

DEDICATION

This thesis is dedicated to Karen Rudloff.

ACKNOWLEDGMENTS

I would like to acknowledge our funding sources: Medical Scientist Training Program (MSTP) NIH T32GM007347 to the Vanderbilt MSTP Program, V Foundation Scholar Award, NIH R37CA263614, Serodino Family Adventure Allee Fund, Vanderbilt-Ingram Cancer Center (VICC) SPORE Career Enhancement Program NIH P50CA098131, Vanderbilt Digestive Disease Research Center (VDDRC) Young Investigator and Pilot Award NIH P30DK058404. I thank the Vanderbilt Division of Animal Care, Dave Flaherty and the Vanderbilt University Medical Center Flow (VUMC) Cytometry Shared Resource Core, Angela Jones and the Vanderbilt Technologies for Advanced Genomics (VANTAGE) Core, and A. Viale and the Sloan Kettering Integrated Genomics Operation Core (IGO). We thank Peter Lauer and Aduro Biotech for providing attenuated *Listeria* strains. We thank Paul Zumbo, Friederike Dündar, Doron Betel for their expertise and analysis of the bioinformatics work in this thesis.

Many individuals contributed to the success of this work over the years. I would like to thank Dr. Nathan Wright and Dr. Christine Alewine for first kindling my passion for translational research and providing me with the foundation necessary to pursue M.D./Ph.D. training. I would like to thank my chair, Dr. Luc Van Kaer and my co-mentor, Dr. Jeff Rathmell for kindly providing their expertise and insight which helped me navigate my graduate school experience. I would also like thank my committee for their critiques and guidance which helped shape the narrative of this thesis and the quality of my training. I would like to thank my mentor, Dr. Mary Philip who provided the home and the training that facilitated my growth as a scientist in everything from mouse colony management, to flow cytometry, to experimental design and execution that facilitated this thesis work. I would like to thank my lab (Jessica Roetman, Carlos

Detrés Román, Megan Erwin, Kristen A. Murray, Gulnara Anzarova, Taylor Bryson, and Sriya Jonnakuti) for their collaboration and support which made many late nights and early morning harvests and experiments even more enjoyable. I would like to thank Natalie Favret who tag-teamed and assisted in countless early timepoint analyses and experimental set ups. I would like to thank my friends, family, my MSTP cohort, and MSTP leadership. Finally, I would especially like to thank my wife, Allie, whose love and support made the completion of all this work possible, and our kids Elliot and Bowen, who remind us that playtime is not optional, and eight hours of sleep is not required for graduate student function.

TABLE OF CONTENTS

LIST OF FIGURES

Figure 5.1 Graphical abstract

CHAPTER 1: INTRODUCTION

Functional CD8 T cell responses

CD8 T cells compose the cytotoxic arm of the adaptive immune response in mice and humans. They specifically identify and destroy cells infected with virus or harboring intracellular bacteria and can detect and destroy cancer cells. Naive T cells circulate throughout the bloodstream, migrating into lymph nodes via interactions between T cell surface CD62L (also called L-selectin) and CC-chemokine receptor 7 (CCR7) with peripheral node addressins (PNA) and chemoattractant CC-chemokine ligand 21 (CCL21) respectively on luminal surfaces of high endothelial venules (HEV)(Forster, Davalos-Misslitz et al. 2008, Zhang and Bevan 2011, Girard, Moussion et al. 2012), or by following CCL21 gradients to white pulp in the spleen (Chauveau, Pirgova et al. 2020). Upon entering secondary lymphoid tissue, $CD8^+$ T cells home to dendritic cells (DC) by following CCL3, CCL4, and CCL17 gradients binding CCR5 or CCR4 and scan for cognate peptide presented on DC major histocompatibility complex class I (MHCI) with T cell receptors (TCR) for approximately one day before returning to the bloodstream via efferent lymphatics (Castellino, Huang et al. 2006, Obst 2015). T cell activation requires three signals. Formation of the TCR-peptide-MHCI interaction composes signal 1 of T cell activation. Canonically, cognate peptide-MHC is recognized on DC that have been primed by recognition of pathogen associated molecular patterns (PAMP), damage associated molecular patterns (DAMP), or inflammatory cytokines such as type I interferons (IFN). Primed DC express a myriad of costimulatory molecules that signal through surface T cells receptors such as CD28, inducible T cell costimulatory (ICOS), or 4-1BB providing T cells with signal 2 (Chen and Flies 2013). The inflammatory or cytokine milieu comprises signal 3 and provides further information for T cells to interpret and integrate on

a population basis. IL-2 is a pleiotropic cytokine described as the classical lymphocyte mitogen, supporting proliferation and expansion of responding populations in a paracrine-autocrine manner. Although IL-2 is not required for T cell expansion *in vivo*, it also plays a role in function fate decisions (Ross and Cantrell 2018). IFNα, IL-12, and to some extend IL-21 are perhaps most critical for the gain of cytolytic and cytokine secretion function, as well as supporting clonal expansion, and ultimately controlling the degree of skew to terminal short lived effectors (Curtsinger, Lins et al. 2003, Mescher, Curtsinger et al. 2006, Joshi, Cui et al. 2007, Agarwal, Raghavan et al. 2009).

T cell biology immediately following TCR signaling is incredibly dynamic. Hours after signaling, T cells increase in cell size, double protein quantity, and increase RNA content 30-fold over resting naive levels (Obst 2015). To support population expansion and gain of effector functions, T cells also undergo rapid metabolic reprogramming (Michalek and Rathmell 2010, Reina-Campos, Scharping et al. 2021). A resting T cell exhibits low level glycolysis and primarily utilizes oxidative phosphorylation (OXPHOS) and fatty acid oxidation (FAO) to produce energy in the form of ATP. Activated T cells transition to a highly anabolic state, rapidly induce nutrient transporters (GLUT1, SLC transporters) on the cell surface and switch to a program driven by aerobic glycolysis, a less efficient process than OXPHOS but 100 fold faster (Reina-Campos, Scharping et al. 2021). Metabolic reprogramming is also linked to epigenetic remodeling, for example import of methionine via SLC7A is critical to maintain production of S-adenosylmethionine (SAM), the universal substrate for methyltransferase reactions on DNA and histones (Sinclair, Howden et al. 2019, Reina-Campos, Scharping et al. 2021). Activated cells can be identified by rapid induction of surface CD69, induced as early as 2 hours following TCR

signaling which contributes to retention of T cells in secondary lymphoid organs (SLO) by downregulating the sphingosine 1 phosphate receptor (S1PR). These “blasting” T cells then enter a rapid expansion phase 24 hours after initial signaling event dividing as much as 3-4 times per 24h period (Badovinac, Haring et al. 2007, Yoon, Kim et al. 2010, Zhang and Bevan 2011). This allows as few as 10-50 antigen specific cells to generate a large population of effectors that can control and eliminate infected cells (Blattman, Antia et al. 2002, Kaech and Cui 2012). Differentiated effector T cell populations upregulate CD44, CXCR3, and S1PR while downregulating CD62L, CCR7, and CD69, and exit SLO via efferent lymphatic channels to the circulation by following S1P gradients (Girard, Moussion et al. 2012). Functional effectors circulate in the bloodstream until encounter with infected tissue. Activated endothelium expressing ICAM-1 and VCAM-1 facilitates adhesion via interactions with LFA-1 and VLA-4. Endothelium-bound and chemotactic gradients of CXCL9, CXCL10, and CXCL11, which are induced by IFNγ, permit extravasation and homing to sites of infection via CXCR3 (Groom and Luster 2011).

The quantifiable cellular readouts of functional CD8 T cells include 1) proliferation, 2) expression of TNFα and IL-2 and the induction of IFNγ, and 3) cytolytic capacity through expression of perforin and granzymes and degranulation. The systems-based readout of a functional T cell response or immune response is clearance of the inciting viral or intracellular bacterial pathogen, with subsequent dissipation of DAMP and PAMP signaling, and declining/disappearing antigen load. Cessation of TCR signaling triggers contraction of the effector population and the development of a long-lived memory population capable of responding to secondary infection or antigen encounter. While the exact model for development of memory is still actively debated, memory T cells reinduce IL-7 receptor (CD127(alpha subunit)) facilitating persistence and

homeostatic proliferation of these populations for up to the duration of host's lifespan (Kaech and Cui 2012). Antigen educated T cells recirculate through bloodstream and SLO until they reencounter antigen during secondary infection, upon which they immediately degranulate and express TNFα, IFNγ, and perforin. Full cytotoxic capacity is regained rapidly, in under 24 hours following secondary activation with the reinduction of granzyme B (Wolint, Betts et al. 2004).

Hypofunctional T cell responses in chronic viral infection

CD8 T cells can also differentiate into hypofunctional states, mainly in the setting of chronic antigen exposure such as chronic infection. "Exhausted" T cells were first described in the context of chronic viral infections caused by hepatitis C virus (Lechner, Wong et al. 2000, Bowen and Walker 2005), hepatitis B virus, and human immunodeficiency virus (HIV)(Betts, Nason et al. 2006) as well as models of murine chronic lymphocytic choriomeningitis virus (LCMV)(Zajac, Blattman et al. 1998, Virgin, Wherry et al. 2009). Due to the inability to clear virus from host cells, the antigen load in the organism remains elevated resulting in constant TCR signaling (Fuller and Zajac 2003, Wherry, Blattman et al. 2003). As a result, T cells enter an exhausted state whose onset coincides with peak of T cell response 7-14 days post infection (Oxenius, Zinkernagel et al. 1998, Wherry, Blattman et al. 2003, Wherry, Ha et al. 2007) with initiation of exhaustion detectable by day five post infection (Utzschneider, Gabriel et al. 2020). While numerous surface inhibitory receptors, soluble molecules (IFN, IL-12, IL-10, TGFβ) or cellular mediators (T regulatory cells) contribute to this phenotype, antigen exposure alone is sufficient to achieve exhausted states (Bucks, Norton et al. 2009). Furthermore, bystander T cells not specific for chronic viral antigen but experiencing the same immune environment will exhibit impaired function and memory formation but to a much lesser degree than antigen specific T cells,

highlighting the dominant role of TCR signaling in driving dysfunction (Stelekati, Shin et al. 2014). Chronic viral specific exhausted T cells have classically been identified by expression of multiple surface inhibitory receptors such as programmed death 1 (PD1), lymphocyte activating 3 (LAG3), cytotoxic T lymphocyte antigen 4 (CTLA4), T cell immunoglobulin and mucin domain-containing protein 3 (TIM3) and 2B4 (CD244) (Wherry 2011). Although exact cellular mechanisms are diverse and a field of active study, these molecules generally dampen down activating signals from TCR (signal 1) and costimulation (signal 2) and attenuated effector function (Chen and Flies 2013). Hypofunctional CD8 T cells during chronic viral infection achieve a host-pathogen stalemate, in which pathogens are not eliminated but controlled, while immunopathology from excessive T cell activation is avoided.

Functional mediators are lost in a conserved and hierarchical manner beginning with the sequential loss of cytokines IL-2, TNFα, and IFNγ (Wherry, Ha et al. 2007). Next, the cytolytic capacity is gradually diminished as measured by granzyme expression, *ex vivo* degranulation potential, and cell killing in *ex vivo* cytotoxicity assays (Wherry 2011). While the loss of cytokine competent T cells is a conserved feature across chronic LCMV studies, the degree of cytotoxic capacity loss is heterogeneous. These differences segregate based on the LCMV strain with Clone 13 driving a loss of cytolytic function (Wherry, Blattman et al. 2003) and LCMV Docile producing a "split" exhausted state with cytokine loss and preserved cytolytic capacity (Agnellini, Wolint et al. 2007). Heterogeneity in loss of function has also been attributed to abundance or burden of viral epitopes with higher burdens associated with more complete dysfunction (Fuller, Khanolkar et al. 2004). Exposure time to antigen also plays a role as dysfunctional T cells in mice and humans can regain previously lost cytokine or cytolytic function following clearance of a protracted LCMV infection

or control of HCV/HIV following antiviral therapy (Lechner, Wong et al. 2000, Rosenberg, Altfeld et al. 2000, Fuller, Khanolkar et al. 2004). Despite loss of effector molecules, both cytokines and cytolytic pathways have been implicated in controlling viral titers and likely contribute to host-pathogen stalemate. IFNγ knock out animals exhibit higher viral loads in all organs and can result in persistence of normally acute LCMV strains (Bartholdy, Christensen et al. 2000). Mice lacking cytotoxic T cell function due to perforin deficiency cannot control acute LCMV infection despite maintenance of Fas induction (Walsh, Matloubian et al. 1994, Fuller and Zajac 2003). Loss of function likely prevents immunopathology to the host, which could result from massive T cell expansion, cytokine release, and death in the setting of chronic infection (Badovinac, Hamilton et al. 2003, McKinney, Lee et al. 2015).

Finally, the proliferative capacity of murine exhausted T cells diminishes with time resulting in reduced capacity to expand and respond to secondary antigen challenge compared to functional memory controls (Wherry and Ahmed 2004). This is also observed in HIV-infected patients following viral control with anti-retroviral therapy (Migueles, Weeks et al. 2009). The reliance of T cell populations on antigen to persist in models of chronic viral infection is a phenomenon known as “antigen addiction” and is due to lack of expression of IL-7 and IL-15 homeostatic cytokine receptors normally induced during memory differentiation (Wherry, Barber et al. 2004). Given enough time, chronic viral specific T cell populations will eventually undergo apoptosis and be deleted from the environment (Wherry 2011).

Differentiation to exhausted T cell states in chronic LCMV has been extensively mapped. A core facet of this pathway is that more stem-like “progenitor exhausted” T cells give rise to a more differentiated “terminally exhausted” cells, defined by high or low transcription factor T cell factor

1 (TCF1) expression, respectively (Utzschneider, Charmoy et al. 2016). Stem-like exhausted T cells maintain properties of self-renewal and are capable of reconstituting T cell populations following transfer to new host or stimulus such as checkpoint blockade (Im, Hashimoto et al. 2016). Terminal exhausted T cells are short lived but are capable of performing cytolytic functions (Miller, Sen et al. 2019). Presence of both progenitor and terminal populations are required to control chronic viral infection (Paley, Kroy et al. 2012). Numerous studies have characterized other transcription factors or surface markers that identify progenitor and terminal exhausted T cells and to elucidate underlying biology. Progenitor (prog) exhausted T cells have been identified with the T follicular helper (Tfh) marker CXCR5, intermediate PD1 expression, and absence of TIM3 (CXCR5+, PD1 int, TIM3-) (Im, Hashimoto et al. 2016). Conversely, terminally exhausted cells are CXCR5-, PD1 hi, TIM3+. Finally, progenitors tend to exhibit a relatively high ratio of the transcription factors TBET to EOMES while terminal exhausted T cells tend to exhibit a low ratio of TBET to EOMES. A recent study aimed at clarifying conflicting results using these markers mapped exhausted differentiation into four states using Ly108 (also known as SLAMF6) as a TCF1 surrogate and CD69. Exhausted T cells begin as a relatively quiescent tissue resident prog1 (Ly108+CD69+) population then transition into a circulating and proliferative prog2 (Ly108+, CD69-) population. Exhausted T cells increase TBET and become cytotoxic but non proliferative prog3 (Ly108-, CD69-) population before becoming a tissue resident terminally exhausted prog4 (Ly108-, CD69+)(Beltra, Manne et al. 2020). While stem-like and terminal exhausted populations have also been found in tumors, the markers established in chronic LCMV models are less reliable in identifying subsets of exhausted tumor-specific T cells (Miller, Sen et al. 2019, Beltra, Manne et al. 2020, Nah and Seong 2022).

Dysfunctional T cell responses in tumors

Tumor specific CD8 T cells (TST) play critical roles in immunosurveillance and destruction of malignantly transformed cells and tumors. However, CD8 T cells in this context are often dysfunctional in that they fail to prevent expansion and metastasis of cancer. The contradicting observation that tumors grow despite being infiltrated by anti-tumor immune populations is termed the Hellstrom paradox (Hellstrom, Hellstrom et al. 1968). While host immune cells and pathogen often reach a stalemate state in chronic viral infections, loss of CD8 T cell function in tumors contributes to immune escape, allows for progression of disease, and drives morbidity and mortality. While the models of tumor immunology are more diverse, the relative hierarchy of dysfunctional onset is preserved between models of tumor and chronic infection (Philip and Schietinger 2021). However, tumors do appear to exhibit a more rapid onset of dysfunction with studies showing naive T cells completely losing cytokine expression capacity within 5 days of tumor encounter (Mognol, Spreafico et al. 2017, Philip, Fairchild et al. 2017). The exact onset of T cell dysfunction within tumors remains poorly defined.

Variability in tumors is in part due to variability in anatomic location of activation. While functional responses tend to follow a pattern of activation in secondary lymphoid tissue followed by trafficking to peripheral sites of infection, T cell activation in tumor bearing hosts is complicated by noncanonical patterns of trafficking, heterogeneous cytokine milieus, abnormal vascularization and endothelial integrity, and formation of tertiary lymphoid structures across tumors (Yu, Lee et al. 2004, Nagy, Chang et al. 2009, Thompson, Enriquez et al. 2010). Canonical effector chemotaxis with CXCL9 and CXCL10 is important for T cell recruitment in some tumors; however, secretion of these ligands is dependent on IFNγ expression in tumor environments, which

is heterogeneous and diminished relative to infections (Slaney, Kershaw et al. 2014). Atypical chemotaxis using CXCR6 expression on T cells and gradients of CXCL16 have also been linked to recruitment of effector T cells to tumors (Slaney, Kershaw et al. 2014), due to presence of CXCL16 expressing DC (Di Pilato, Kfuri-Rubens et al. 2021). Increased permeability of tumor neovasculature is well described and provides the rationale for targeted nanoparticle therapy and matrix targeting immunomodulatory treatments (Nagy, Chang et al. 2009, Mansurov, Ishihara et al. 2020). This principle also means that naive or memory T cells can be activated directly in tumors instead of only on antigen-presenting cells (APC) in secondary lymphoid tissue. This has been definitively shown in MHC-I knockout mice grafted with MHC-I wild-type (WT) subcutaneous tumors resulting in activation of transferred T cells (Thompson, Enriquez et al. 2010) or tumors engineered to express LIGHT (Yu, Lee et al. 2004). In line with these findings, immune cell tracking with photoconversion in subcutaneous tumors showed naive or stem like CD8 populations to activate in tumors and participate in a bidirectional migration between tumor and TDLN (Li, Tuong et al. 2022). Furthermore, the vasculature perfusing tumors has been associated with HEV like structures that can provide an entry point for CD62L high tumor specific T cells such as naive, central memory, or activated stem-like dysfunctional T cells; the quantity of intratumoral HEV structures correlated with responsiveness to CTLA checkpoint blockade (Asrir, Tardiveau et al. 2022). Thus, tumors can provide a sufficient and dynamic environment for the activation of T cells regardless of differentiation status.

Upon entry into tumors, TST must contend with a myriad of challenges. These include hostile environmental factors including hypoxia, acidic pH and metabolic byproducts as well as cellular regulators (Treg, myeloid derived suppressor cells)(McLane, Abdel-Hakeem et al. 2019). For example molecules such as lactate (Quinn, Jiao et al. 2020), IDO, or adenosine can diminish

effector T cell proliferation and functional status (Reina-Campos, Scharping et al. 2021). Furthermore, metabolites such as lactate can selectively potentiate regulatory T cell responses to block effector responses (Watson, Vignali et al. 2021). Competition for nutrients in tumors has also been suggested as early mechanism for dysfunction (Reina-Campos, Scharping et al. 2021), with implications in both failures of anabolic programming and long term differentiation through aberrant epigenetic programming (Sinclair, Howden et al. 2019). The differential induction and engagement of metabolic regulators may be able to directly control effector molecule expression via post transcriptional regulatory mechanisms (Chang, Curtis et al. 2013).

T cell intrinsic factors also influence functional states in tumors. Best-characterized are the inhibitory receptors that are often found in tumor reactive T cells. Similar to chronic viral infection, these include PD1, CTLA4, LAG3, TIM3, 2B4, CD38, CD39, and CD101 (Schietinger, Philip et al. 2016, Philip, Fairchild et al. 2017). These dampen T cell activation by blocking ligation or signaling of CD28, CTLA4 (Krummel and Allison 1995) and PD1 (Hui, Cheung et al. 2017) respectively, or decreasing immediate TCR signaling via LAG3 (Guy, Mitrea et al. 2022). PD1, CTLA4, and LAG3 are particularly relevant as they provide the basis for checkpoint immunotherapy which can unleash antitumor immunity (Hodi, O'Day et al. 2010). While PD1 targeted therapies are the most common form of immunotherapy and can produce complete responses in metastatic disease, the fraction of patients who benefit from even partial responses are below 20% (Haslam and Prasad 2019). For murine tumor models and patients with cancer, there is growing evidence from the field that checkpoint blockade does not rescue function in tumors but reinvigorates precursor dysfunctional T cells, often PD1 and TCF1 double positive in secondary or tertiary lymphoid tissue (Jansen, Prokhnevska et al. 2019, Miller, Sen et al. 2019,

Philip and Schietinger 2021). Even with the establishment of stem-like populations to replenish effector T cells in the context of checkpoint blockade, we do not know how long previously functional T cells remain functional upon encountering tumor antigen.

As in models of chronic viral infection, TCR signaling in tumors plays a dominant role in driving T cell dysfunction. Studies by us and others have shown that the initiation of dysfunctional states requires TCR signaling, and bystander T cells exhibit little to no functional deficits from just existing in the tumor environment (Schietinger, Philip et al. 2016, Mognol, Spreafico et al. 2017). The degree of tumor burden and thus the antigen burden, also appears as a key factor for predicting responses to immunotherapy. Growing literature in the clinic suggests that baseline tumor burden negatively correlates with response rate despite successful invigoration of patient immune cells (Huang, Postow et al. 2017, Kim, Cassella et al. 2020, Dall'Olio, Marabelle et al. 2022, Matoba, Minohara et al. 2022). This observation has been made in genetic murine models of cancer (Tichet, Wullschleger et al. 2023). While evolution of malignant cells can alter epitope expression, tumor vasculature, or tumor microenvironment, it is also proposed that an imbalance of activated T cells relative to tumor targets itself provides a barrier to responses (Huang, Postow et al. 2017). Thus, despite appropriate immune responses and reservoirs of stem populations, T cell populations are spent before they can clear tumor. As T cell function is often not measured in these studies, the duration of effector function following activation in tumor is unknown and rapid functional losses could contribute to checkpoint blockade failures. Mapping naive and effector functional responses on contact with tumors would provide insight to these unanswered questions in the field.

Key transcription factors of early activation

T cells rapidly integrate external signals to initiate fate decisions by the activation and translocation of transcription factors (TF) from the cytoplasm to the nucleus. These include nuclear factor of activated T cells (NFAT), Fos, Jun, Bach, BATF, mTOR, NFκB, and STAT family members. The degree and combination of transcription factors that drive fate decisions can be influenced by TCR signaling strength (Conley, Gallagher et al. 2016), stability of signaling (Marangoni, Murooka et al. 2013), the presence of costimulation (Yukawa, Jagannathan et al. 2020), nutrient availability (Reina-Campos, Scharping et al. 2021), or cytokine milieu (Hu, Li et al. 2021). A second wave of TF considered to be master regulators for T cell function such as T-BOX family members TBET and EOMES are then induced and facilitate full gain of cytokine and cytolytic potential (Intlekofer, Takemoto et al. 2005).

NFAT family members, NFAT1, NFAT2, and NFAT4 in T cells, are both essential for T cell activation and implicated in driving dysfunction of T cells. NFAT is dephosphorylated by calcineurin in a calcium and calmodulin-dependent manner, allowing for translocation into the nucleus and transcription of target genes (Macian 2005). The degree of NFAT activation is tunable and correlates with the TCR signaling strength and subsequent calcium flux (Dolmetsch, Lewis et al. 1997), regulated by the relative degree of ITK signaling (Conley, Gallagher et al. 2016), allowing for customization of T cell responses based on antigen affinity and load. NFAT binding partners such as NFκB and AP1 allow for further customization of transcriptional programs. In particular, a balance of NFAT and AP1 has been shown to be critical (Macian, Lopez-Rodriguez et al. 2001). For example, *Tnf* and *Ifng* both contain NFAT binding motifs for driving transcription, however, NFAT:AP1 dimers seem to be required for optimal induction of *Ifng* transcription (Rao,

Luo et al. 1997, Macian, Lopez-Rodriguez et al. 2001). Along with relative TCR signaling, costimulation has also been implicated in providing optimal NFAT:AP1 balance by inducing components of the AP1 heterodimer. CD28 signaling and PI3K activation induces c-Jun (Atsaves, Leventaki et al. 2019) and JunB (Yukawa, Jagannathan et al. 2020) in a calcium signaling independent manner. Furthermore, CD28 engagement augments JNK signaling, inducing Elk-1 transactivation of c-*Fos* gene (Atsaves, Leventaki et al. 2019). Along with optimal induction of effector genes, AP1 downstream of CD28 ligation appears critical for facilitating epigenetic remodeling of enhancer regions during the first hours after T cell activation *in vitro* (Yukawa, Jagannathan et al. 2020).

In line with the studies above, these pathways have been further analyzed in context of tumors or models of chronic viral infection. Models of chronic viral infection have implicated NFAT as a driver of dysfunction associated genes (Scott-Browne, Lopez-Moyado et al. 2016), which have been validated in pre malignant and malignant tumor models (Schietinger, Philip et al. 2016, Philip, Fairchild et al. 2017). NFAT engineered to be incapable of interacting with AP1 produces T cell phenotypes and epigenetic profiles that mimic T cell exhaustion (Martinez, Pereira et al. 2015). While comparisons between acute and chronic viral infections usually involved analysis between cells no longer receiving TCR signaling and cells receiving continuous signaling, respectively, the relative NFAT induction is important. Studies performed with altered peptide ligands in tumors have shown increased degree of NFAT correlates with kinetics of dysfunctional onset (Shakiba, Zumbo et al. 2022) and studies in early chronic viral infection attribute initiation of dysfunction to higher antigen burdens relative to early acute infections (Utzschneider, Gabriel et al. 2020). In line with these observations, interventions to rescue function by attenuating TCR signaling pharmacologically with the tyrosine kinase inhibitor dasatanib or with a degradable

chimeric antigen receptor (CAR)-T construct have provided some benefit in cytokine production and antitumor immunity in some models (Weber, Parker et al. 2021). Indeed, TST interacting with intermediate affinity ligands provided the most durable anti-tumor responses relative to high affinity antigen (Shakiba, Zumbo et al. 2022). However, it is possible TCR signaling, and corresponding NFAT signaling, may need to be balanced as relatively lower affinity TCR clones can be outcompeted in organisms or tumor environment (Burger, Cruz et al. 2021). Rescue protocols targeting AP1 have also been attempted to counterbalance relative excess of NFAT in tumors. Jun overexpression in CAR-T cells produced moderate gains in IFNγ and degranulation with enhanced control of subcutaneous tumors (Lynn, Weber et al. 2019).

Inhibitory members of the AP1 family can further tune T cell responses and have been implicated in T cell functional and dysfunctional differentiation. Members of the BACH family (BACH1, BACH2) actively compete for AP1 binding sites. While they themselves do not induce gene expression, BACH works to block the induction of genes in an AP1 dependent manner (Roychoudhuri, Clever et al. 2016). In normal T cell development BACH2 has been implicated in restraining terminal effector differentiation and promoting a more memory phenotype. Indeed, T cells with higher BACH2 tend to be lower in cytokines or cytolytic molecules (Roychoudhuri, Clever et al. 2016). Extending off this observation was the finding that BACH2 is necessary to produce progenitor exhausted populations in models of chronic LCMV (Utzschneider, Gabriel et al. 2020).

BATF is another inhibitory member of the AP1 family, although with more conflicting roles in function and dysfunction. Implicated as a TF driving dysfunction at later timepoints (Quigley, Pereyra et al. 2010), knock out of BATF actually produces a less functional T cell population

(Grusdat, McIlwain et al. 2014). Follow up studies revealed that while BATF does suppress function, this role appears to be restricted to early differentiation and coincides with BATF mediated amplification of TCR signaling and TBET/EOMES induction (Kurachi, Barnitz et al. 2014). Thus, BATF has been labeled as an early differentiation checkpoint where effector differentiation is transiently restrained until sufficient signaling and master TF have been acquired to ensure successful differentiation. BATF has subsequently been identified as a critical chromatin remodeler for T cell differentiation into functional cytotoxic effectors (Tsao, Kaminski et al. 2022). Opposing BACH, BATF has also been implicated in driving a more terminal exhausted population early in models of chronic LCMV infection (Utzschneider, Gabriel et al. 2020).

Signal 3 cytokines also contribute to early T cell fate decisions in a signal transducer and activator of transcription (STAT) dependent manner providing a direct connection between the cytokine context of activation and downstream TF. T cells respond to and are informed by a myriad of cytokines during activation, providing specific information to customize differentiation. Type I interferons (IFNα and IFNβ) are induced with intracellular infections and are rapidly expressed alarmins that can inform T cell activation environment. These cytokines inform T cell differentiation through several pathways including STAT1 and STAT4 (Hu, Li et al. 2021). IL-12 signals predominantly through STAT4 to induce master TF and downstream effector genes such as IFNγ (Curtsinger, Lins et al. 2003). Finally, IL-2 can signal through STAT5a and STAT5b in a paracrine or autocrine fashion from CD8 T cells or from supporting CD4 helper T cells (Hu, Li et al. 2021). The functional result is the skewing of the global T cell population from a memory precursor to a terminal effector dominated population. There are upcoming studies testing the feasibility of STAT activation in the rescue or preservation of CD8 or CAR-T cells in tumors to

enhance therapeutic effect.

Following the first wave of TF a secondary wave is induced in activated populations that facilitates full differentiation to functional effectors. The predominant master TF associated with effector function gain are TBET and EOMES (Joshi, Cui et al. 2007, Cruz-Guilloty, Pipkin et al. 2009), T-BOX family TF that confer gain of IFNγ, granzyme B, and perforin during naive to effector T cell differentiation (Tsao, Kaminski et al. 2022). T cells with double knock out of TBET and EOMES lose cytotoxic lymphocyte functionality and aberrantly express IL-17 (Intlekofer, Banerjee et al. 2008). Induction of these transcription factors is multifactorial, but IL-12 and IFNα are among the clearest drivers of TBET and EOMES and impact downstream skewing (Joshi, Cui et al. 2007). High IL-12 and subsequent STAT4 correlates with excess TBET over EOMES through an mTOR dependent mechanism and blocking this pathway with rapamycin will produce excess EOMES over TBET (Rao, Li et al. 2010). The ratio of TBET and EOMES determines if cells are destined to differentiate into terminal effectors or long-lived memory populations with TBET highest immediately following activation and in terminal effectors. EOMES high cells tend to become long lived memory populations (Intlekofer, Takemoto et al. 2005). Again, these "functional" TF are also involved in the formation of exhausted T cells in models of chronic viral infection with parallel outcomes. TBET high populations exhibit the most cytolytic function but are a transient population, becoming EOMES high populations that are dysfunctional but persist longer (Paley, Kroy et al. 2012). Due to the dual roles in function and dysfunction, TBET and EOMES have not been heavily targeted for functional rescue; however, cytokine receptor modulation in CAR-T cells has indirectly shown that TBET induction potentiates anti-tumor immunity in subcutaneous models. TBET has also been shown to downregulate PD1 surface expression on T cells which may

preserve functional states (Kao, Oestreich et al. 2011). It is also worth noting that these studies were carried out in chronic viral infection and relatively low expression of both TBET and EOMES are found in tumor infiltrating T cells suggesting that inducing these TF could rescue function in tumors (Beltra, Manne et al. 2020).

TCF1 is a master T cell transcription factor expressed in stem-like populations best equipped to persist long term (Gounari and Khazaie 2022). TCF1 is high in antigen naive and quiescent antigen educated T cells such as memory populations. During primary and secondary activation in acute infection models, the gain of TBET and granzyme B and the loss of CD62L correlates with the drop of TCF1 to low or negative states (Danilo, Chennupati et al. 2018). These cells usually represent the relatively short-lived terminal effector populations that migrate to tissues and actively eliminate infected cells before undergoing apoptosis in the contraction phase following antigen clearance (Joshi, Cui et al. 2007, Joshi and Kaech 2008). TCF1 has also garnered attention in the context of chronic viral infections to identify dysfunctional populations that can respond to rescuing therapies such as checkpoint blockade versus those that are in a terminal exhausted state. The TCF1 positive stem-like dysfunctional T cells can express TBET and display low to intermediate PD1 and Ly108 (Beltra, Manne et al. 2020). Terminal exhausted TCF1 negative cells express EOMES, are PD1 and TIM3 positive and lose Ly108. The maintenance of TCF1 high stem like populations has also been implicated in continuing endogenous anti-tumor immunity (Jansen, Prokhnevska et al. 2019, Connolly, Kuchroo et al. 2021) and being the responsive population to checkpoint blockade (Im, Hashimoto et al. 2016, Miller, Sen et al. 2019, Dammeijer, van Gulijk et al. 2020).

Studies aimed at identifying drivers of dysfunctional T cell states identified Thymocyte selection-

associated HMG Box (TOX), in chronic viral infections and tumors. TOX family consists of four members TOX1, TOX2, TOX3, and TOX4. TOX1 was originally identified as a TF critical for development of double positive thymocytes during positive selection as well as CD4 development by facilitating ThPOK, natural killer (NK) cell development by downregulating expression of ID2 and TBET inhibitors, follicular helper CD4 (Tfh) cells by supporting TCF1, LEF1, and PD1 expression in a BCL6 dependent manner, and of secondary lymphoid organogenesis by lymphoid tissue inducer cells (LTi). While TOX2 works in concert with TOX1 to support NK cell and Tfh cell development and function, TOX3 and TOX4 appear less defined with associations in supporting neuronal and breast cancer survival or generally regulating cell cycle in pluripotent stem cells. In the context of dysfunctional CD8 T cell differentiation TOX1 and TOX2 have been identified as drivers in both models of chronic LCMV dysfunction and in murine tumors (Seo, Chen et al. 2019, Han, Wan et al. 2022). TOX has also been identified in tumor infiltrating lymphocytes and high TOX expression has been correlated to anti-PD1 checkpoint blockade responses in non-small cell lung cancer (NSCLC)(Kim, Park et al. 2020). However, unlike murine T cells where TOX does not play a role in memory T cell differentiation, functional human effector memory and to a lesser extent, memory T cells express TOX, confounding its role as an exhaustion specific marker (Sekine, Perez-Potti et al. 2020). While exact molecular mechanisms are incompletely understood, knockout of TOX in murine CD8 T cells blocks differentiation into terminally fixed dysfunctional T cells and prevented epigenetic opening of exhaustion associated chromatin signatures including inhibitory receptors (PD1)(Scott, Dundar et al. 2019). Immunoprecipitation and mass spectrometry has identified both activating chromatin remodelers such as components of the HBO1 histone acetyltransferase complex and suppressive chromatin remodelers such as DNMT1, LEO1, PAF1, SAP130 and SIN3A (Khan, Giles et al. 2019).

Epigenetic programming of T cell dysfunction

In line with the pattern of TF induction and dysfunctional stability described above, studies of tumor-specific T cells and dysfunctional differentiation identified two distinct chromatin states. The first was established rapidly within five days of contacting tumor antigen and associated with complete loss of cytokine function. TF motif analysis identified NFAT family (NFAT1 and NFAT2) and AP1 family (JunB, JunD, Bach1) as drivers of dysfunctional differentiation state 1 (Mognol, Spreafico et al. 2017, Philip, Fairchild et al. 2017). These early dysfunctional T cells remained high for TCF1 and were further characterized by the capability to be rescued by removal from antigen and IL-15/IL-7 supplementation (Schietinger, Philip et al. 2016, Philip, Fairchild et al. 2017). State 2 occurred two weeks after exposure to tumor antigen and was associated with loss of TCF1 and gain of TF such as E2F, ETS and KLF on TF motif analysis (Philip, Fairchild et al. 2017, Miller, Sen et al. 2019). Further analysis on TF that were specific to tumor activated T cells and not naive and memory T cells further identified TOX as critical for terminal dysfunction. This is supported by the fact that TOX KO cells expanded normally up until day 8 in tumors, TOX KO T cells did not persist >2 weeks relative to WT T cell controls (Scott, Dundar et al. 2019). Functionally, state 2 represents a fixed dysfunctional state, unable to be rescued following removal from antigen and exposure to IL-15/IL-7. Poised epigenetic states of functional effector or memory T cells also underwent rapid chromatin remodeling at an identical pace to naive T cells rapidly reaching dysfunctional phenotypes within days and corresponding fixed dysfunctional epigenetic signature within 14 days of encountering tumor antigen (Mognol, Spreafico et al. 2017, Philip, Fairchild et al. 2017). These studies underscore that even previous functional differentiation and epigenetic remodeling does not protect T cells from dysfunctional reprogramming in tumors.

Exactly how epigenetic modification programs functional or dysfunctional states remains an area

of active study. Globally, differential chromatin accessible regions between acute viral infection or chronic viral infections in mice or humans tend to have relatively few differences around transcriptional start sites (~5%) while intergenic and intronic regions contain the most differential accessible chromatin regions (35 and 45% respectively)(Sen, Kaminski et al. 2016, Mognol, Spreafico et al. 2017). Thus, programming of different functional states is, in part, due to enhancer regions in or adjacent to target genes. A notable example of a dysfunction associated regulatory region is the -23kb region upstream of the Pdcd1 murine locus which was found to be uniquely opened in exhausted T cells responding to chronic LCMV infection (Sen, Kaminski et al. 2016) and in subcutaneous tumor models with tumor-specific T cells (Mognol, Spreafico et al. 2017) relative to bystander T cell controls. Targeting and mutation of this enhancer region with Cas9 gRNA led to decreased expression of PD1 on the cell surface (Sen, Kaminski et al. 2016). This concept has been further shown in the context of methylation. DNTM3a deletion models have been shown to slow global dysfunctional epigenetic reprogramming of CAR-T cells and mitigate dysfunctional phenotypes *in vitro* (Prinzing, Zebley et al. 2021). Again, exhaustion associated demethylation changes at promoter for *Pdcd1* can be found in dysfunctional T cells (Ahn, Youngblood et al. 2016). Taken together, epigenetic programming underlies T cell dysfunction in tumor and chronic viral models. Studies aimed at understanding the initiation of dysfunctional programming may shed light on the key drivers and epigenetic regulators of dysfunctional phenotypes that could be used in therapeutic design.

Proliferation and autopilot in early differentiation

Proliferation, the first functional output of T cell activation, serves to supply enough effectors to effectively repel a foreign pathogen. However, the act of cellular division has been implicated

more directly in facilitating T cell differentiation from naive to effector states. Seminal work with cellular division tracking dyes following CD4 T cell activation have shown that function appears to be gained in an incremental manner with the most divided cells exhibiting the most cytokine expression (Bird, Brown et al. 1998). Pharmacologic inhibition of cell division stunts the functional gain of T cells activated *in vitro*. Furthermore, treatment of cells with histone deacetylating agents or demethylating agents can potentiate or augment the gain of cytokine expression following stimulation, respectively. This principle has been similarly applied to CD8 T cells where cytokine expression and cytotoxicity mediators are incrementally gained with cell division and undivided cells are poor expressers of IFNγ (Auphan-Anezin, Verdeil et al. 2003).

T cells do not need sustained TCR signaling to proliferate and differentiate. The instructions for differentiation to effector and memory CD8 T cells can be programmed with brief periods of TCR signaling (Obst 2015). This was first shown by experiments providing brief *in vitro* stimulation, which produced populations that continued to expand upon transfer into mice (Kaech and Ahmed 2001); this antigen independent continuation of differentiation was termed "autopilot" T cell differentiation. While non-autopilot CD8 T cell expansion consists of around 15-20 cell divisions from activation to peak of response in models of acute LCMV and *Listeria* infection (Badovinac, Haring et al. 2007, Obst 2015) experiments that limited duration of *Listeria* infection to <24h with antibiotic therapy showed minimal differences in T cell expansion between normal and truncated *Listeria* infection (Williams and Bevan 2004). *In vitro* studies with anti CD3/CD28 bead or transgenic antigen presenting cell line stimulation have shown that interactions as brief as 2.5 hours were sufficient for T cells to divide for days in culture (van Stipdonk, Lemmens et al. 2001). However, the requirements for continued proliferation *in vivo* are more stringent with a signaling

duration between 20-24 hours (Obst 2015).

Opposing studies have pointed out that autopilot is not a process that occurs completely devoid of secondary signaling (Mescher, Curtsinger et al. 2006). While T cells can activate and undergo division with periods of antigen stimulation in isolation, these populations exhibited diminished clonal expansion and peak of response numbers. These cells expressed limited effector cytokines exhibiting despite undergoing initial cell divisions, a state of "split anergy" (Otten and Germain 1991). Authors termed this state activation-induced non-responsiveness to separate it from a canonical effector and memory differentiation pathway. Follow up studies described how T cell supplementation with signal 3 cytokines (IL-12, IFNα) or IL-2 rescued the expansion and cytokine deficits in the context of transient TCR signaling (Mescher, Curtsinger et al. 2006).

While there are discrepancies in the literature, there is some form of programming that occurs incredibly rapidly following T cell contact with antigen. The "autopilot" differentiation suggests underlying epigenetic or transcriptional programming. However, the general time range of less than 24h of TCR signaling to trigger autopilot would suggest this occurs in an undivided population, counter to previous work in the field (Bird, Brown et al. 1998). Furthermore, the rapid encoding of differentiation programs underscores the consequence of even brief TCR signaling events on the long-term decision making of T cell populations.

Rationale for dissertation research

T cell differentiation has been the focus for research for years to improve vaccination efficacy, modulate the immune system for immunosuppressive or immunostimulatory effect, and advance our understanding of how organisms reject foreign pathogens or tissues. However, early T cell

differentiation including the first hours and cell divisions after antigen encounter is relatively understudied. There are notions in the field that more time must pass for T cells to fully acquire functional or dysfunctional phenotypes and initial TCR signaling is insufficient to impact T cell differentiation. There are also technical barriers, as studies using polyclonal populations or even adoptive transfer methods must be able to identify and isolate the few antigen specific T cells available for analysis, limiting experimental feasibility. This is particularly true for transcriptional and epigenetic studies. Thus, virtually all studies analyzing T cells immediately after TCR signaling use *in vitro* methods with relatively artificial methods of stimulation which are not able to recapitulate the spectrum of activation environments *in vivo*. As *in vitro* activation does not classically reproduce dysfunctional differentiation seen in chronic viral models or tumors, early dysfunctional differentiation is even less well understood.

An open question for dysfunctional development is the role of cell division in facilitating differentiation on an epigenetic, transcriptional, and functional level. This has been described in functional differentiation extensively. However, it is worth noting that many of these experiments were initially performed *in vitro*. Furthermore, recent studies showing significant pre-division chromatin remodeling can occur with *in vitro* stimulation challenges the notion that epigenetic remodeling requires proliferation (Yukawa, Jagannathan et al. 2020). The work establishing the premise of autopilot division in differentiation indicates some degree of differentiation instructions are programmed with brief TCR signaling again, all prior to cell division. Whether this programming is facilitated by signaling, transcriptional or epigenetic changes remains to be seen. This begs the question, how much if any dysfunctional programming is encoded with brief encounters of T cell and tumor? This has powerful implications in kinetics of dysfunctional programming and could limit the degree of anti-tumor immunity on secondary encounters

following tumor resection or cure.

The early kinetics of T cell dysfunction in tumors is relatively understudied. CD8 T cells are completely dysfunctional five days after activation in tumors, accompanied by unique epigenetic and transcriptional profiles. This suggests T cell dysfunction in tumors occurs much faster than previous studies described. We do not know exactly when T cell dysfunction is first initiated and completed for either naive or previously functional effector T cell populations. It is also widely assumed that previously functional effectors can successfully initiate and maintain functional responses after secondary antigen encounter in tumors. This provides the basis for adoptive cell therapies and chimeric antigen receptor (CAR-T) therapies; however, this remains largely untested in solid tumors.

Most studies aimed at identifying drivers of T cell dysfunction are focused at relatively late timepoints in T cell differentiation. While candidates have been identified (TOX), attempts to rescue function by genetic KO of these candidates have failed to significantly alter T cell cytokine or cytolytic production across tumors or chronic viral infection. Furthermore, after weeks in tumors or chronic viral infection, established epigenetic remodeling produces a fixed dysfunctional state, not rescuable by inflammation or checkpoint blockade. Identifying the first drivers of T cell dysfunction may prove more fruitful for inducing or maintaining T cell functional states in tumors. Furthermore, there is growing consensus in the field that pharmacologic rescue of T cells with checkpoint blockade does not rescue intratumoral T cells but instead unleashes a proliferative burst of stem like or progenitor dysfunctional T cells sequestered in secondary or tertiary lymphoid tissue. This further hints at the importance of understanding early dysfunctional T cell differentiation and using that understanding as a basis for designing targeted therapies to prolong

anti-tumor immunity. Altogether, this dissertation advances our basic understanding of functional and dysfunctional differentiation, shedding light on previously unmapped aspects of the earliest timing and drivers of loss of effector function.

CHAPTER 2: PROLIFERATION AND FUNCTION DURING THE FIRST HOURS AND DIVISIONS FOLLOWING T CELL ACTIVATION

Introduction

T cell differentiation to functional states has been linked to proliferation with incremental gains in cytokines or cytolytic capacity with each division (Bird, Brown et al. 1998). Cell division is interrogated using cell proliferation dyes such as carboxyfluorescein succinimidyl ester (CFSE) or Cell Trace Violet (CTV). Upon addition to aqueous solutions and cytoplasmic cell esterases, reactive ester groups conjugated to fluorescent moieties are unlocked allowing for covalent binding of dyes to amino groups on target cells. This produces a stained cell population that fluoresces at a uniform brightness when used with flow cytometry. On activation, dye labeled proteins are equally distributed across daughter cells producing a population with half the fluorescent intensity of the parent population (Quah, Warren et al. 2007). These "proliferation peaks" can be used in concert with intracellular and surface marker antibody stains to assess activation and functional status in a cell division dependent manner. These studies were originally carried out in CD4 T cells and extensively employed for *in vitro* methodologies. It remains unknown if early loss of effector function is initiated or if functional loss is dependent on cell division. By identifying the exact timing of dysfunctional or functional onset, we may be able to identify critical drivers or pathways to therapeutically target.

To assess both functional and dysfunctional differentiation *in vivo* we utilized a model of acute intracellular infection with *Listeria monocytogenes* (LM) and an autochthonous murine hepatocellular carcinoma (HCC) model, respectively. To produce HCC bearing mice, our lab

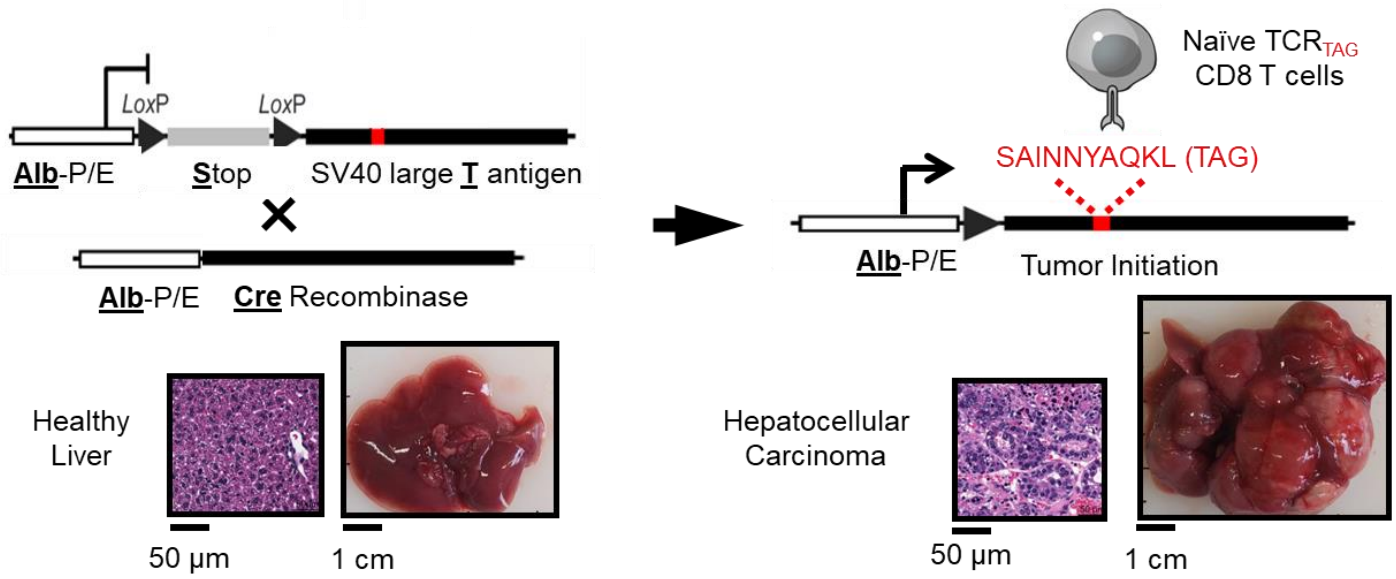

Figure 2.1 Genetic model of murine hepatocellular carcinoma. Albumin lox-stop-lox large T antigen (AST) mice are crossed with Alb-Cre mice (left) facilitating oncogene activation (right). Mice develop advanced multifocal hepatocellular carcinoma by adulthood.

leverages the albumin lox-stop-lox large T antigen system (AST). The large T antigen is a viral oncogene derived from the simian SV40 virus and inhibits the tumor suppressor function of P53 and Rb (Ahuja, Saenz-Robles et al. 2005). All experiments in this thesis were performed with ASTxAlb-Cre mice, which produce a constitutively active oncogene in hepatocytes culminating in oncogenesis initiated at birth and producing adult mice bearing multifocal advanced liver tumors (**Figure 2.1**). The TAG epitope is an MHCI restricted peptide derived from the oncogene that is presented on malignant hepatocytes. Our model of LM is attenuated with a double deletion of ActA and internalin B severely limiting its capability of cell-to-cell spread and limiting its invasion to primarily phagocytic cells (Brockstedt, Giedlin et al. 2004). LM promotes inflammatory environment consisting of type I IFN, IFNγ, and IL-12 and licensing of professional antigen presenting cells(Sinnathamby, Lauer et al. 2009) and infection is cleared within 3 days (Brockstedt, Giedlin et al. 2004). LM is engineered to express the TAG epitope (LM_{TAG}) providing

a conserved model antigen between tumors and infection. In conjunction with these systems, we use transgenic TAG (TCR_{TAG}) specific CD8 T cells, which will recognize and activate on TAG peptide presented in context of MHCI in tumors and infection. By adoptively transferring TCR_{TAG} into tumor bearing or infected mice, we control the exact timing of activation of a clonal T cell population and can compare differentiation and functional outcomes hour by hour and cell division by cell division.

Naive T cell activation in infection and tumors

We first asked how the activation and expansion would compare between effector and tumor activation conditions. Naive TCR_{TAG} T cells were CFSE labelled and transferred into mice infected with LM_{TAG} or mice bearing advanced liver tumors and harvested at timepoints between 12 and 60 hours post transfer to capture full range of cell divisions (**Figure 2.2a**) TCR_{TAG} populations expanded comparably in both tumors and infection both at early timepoints (60h) and at a peak of response timepoint (5d). TCR_{TAG} in both conditions exhibited a contraction phase, reaching comparable numbers by 21d despite persistent antigen in the tumor environment (**Figure 2.2b**). TCR_{TAG} isolated from infected spleens and organs from tumor bearing mice exhibited highly similar early proliferation kinetics as evidenced by similar CFSE dilution at early timepoints (**Figure 2.2c)**. Together with expansion data, this indicates that the functional readout of cell division and clonal expansion was highly similar between infection and tumor.

To assess activation status of TCR_{TAG} across timepoints and conditions we performed surface staining for T cell activation and immunophenotypic markers (**Figure 2.2c**). TCR_{TAG} induced CD69 similarly by 12h in infection and tumors and began to incrementally downregulate surface

expression with cell division at subsequent timepoints indicating similar rapid TCR signaling across conditions. TCR_{TAG} induced CD44, a marker indicating antigen-education status, comparably across conditions with tumors exhibiting slightly more homogenously high expression at early divisions relative to infection activated condition. CD62L was homogenously downregulated at 12h with higher drop occurring in tumors. This is consistent with observations of induced ADAM17 cleavage following TCR signaling (Link, Lucke et al. 2017). CD62L is recovered and remains high in tumors but undergoes a secondary downregulation primarily in the infection group producing a CD44+ CD62L- effector surface immunophenotype. TCR_{TAG} exhibited similar levels of the inhibitory receptor LAG3 which is influenced by both inflammation and degree of TCR signaling (Nguyen and Ohashi 2015). PD1 was induced to a higher degree in tumor bearing animals with the highest expression in tumors. While TCR_{TAG} in infection also induced PD1, expression was lower and more transient. While PD1 is categorized as an inhibitory receptor, it also serves as an activation marker, giving a clear readout of TCR signaling status and strength (Ahn, Araki et al. 2018). This pattern likely represents the relatively higher and persistent antigen load in tumors relative to a lower load in context of inflammation that goes down as infection is cleared. Inflammation induced TBET may also contribute to lower PD1 in infection (Kao, Oestreich et al. 2011).

To assess cytokine and cytolytic mediators we focused on the 48h and 60h timepoints capturing most cell divisions following activation (**Figure 2.3a**). Strikingly, we found that despite robust proliferation and expansion, TCR_{TAG} activated in tumors failed to express TNFα and IFNγ as early as two days after activation in contrast to infection activated TCR_{TAG} which converted to a

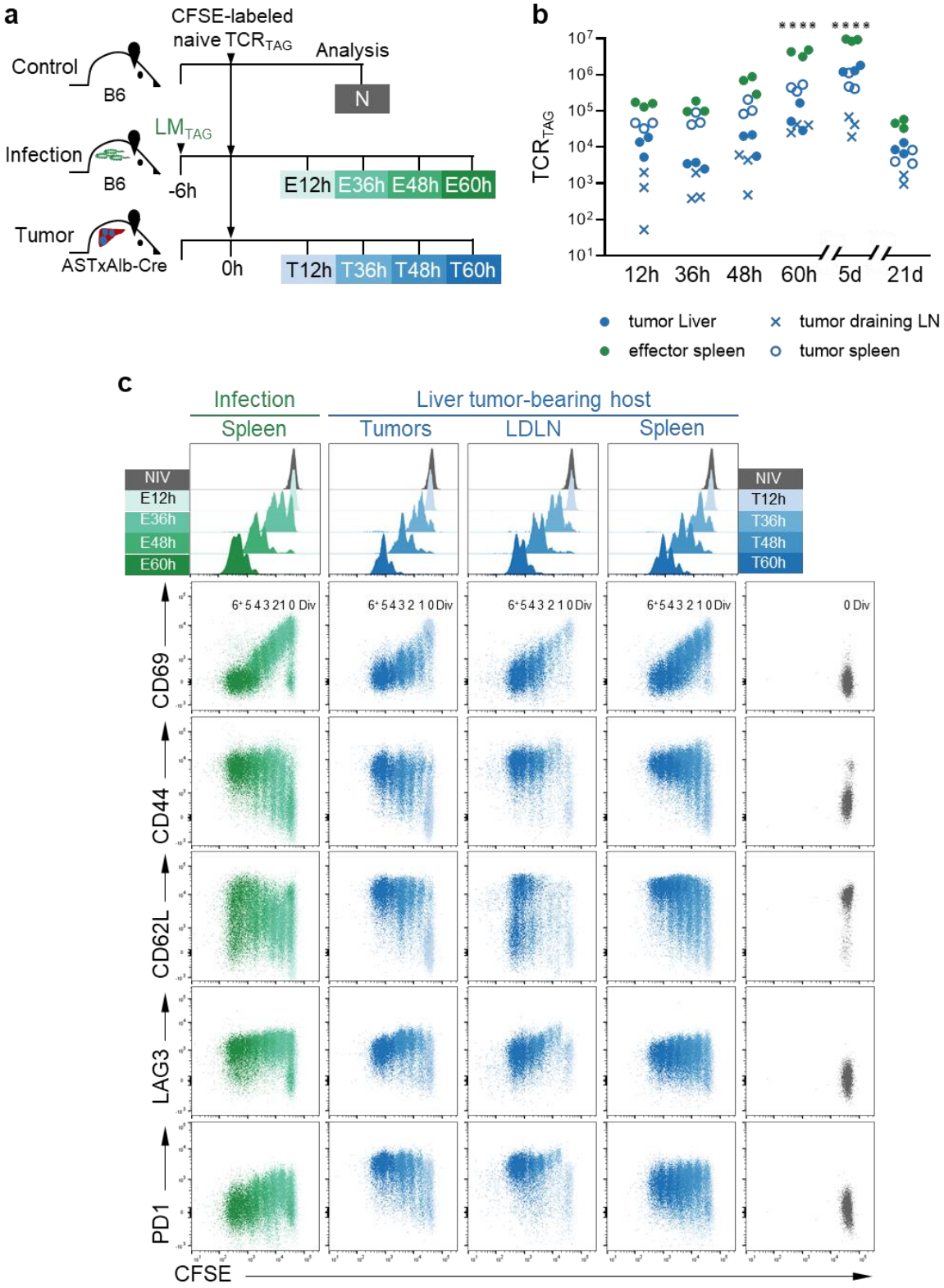
a
CFSE-labeled
naive TCR$_{TAG}$
Analysis
Control
B6
N
LM$_{TAG}$
Infection
B6
-6h
E12h E36h E48h E60h
Tumor
ASTxAlb-Cre
0h
T12h T36h T48h T60h
b
TCR$_{TAG}$
10^7
10^6
10^5
10^4
10^3
10^2
10^1
****
****
12h 36h 48h 60h 5d 21d
tumor Liver
tumor draining LN
effector spleen
tumor spleen
c
Infection
Liver tumor-bearing host
Spleen
Tumors
LDLN
Spleen
NIV
E12h
E36h
E48h
E60h
NIV
T12h
T36h
T48h
T60h
6+5 4 3 2 1 0 Div
6+5 4 3 2 1 0 Div
6+5 4 3 2 1 0 Div
6+5 4 3 2 1 0 Div
0 Div
CD69
CD44
CD62L
LAG3
PD1
CFSE

Figure 2.2 TST undergo robust proliferation and activation in infection and tumors. a, Experimental scheme: CFSE-labeled naive TCR_{TAG} (Thy1.1) were adoptively transferred into B6 (Thy1.2), LM_{TAG}-infected B6 (Thy1.2), or ASTxAlb-Cre mice (Thy1.2) bearing late-stage liver tumors. TCR_{TAG} were re-isolated at 12, 36, 48, and 60 hours (h) from infected spleen or tumor livers for flow cytometric analysis (Naive *in vivo* (N; grey); Effector (E; green); Tumor (T; blue)). **b,** Counts of TCR_{TAG} per organ; black bars represent population mean. **c**, Live $CD8^+$ $Thy1.1^+$ TCR_{TAG} CFSE dilution and expression of surface markers at each timepoint from LM_{TAG}-infected spleens (green) or for tumor-bearing mice (blue), from liver tumors, liver draining lymph nodes (LDLN), and spleens, shown relative to naive *in vivo* control (N; grey). Each timepoint is concatenated from 3-4 biologic replicates.

functional double positive population (**Figure2.3b**). When analyzed by cell division there was not a pattern of decreasing function with cell division across organs in tumor bearing mice indicating dysfunction was established by the earliest divisions or even predivision (**Figure 2.3c)**. This pattern was also found for cytolytic mediators. TCR_{TAG} activated in tumors largely failed to degranulate and did not express granzyme B in contrast to infection activated controls (**Figure 2.3c)**. Perforin was expressed in TCR_{TAG} activated in tumors but to a lesser degree and in a smaller fraction of the population relative to infection control. These data indicate a stark decoupling of proliferative capacity and function while suggesting functional mediators are differentially regulated in tumors.

We next asked what master TF were present during the initial divisions following T cell activation in tumors or infection. We harvested TCR_{TAG} at timepoints between 12 and 60 hours post transfer to capture full range of cell divisions (**Figure 2.4a**). Infection activated T cells robustly induced the TF TBET and EOMES which also correlates with the relative gain in cytokine and

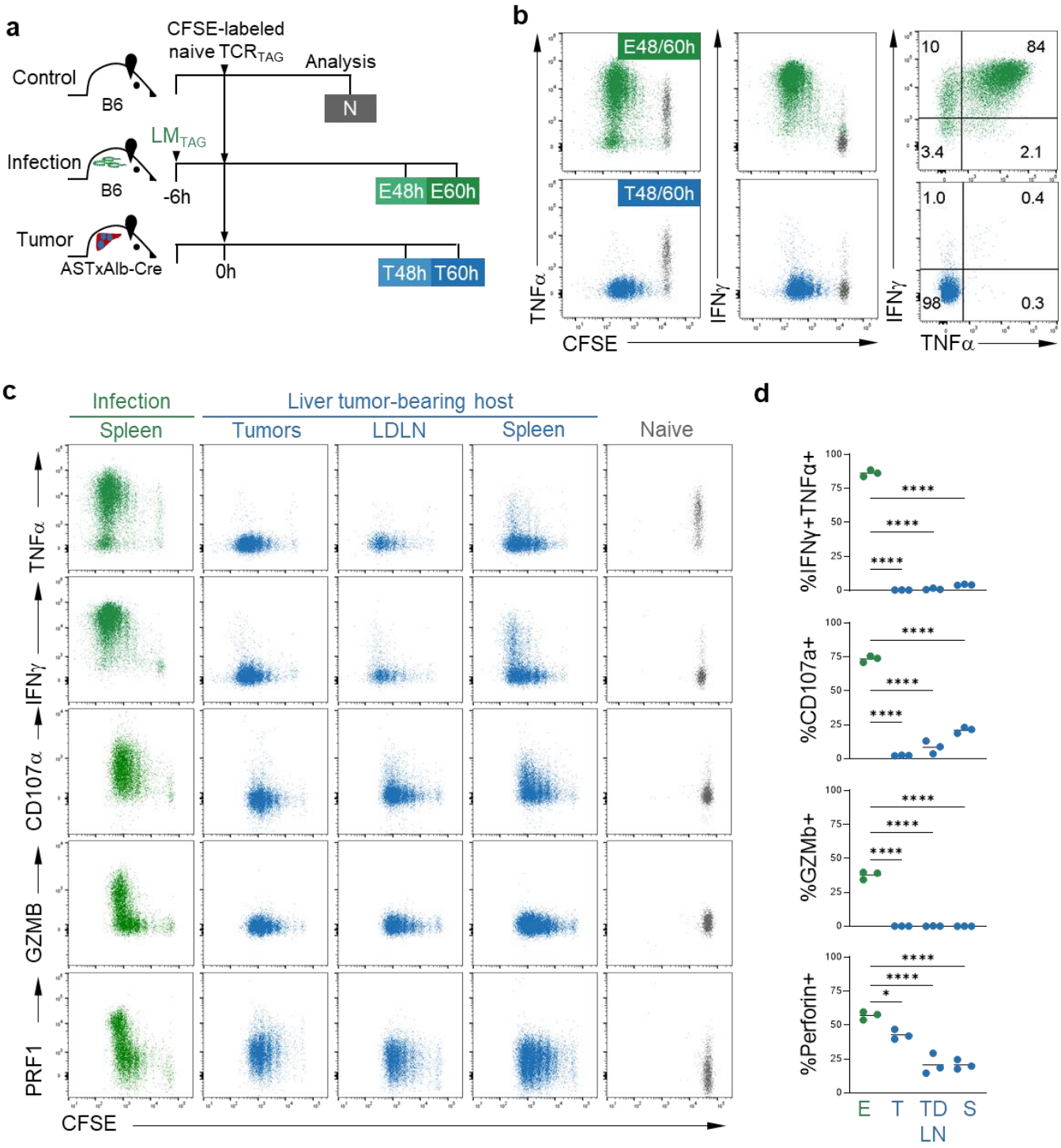
a
CFSE-labeled naive TCR$_{TAG}$
Analysis
Control
B6
N
LM$_{TAG}$
Infection
B6
-6h
E48h E60h
Tumor
ASTxAlb-Cre
0h
T48h T60h
b
E48/60h
T48/60h
TNFα
CFSE
IFNγ
IFNγ
TNFα
10
84
3.4
2.1
1.0
0.4
98
0.3
c
Infection
Liver tumor-bearing host
Spleen
Tumors
LDLN
Spleen
Naive
TNFα
IFNγ
CD107α
GZMB
PRF1
CFSE
d
%IFNγ+TNFα+
%CD107a+
%GZMb+
%Perforin+
****
****
****
*
E
T
TD LN
S

Figure 2.3 TST are dysfunctional during the first cell divisions following tumor contact. a, Experimental scheme: CFSE-labeled naive TCR_{TAG} (Thy1.1) were adoptively transferred into B6 (Thy1.2), LM_{TAG}-infected B6 (Thy1.2), or ASTxAlb-Cre mice (Thy1.2) bearing late-stage liver tumors. TCR_{TAG} were re-isolated at 48 and 60 hours (h) from infected spleen or tumor livers for flow cytometric analysis (Naive *in vivo* (N; grey); Effector (E; green); Tumor (T; blue)). **b,** TCR_{TAG} IFNγ and TNFα expression following 4h *ex vivo* peptide stim for 36h time point (divisions 1-3) in LM_{TAG}-infected spleens or tumor livers. **c,** TCR_{TAG} from pooled 48 and 60h timepoints. TNFα, IFNγ, and CD107a expression following 4h *ex vivo* TAG peptide stimulation. Granzyme B (GZMB) and perforin (PRF1) expression immediately *ex vivo* from infected or tumor bearing mice relative to N. **d,** Summary plots of effector molecules from effector spleens, tumors, TDLN, and tumor spleens. **P*<0.05, *****P* <0.0001 determined by one-way ANOVA with post hoc Sidak's test. Experiments were repeated twice with n=3-4 mice per group.

cytolytic function. Interestingly, both TF exhibited some induction even before the first cell division. Infection activated T cells did induce TOX in line with observations that TOX is NFAT induced in both functional and dysfunctional environments (**Figure 2.4b)**. In contrast, while tumor activated T cells did induce EOMES, expression was fleeting, with most TCR_{TAG} exhibiting negative expression by division 4 and within 48h in tumor. TBET was uniformly negative in tumor activated TCR_{TAG}. TOX was expressed more in tumor activated TCR_{TAG} and maintained a more homogenous expression level, again likely representing a relatively higher and persistent antigen burden relative to infection controls (**Figure 2.4b**).

The exceedingly rapid onset of T cell dysfunction led us to ask if functional or dysfunctional phenotypes were initiated before cell division. To address this question, we implemented the same experimental design with more rapid, predivision analysis timepoints (**Figure 2.5a**). At 6, 12, and 18h after transfer into infected animals or tumor bearing animals TCR_{TAG} remained undivided as evidenced by single CFSE peak (**Figure 2.5b)**. Despite being undivided, the majority of TCR_{TAG} across timepoints and conditions received TCR signaling as CD69 was near uniformly induced even at 6h (**Figure 2.5b)**. Despite similar levels of predivision activation, TCR_{TAG} maintained

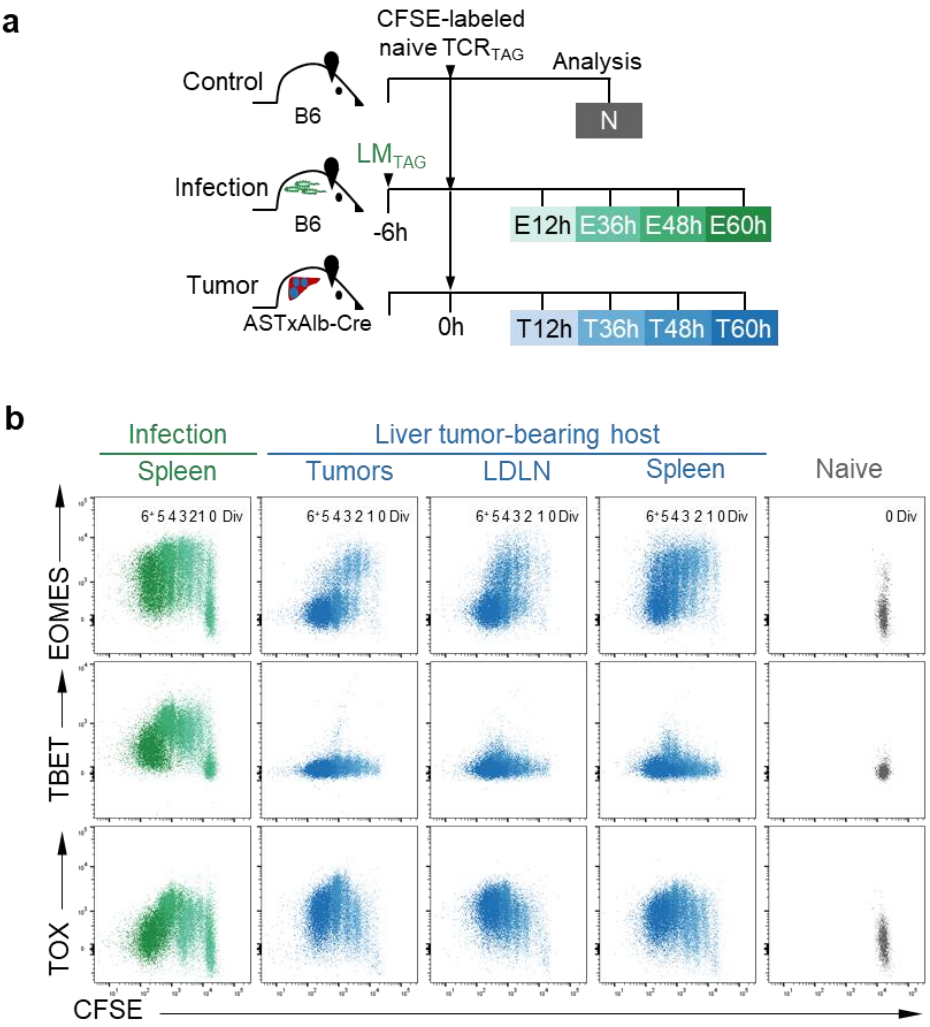

Figure 2.4 TST exhibit unique transcription factor profile following activation in tumors. a, Experimental scheme: CFSE-labeled naive TCR_{TAG} (Thy1.1) were adoptively transferred into B6 (Thy1.2), LM_{TAG}-infected B6 (Thy1.2), or ASTxAlb-Cre mice (Thy1.2) bearing late-stage liver tumors. TCR_{TAG} were re-isolated at 48 and 60 hours (h) from infected spleen or tumor livers for flow cytometric analysis (Naive *in vivo* (N; grey); Effector (E; green); Tumor (T; blue)). **b,** transcription factor expression by cell division. Dot plots represent concatenation of 3-4 biological replicates.

TNFα and gained IFNγ and GZMB expression with time in infection. This was in sharp contrast to tumor activated TCR_{TAG}, which rapidly shut down basal TNFα expression and failed to gain appreciable IFNγ or GZMB expression (**Figure 2.5c, d and Figure 2.6b**). Notably, functional gain and loss did not correlate with any TOX expression, which remained negative during the first 18h after activation (Figure 2.5e).

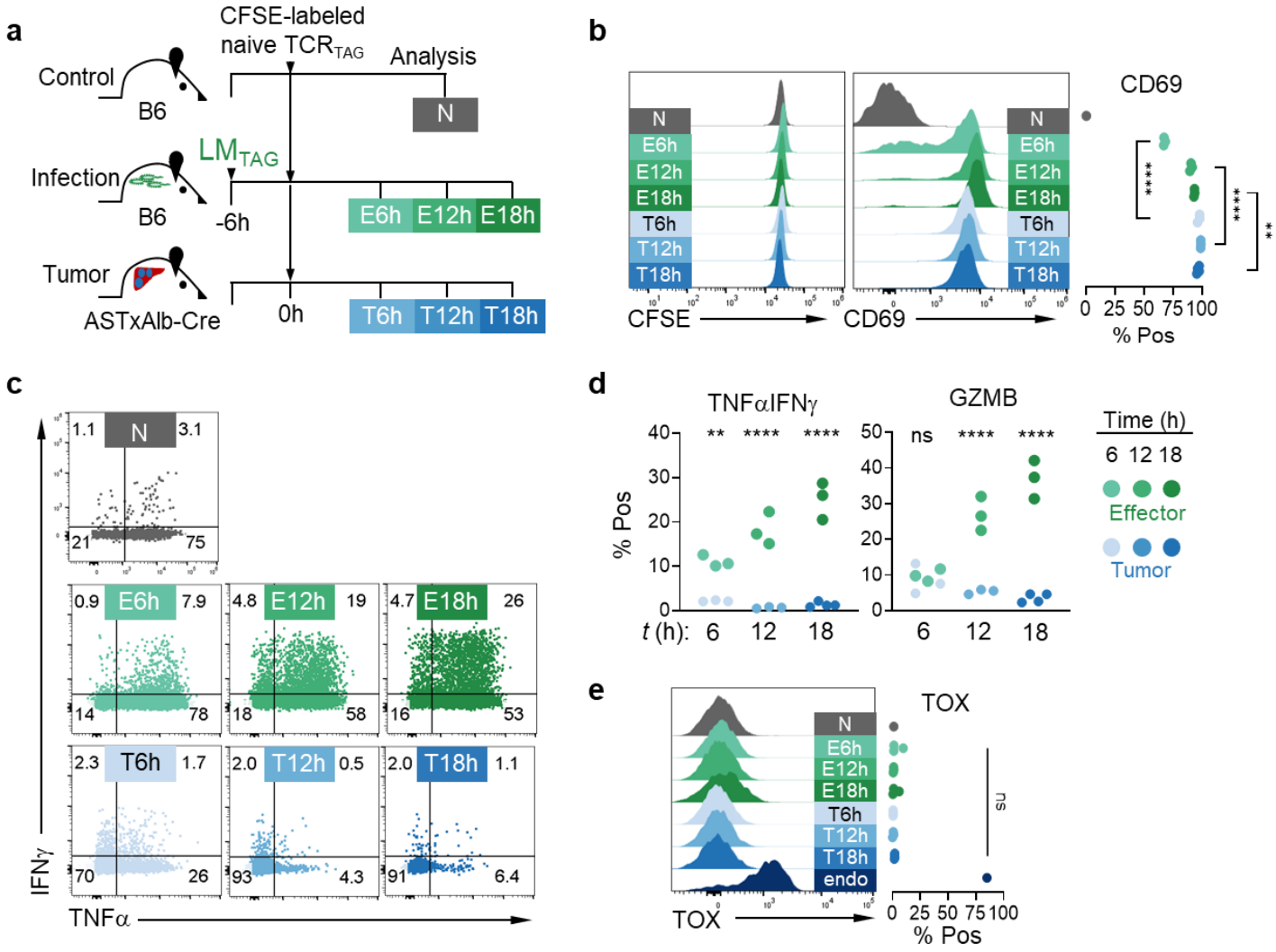

Figure 2.5 Tumor-induced TST dysfunction is established prior to cell division. **a**, Experimental scheme: CFSE-labeled naive TCR_{TAG} (Thy1.1) were adoptively transferred into B6 (Thy1.2), LM_{TAG}-infected B6 (Thy1.2), or ASTxAlb-Cre mice (Thy1.2) bearing late-stage liver tumors, and lymphocytes were re-isolated from tumor livers (blue) and infected spleens (green) at 6, 12, and 18h post-transfer for analysis by flow cytometry. **b**, Live $CD8^+$ $Thy1.1^+$ TCR_{TAG} CFSE dilution at each timepoint (left) and histogram and summary plot of CD69 expression (right) shown in comparison to naive *in vivo* (N; grey). **c**, TCR_{TAG} intracellular IFNγ and TNFα production after 4h *ex vivo* TAG peptide stimulation, with inset numbers indicating percentage of cells in each gate. Gates set based on no stim controls. **d**, Summary plots of TNFαIFNγ double-positive and *ex* vivo GZMB expression in TCR_{TAG}. Each symbol represents an individual mouse. e, Histograms and summary plots of TOX expression. $CD8^+$ $CD90.1^-$ $PD1^{hi}$ endogenous (endo) dysfunctional T cells are shown as the positive control for TOX staining. Histograms show representative data of group. $^{**}P<0.01$, $^{****}P<0.0001$ determined by two-way ANOVA with post hoc Tukey test. Experiments were repeated twice with n=3-4 mice per group.

This indicates that initiation of dysfunction in tumors is independent of TOX. Surface expression of additional activation markers showed that CD44 was induced later in the predivision phase and induction rose sharply in the tumor activated TCR_{TAG} group (**Figure 2.6a**). While LAG3 was induced similarly between groups, PD1 again was more in tumor activated TCR_{TAG}. Taken together, this supports the notion of a relatively high strength of TCR signaling that begins on first contact in TCR_{TAG} activated in tumors.

To validate our findings of rapid, predivision functional and dysfunctional fate decisions in a secondary model, we turned to murine melanoma cell line B16 engineered to express the model antigen ovalbumin (B16-OVA) in conjunction with OVA-specific CD8 T cells (TCR_{OTI}). B16-OVA was introduced into B6 mice by intravenous tail vein injection thus establishing lung tumors. After tumors were established, naive TCR_{OTI} was adoptively transferred into tumor bearing mice or mice inoculated with LM_{OVA} and then isolated from lung tumors or spleens of infected animals at 16h and 48h (**Figure 2.7a**). As seen with TCR_{TAG}, TCR_{OTI}, rapidly activated in lung tumors as seen by CD69 induction in both infection and tumor conditions while remaining undivided at 16h. While undivided, both infection and tumor conditions induced PD1 surface expression with higher levels being found on tumor activated TCR_{OTI} (**Figure 2.7b**). Cytokine expression patterns of TCR_{OTI} also matched previous findings where infection activated cells maintained TNFα and majority were already expressing IFNγ and GZMB prior to first cell division. In stark contrast, TCR_{OTI} activated in tumors failed to induce significant amounts of IFNγ or GZMB while also rapidly shutting down baseline TNFα production (**Figure 2.7c, e, and f)**.

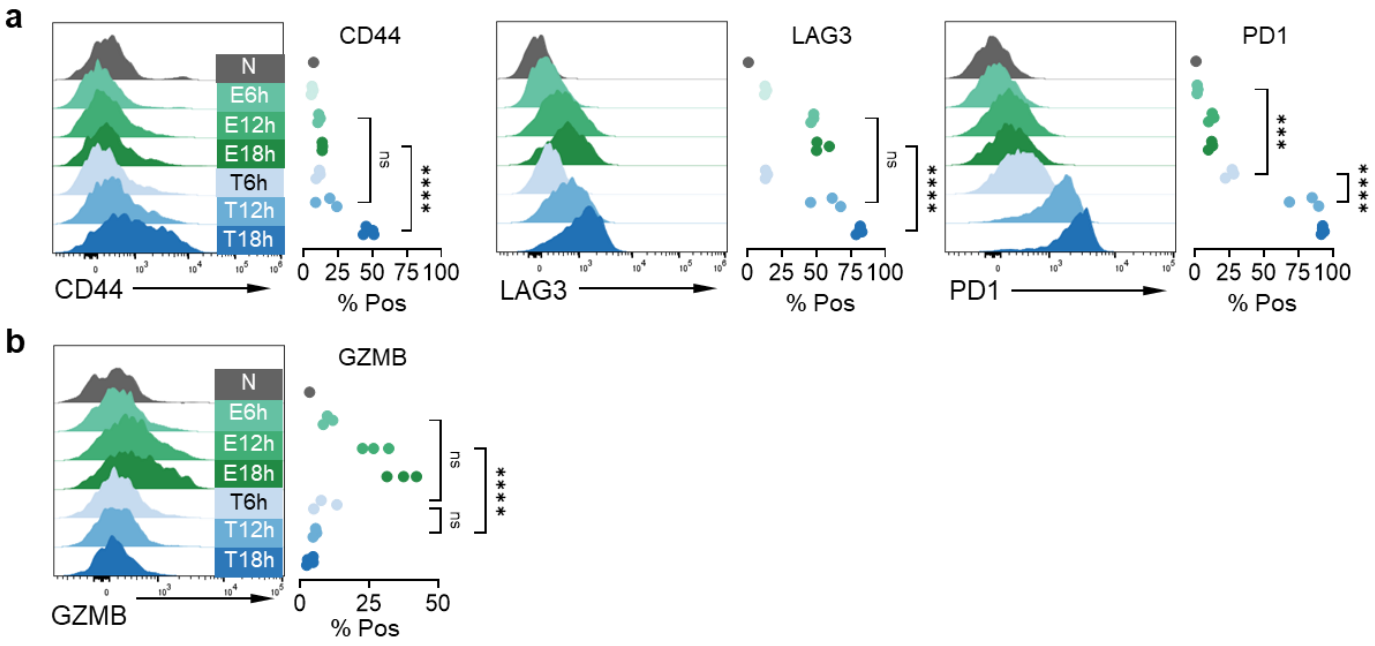

Figure 2.6 Predivision activation in tumors and infection. Live $CD8^+$ $Thy1.1^+$ TCR_{TAG} analyzed from spleens of infected mice (green) and liver tumors from tumor-bearing hosts (blue) at 6, 12, and 18h. **a,** Representative histograms of CD44, LAG3, and PD1 expression profiles. **b,** *Ex vivo* GZMB expression. Summary plots are shown to the left with each point representing an individual mouse. ***P<0.001, ****P <0.0001 determined by two-way ANOVA with post hoc Tukey test.

Functional or dysfunctional differentiation with additional times and the onset of cell division was also evaluated at 48h. Again, both infection and tumor activated TCR_{OTI} expanded robustly as evidenced by dilution of CFSE (**Figure 2.7d).** Both conditions induced and incrementally downregulated CD69 and induced CD44 expression (**Figure 2.7d**). While similar numbers expressed LAG3 and to similar expression levels, PD1 was induced more in the tumor condition than the infection condition in line with TCR_{TAG} experiments.

Taken together, differentiation began before cell division with dysfunctional states obtained before cell division. The rapid onset of dysfunction in naive CD8 T cells upon encountering tumor is not

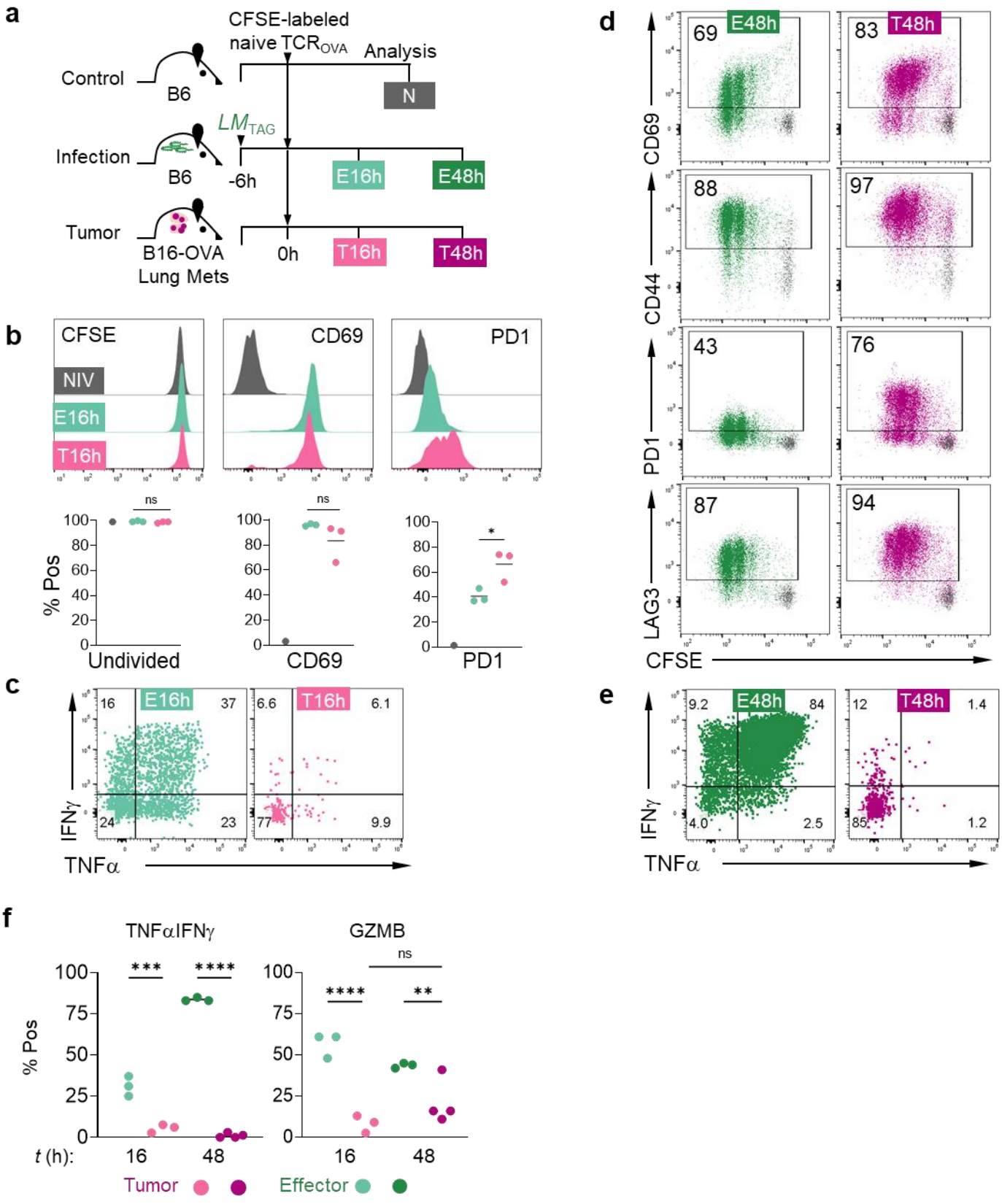
a
CFSE-labeled naive TCR$_{OVA}$
Analysis
N
Control
B6
LM_{TAG}
Infection
B6
-6h
E16h
E48h
Tumor
B16-OVA Lung Mets
0h
T16h
T48h
b
CFSE
NIV
E16h
T16h
CD69
PD1
ns
ns
*
% Pos
Undivided
CD69
PD1
c
16
E16h
37
6.6
T16h
6.1
24
23
77
9.9
IFNγ
TNFα
d
69
E48h
83
T48h
88
97
43
76
87
94
CD69
CD44
PD1
LAG3
CFSE
e
9.2
E48h
84
12
T48h
1.4
4.0
2.5
85
1.2
IFNγ
TNFα
f
TNFαIFNγ
GZMB
***
****
ns
****
**
% Pos
t (h):
16
48
16
48
Tumor
Effector

Figure 2.7 T cells activated in lung tumors exhibit dysfunction predivision but still expand robustly. CFSE-labeled naive TCR_{OTI} (Ly5.1) were adoptively transferred into B6 (Ly5.2), LM_{OVA}-infected B6 (Ly5.2), or B6 mice (Ly5.2) bearing lung tumors, and lymphocytes were re-isolated from lung tumors (pink) and infected spleens (green) at 16 and 18h post-transfer for analysis by flow cytometry. **b**, Live $CD8^+$ $Ly5.1^+$ TCR_{OTI} CFSE dilution at each timepoint (left), CD69 expression (middle), and PD1 expression (right) shown in comparison to naive *in vivo* (N; grey). Summary plots below where each point represents an individual mouse and black lines represent the mean. ns = not significant and $*P<0.05$ determined by unpaired two tailed Students T test. **c**, TCR_{OVA} intracellular IFNγ and TNFα production after 4h *ex vivo* OVA peptide stimulation, with inset numbers indicating percentage of cells in each gate. Gates set based on no stim controls. **d**, Summary plots surface markers by CFSE at 48h. Gates based on N control and inset represents percent population in gate. **e,** TCR_{OVA} intracellular IFNγ and TNFα production after 4h *ex vivo* OVA peptide stimulation, with inset numbers indicating percentage of cells in each gate. Gates set based on no stim controls. TCR_{OVA} intracellular IFNγ and TNFα production after 4h *ex vivo* OVA peptide stimulation, with inset numbers indicating percentage of cells in each gate. Gates set based on no stim controls. **f,** summary plots of cytokines and GZMB where each point represents an individual mouse $**P<0.01$, $****P<0.0001$ determined by two-way ANOVA with post hoc Tukey test. Experiments were repeated twice with n=3-4 mice per group.

unique to liver tumors as T cells activated in B16-OVA lung tumors exhibited similar phenotypes. Thus dysfunction cannot be solely attributed to the relatively immunosuppressive environment of livers in general (Crispe, Dao et al. 2000, Li and Tian 2013, Doherty 2016) or the relatively accessible antigen through fenestrated epithelium (Guidotti, Inverso et al. 2015). Furthermore, the use of two different model antigens and T cell clonotypes suggests these results may be more generalizable of T cells encountering antigen in established tumors.

Kinetics of effector T cell function loss in tumors

We next asked if previously activated and committed effector T cells would also rapidly lose function on contact with tumors. To answer this, we generated effector TCR_{TAG} by transferring naive TCR_{TAG} into mice infected with LM_{TAG} and harvesting effectors at 5d post transfer, roughly peak of response. Effector TCR_{TAG} (E5d) were CFSE labeled and adoptively transferred into time matched infected animals or ASTxAlb-Cre liver tumor bearing mice (**Figure 2.8a**). As seen in

naive populations, E5d robustly proliferated on secondary encounter with antigen in tumor bearing mice (**Figure 2.8b**). E5d induced the IL-7 receptor subunit CD127 while tumor activated E5d did not indicating impaired memory differentiation in the context of persistent antigen (**Figure 2.8b**). E5d transferred into infection matched controls exhibited full cytokine function with strong double positive TNFα and IFNγ. Remarkably, E5d transferred into tumor bearing hosts lost the majority of the cytokine double positive population by 12h after transfer, prior to first cell division (**Figure 2.8c**). This was worsened with time and cell division, producing a majority double negative population in as little as 36h following tumor encounter (**Figure 2.8c, d**). Again, this functional loss was specific to liver tumors as E5d transferred into time matched infection controls exhibited identical function when reisolated from livers or spleens (**Figure 2.8e**). When TNFα and IFNγ were compared to CFSE, we found that exposure time to tumors appeared more important for effector function loss than cell division, with most cytokine being lost predivision which was worsened in undivided cells with another 24h of tumor exposure (**Figure 2.8f, g**). This suggests that initiation of cytokine dysfunction begins with tumor contact and that chronic antigen signaling is not required. Furthermore, the stable function and induction of CD127 indicate that memory differentiation is not negatively affected by the adoptive transfer workflow and does not contribute to functional loss.

We next asked if cytotoxicity is also rapidly lost in tumors. E5d were transferred into liver tumor bearing ASTxAlb-Cre mice and cells were harvested 1, 2, 3, and 4 days later (**Figure 2.9a**). Similar to naive TCR_{TAG} E5d underwent clonal expansion on secondary encounter with antigen in tumors (**Figure 2.9b**). E5d encountering tumors induced PD1 by 1d corroborating expansion data

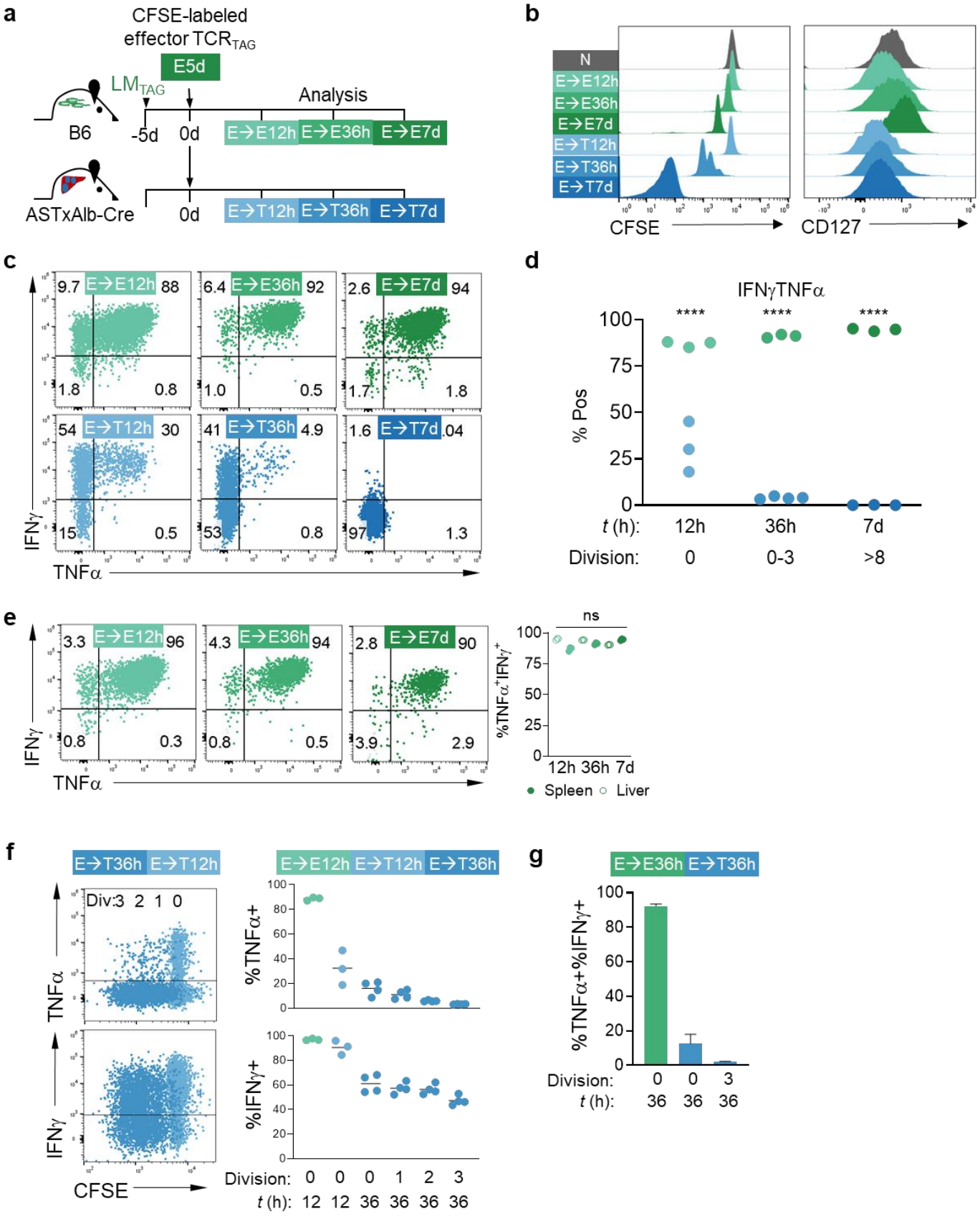
a
CFSE-labeled effector TCR$_{TAG}$
E5d
LM$_{TAG}$
Analysis
B6
-5d
0d
E→E12h E→E36h E→E7d
ASTxAlb-Cre
0d
E→T12h E→T36h E→T7d
b
N
E→E12h
E→E36h
E→E7d
E→T12h
E→T36h
E→T7d
CFSE
CD127
c
9.7 E→E12h 88
1.8 0.8
6.4 E→E36h 92
1.0 0.5
2.6 E→E7d 94
1.7 1.8
54 E→T12h 30
15 0.5
41 E→T36h 4.9
53 0.8
1.6 E→T7d .04
97 1.3
IFNγ
TNFα
d
IFNγTNFα
****
****
****
% Pos
100
75
50
25
0
t (h): 12h 36h 7d
Division: 0 0-3 >8
e
3.3 E→E12h 96
0.8 0.3
4.3 E→E36h 94
0.8 0.5
2.8 E→E7d 90
3.9 2.9
IFNγ
TNFα
ns
%TNFα+IFNγ+
100
75
50
25
0
12h 36h 7d
Spleen
Liver
f
E→T36h E→T12h
Div:3 2 1 0
TNFα
IFNγ
CFSE
E→E12h E→T12h E→T36h
%TNFα+
%IFNγ+
100
80
60
40
20
0
Division: 0 0 0 1 2 3
t (h): 12 12 36 36 36 36
g
E→E36h E→T36h
%TNFα+%IFNγ+
100
80
60
40
20
0
Division: 0 0 3
t (h): 36 36 36

Figure 2.8 Committed effectors rapidly lose cytokine function in tumors. a, Experimental scheme: committed effectors were generated by transferring naive TCR_{TAG} into LM_{TAG}-infected B6 mice and harvesting splenocytes 5 days (d) post transfer (E5d). E5d were CFSE-labeled and transferred into time-matched infected mice or tumor-bearing mice. TCR_{TAG} were re-isolated from infected spleens (green) or tumor livers (blue) of secondary recipients 12h, 36h, and 7d post-transfer. All flow plots are gated on live $CD8^+$ $Thy1.1^+$ cells. **b**, CFSE dilution and CD127 expression with naive TCR_{TAG} (N; grey) shown for comparison. **c**, TCR_{TAG} IFNγ and TNFα production after 4h *ex vivo* TAG peptide stimulation, with inset numbers indicating percentage of cells in each gate. Gates set based on no peptide stimulation controls. **d**, Summary plots of TNFαIFNγ double-positive TCR_{TAG}. Each symbol represents an individual mouse. **e**, TCR_{TAG} IFNγ and TNFα production from livers of infected mice after 4h *ex vivo* TAG peptide stimulation, with inset numbers indicating percentage of cells in each gate. **f,** Overlay of concatenated 12 and 36h timepoints from tumor livers showing TCR_{TAG} CFSE dilution and TNFα and IFNγ production following 4h TAG peptide stimulation (left). Summary plots of TNFα and IFNγ production (right) where each symbol represents a single mouse. **g,** Summary plot of IFNγTNFα double-positive TCR_{TAG} by cell division 36h post-transfer. ****P<0.0001 determined by two-way ANOVA with post-hoc Tukey test. Experiments were repeated three times with n=3-4 mice per group.

and indicated that effectors rapidly activate in tumors similar to naive populations. Notably, PD1 did not increase during the time course (**Figure 2.9c**). Relative to quiescent effector controls which are immediately capable of degranulating following secondary stimulation, E5d in tumors could only degranulate during the first day of contact with tumor. By 2d and beyond, effectors were largely incapable of degranulation despite persistent antigen. Relative to quiescent effector control which are baseline negative for granzyme B, E5d in tumors appropriately reinduced granzyme but expression was fleeting and majority were granzyme B negative by 2d and beyond (**Figure 2.9c**). Perforin, which was induced to lower degree in naive tumor activated TCR_{TAG} is maintained positive in committed quiescent effectors. Perforin underwent a secondary induction to even higher expression levels but returned to "baseline" positive levels after 2d (data not shown).

To validate the rapid onset of dysfunction in effector T cells we once again turned to our B16-OVA lung tumor system. Effector TCR_{OTI} were generated by adoptive transfer of TCR_{OTI} into LM_{OVA} infected animals and harvest from spleens at 5d (E5d). E5d were CFSE labelled and

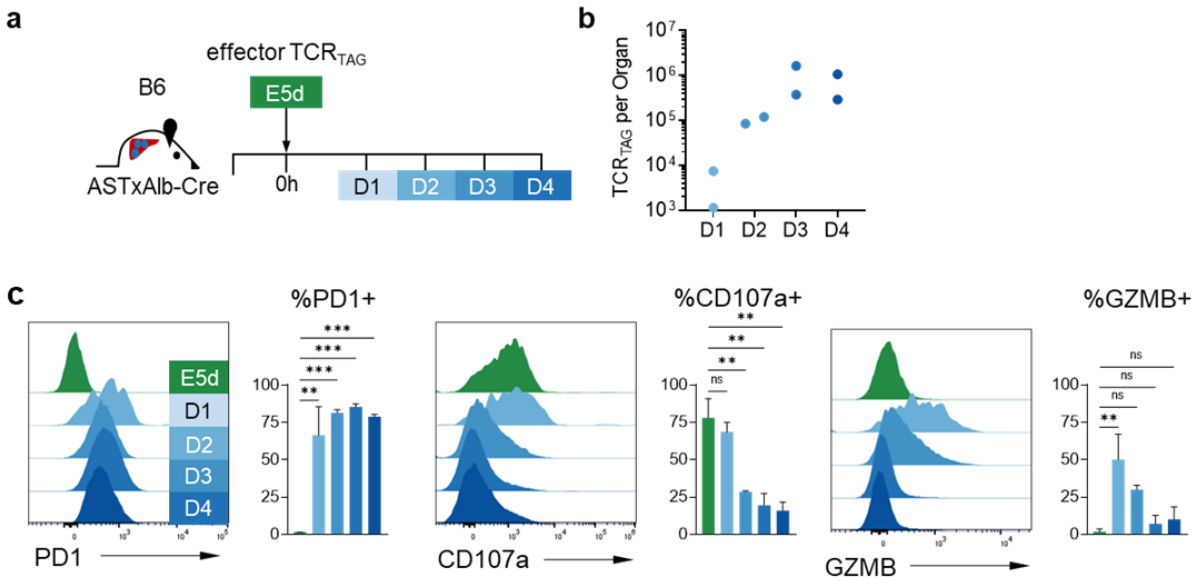

Figure 2.9 Committed effectors rapidly lose cytolytic function in tumors. a, Experimental scheme: committed effectors were generated by transferring naive TCR_{TAG} into LM_{TAG}-infected B6 mice and harvesting splenocytes 5 days (d) post transfer (E5d). TCR_{TAG} were re-isolated tumor livers (blue) of secondary recipients 1, 2, 3, and 4d post-transfer. **b,** Quantity of TCR_{TAG} in liver tumors over time where each point represents an individual mouse. **c,** Histogram of representative PD1 expression, CD107a localization following 1h TAG peptide stim, and *ex vivo* granzyme B expression at each timepoint. Summary bar plots of each marker shown where error bars represent standard deviation. Ns = not significant, ** P<0.01, and ***P<0.001 determined by two-way ANOVA with post-hoc Dunnett's multiple comparison test. Experiments were performed once with n=2 mice per group.

transferred into time matched infection controls or mice bearing B16-OVA lung tumors (**Figure 2.10a**). Similar to TCR_{TAG} E5d, TCR_{OTI} E5d expanded in tumors and rapidly activated as evidenced by PD1 expression (**Figure 2.10b**). Again, despite robust proliferation, E5d activated in lung tumors began to rapidly lose function with majority of cytokine double positive population lost within 24h and prior to the first cell division. This phenotype was worsened with an additional day in tumors and the initiation of cell division with substantial percentage of the population double negative by 48h (**Figure 2.10c, d)**.

Discussion

Taken together, the findings described in this chapter indicate that even previously differentiated

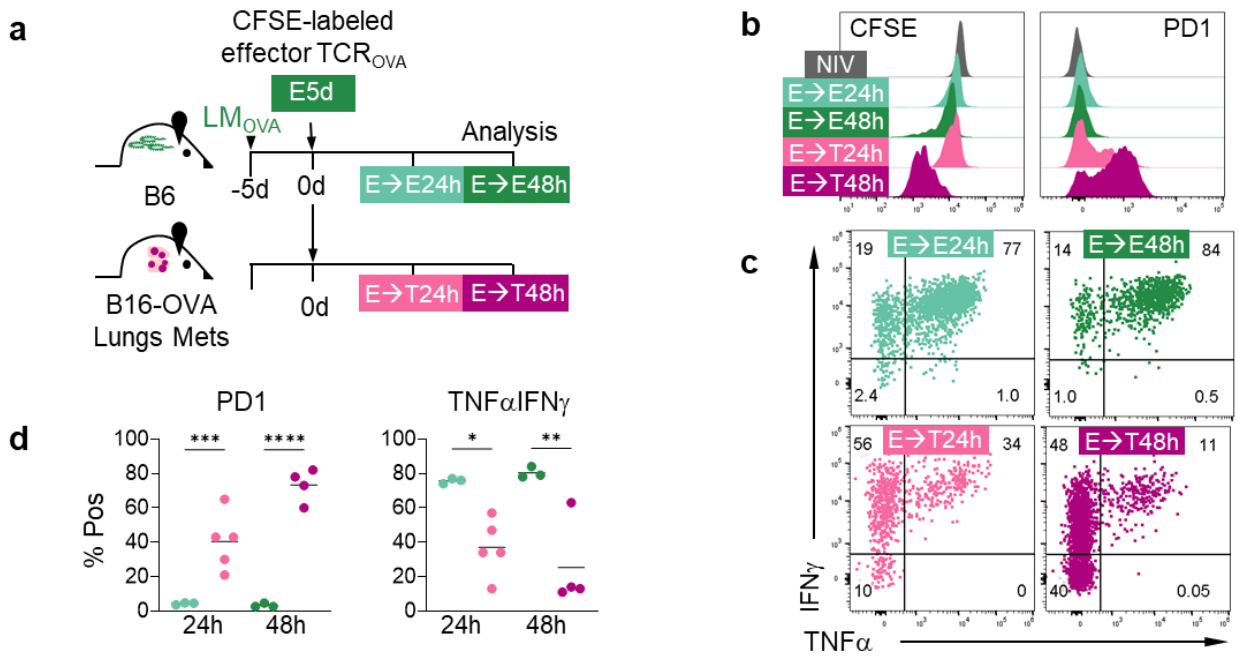

Figure 2.10 Committed effectors rapidly lose function in melanoma lung metastases. a, Experimental scheme: committed effectors were generated by transferring naive TCR_{OVA} into LM_{OVA}-infected B6 mice and harvesting splenocytes 5 days post transfer (E5d). E5d were CFSE-labeled and transferred into time-matched infected mice or lung tumor-bearing mice. TCR_{OVA} were re-isolated from infected spleens (green) or lung tumors (pink) of secondary recipients 24h and 48h post-transfer. All flow plots are gated on live $CD8^+$ $Ly5.1^+$ cells. **b,** CFSE dilution and PD1 expression with naive TCR_{TAG} (N; grey) shown for comparison. **c,** TCR_{OVA} IFNγ and TNFα production after 4h *ex vivo* OVA peptide stimulation, with inset numbers indicating percentage of cells in each gate. Gates set based on no peptide stimulation controls. **d,** Summary plots of TNFα and IFNγ production where each symbol represents a single mouse. **P*<0.05, ** *P*<0.01, and *****P*<0.0001 determined by two-way ANOVA with post-hoc Tukey test. Experiments were performed once with n=3-4 mice per group.

committed effectors lose function rapidly in tumors. This finding is not dependent on liver tumors or the TAG antigen as effector T cells responding to tumors in the lung also rapidly initiated effector function loss. The rapid initiation of functional losses was not specific to single clonal T cell population or epitope. Rapid dysfunction was not specific to tumor type either, with both HCC and murine melanoma producing similar kinetics. The effector functional losses of effector T cells indicates that rapid dysfunctional onset is not solely due to lack of costimulation or inadequate priming of naive populations. The rapid shutdown of TNFα in the naive population and the

initiation of TNFα and IFNγ loss in effectors, indicates that there is an active component driving dysfunction in T cells activated in the context of tumors. It is worth noting that effector T cells progressively lose TNFα followed by IFNγ which recapitulates the hierarchical cytokine loss first observed in models of chronic viral infection (Wherry, Blattman et al. 2003), but occurs at a much more rapid pace. These kinetics match independent studies of *in vitro* generated effector T cells in subcutaneous tumors (Mognol, Spreafico et al. 2017). A striking difference between tumors and chronic viral infection though appears to be the kinetics and uniform loss of cytotoxicity in tumors. While T cells in chronic viral infections may incompletely lose or keep cytolytic mediators during late dysfunction (Fuller, Khanolkar et al. 2004). This indicates that even T cells that are properly activated in secondary lymphoid tissue or *in vitro* would rapidly lose function in tumors and these fleeting functional states may fail to mediate successful anti-tumor immunity.

CHAPTER 3: EPIGENETIC AND TRANSCRIPTIONAL UNDERPINNINGS OF EARLY T CELL DIFFERENTIATION

Introduction

Epigenetic remodeling is believed to facilitate transcriptional and functional differentiation of T cells from naive to effector and effector to memory states(Bird, Brown et al. 1998). This remodeling facilitates epigenetic opening of effector genes allowing for expression and function. Epigenetic states also allow for previously activated memory T cells to more rapidly induce secondary functional responses, as epigenetic states maintain open chromatin of effector genes such as *Ifng* in a lowly transcribed "poised" state (Gray, Kaech et al. 2014). Observations across the immune system have suggested that epigenetic remodeling is dependent of activated cells initiating cell division (Bird, Brown et al. 1998, Tangye and Hodgkin 2004, Kreslavsky, Gleimer et al. 2012, Scharer, Barwick et al. 2018). However studies performed *in vitro* (Yukawa, Jagannathan et al. 2020*)* and autopilot differentiation observed following brief <24h antigen encounters (Obst 2015) suggest that some degree of differentiation instructions are programmed, possibly through epigenetic mechanisms. Our findings from Chapter 1 suggest that both functional and dysfunctional T cell differentiation begin prior to cell division and led us to hypothesize that epigenetic remodeling occurs within 24 hours of activation *in vivo* prior to cell division.

To assess global chromatin landscape at early timepoints we implemented Assay for Transposase-Accessible Chromatin with sequencing (ATAC-SEQ)(Buenrostro, Giresi et al. 2013). This technique leverages mutated transposase preloaded with adapter fragments. Intact nuclei are isolated from sorted T cells and exposed to transposases. Transposase accessible chromatin is

tagged with adapters for downstream amplification and sequencing. This provides a population snapshot of global chromatin signatures from T cells activated in both tumors or infection across time and with cell numbers that prohibit use of other epigenetic techniques such as CHIP-SEQ. When run in parallel with RNA-Sequencing (RNA-SEQ), we can assess the chromatin changes, putative TF drivers, and corresponding transcriptional changes that are occurring at these early timepoints.

As epigenetic remodeling has been shown to program and stabilize functional (Gray, Kaech et al. 2014) or dysfunctional (Mognol, Spreafico et al. 2017, Philip, Fairchild et al. 2017, Abdel-Hakeem, Manne et al. 2021) T cell phenotypes, we wanted to evaluate the stability of early T cell differentiation decisions. Given enough time in tumors, T cells will enter fixed dysfunctional states incapable of expressing cytokines or being rescued by checkpoint blockade or inflammation (Philip, Fairchild et al. 2017). In chronic viral models, T cells exposed to antigen for 3-4 weeks will fail to acquire true memory phenotypes or chromatin signatures, instead exhibiting an epigenetically "scarred" profile (Abdel-Hakeem, Manne et al. 2021, Hensel, Gu et al. 2021, Yates, Tonnerre et al. 2021). It remains unclear how soon dysfunctional phenotypes can be stabilized and what the kinetics of epigenetic scarring in tumors are.

Predivision epigenetic and transcriptional remodeling coincides with predivision functional differentiation

Due to the surprising degree of functional differentiation we observed prior to cell division in adoptively transferred naive T cell populations, we asked if chromatin and corresponding transcriptional remodeling could also be detected within hours after T cell activation in tumors or

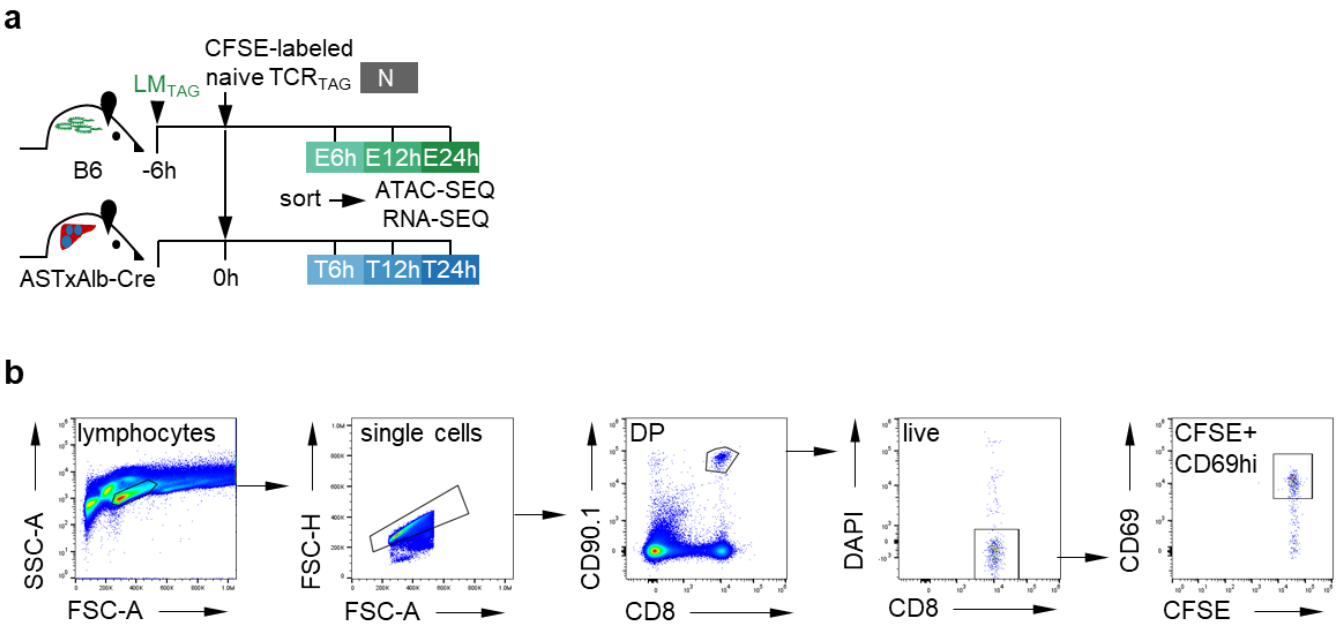

Figure 3.1 Isolating TCR_{TAG} for sequencing workflows. a, Experimental scheme: CFSE-labeled naive TCR_{TAG} (Thy1.1) were adoptively transferred into B6 (Thy1.2), LM_{TAG}-infected B6 (Thy1.2), or ASTxAlb-Cre mice (Thy1.2) bearing late-stage liver tumors, and lymphocytes were re-isolated from tumor livers (blue) and infected spleens (green) at 6, 12, and 24h post-transfer sorting. **b,** Cell sorting gating strategy for isolating single cell, live (DAPI-negative), activated TCR_{TAG} from infected spleens or liver tumors. DP, double-positive; DAPI negative, live population.

infection. To address these questions, we transferred CFSE labelled naive TCR_{TAG} into LM infected animals or ASTxAlb-cre mice (**Figure 3.1a**). We used cell sorting to separate live, congenic, CD8 TCR_{TAG} T cells that were CD69 positive indicating TCR signaling had been received *in vivo* (**Figure 3.1b**). Sorted cells were submitted for chromatin accessibility analysis by ATAC-SEQ and gene expression by RNA-SEQ.

To our surprise, we found that CD8 T cells underwent large scale chromatin remodeling starting as early as 6h following activation in tumors and infection. Up to 40,000 peaks opened or closed in both conditions. Intriguingly, the quantity of chromatin remodeling did not increase with time pre cell division. The largest remodeling event took place immediately after TCR signaling with

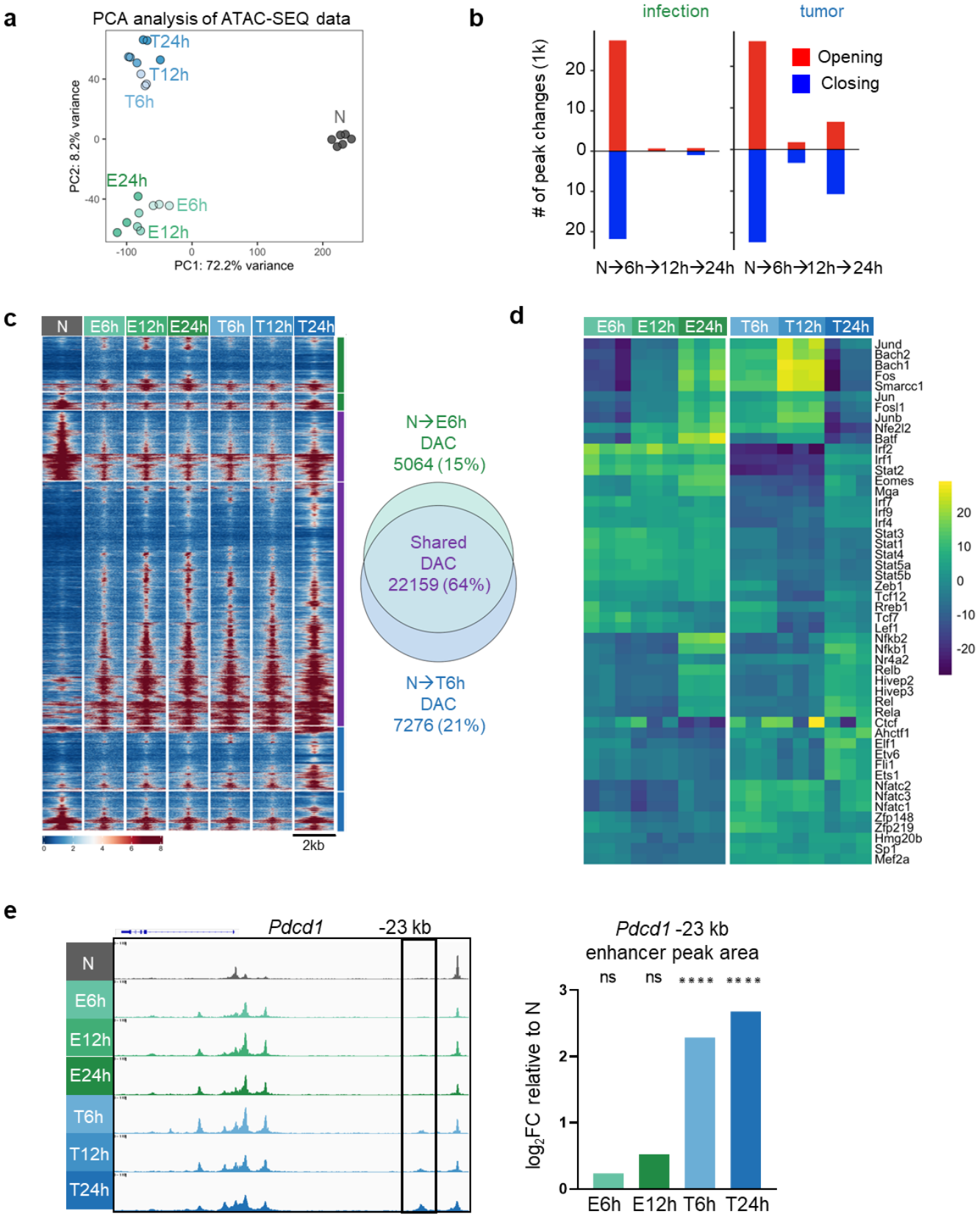
a
PCA analysis of ATAC-SEQ data
T24h
T12h
T6h
N
E24h
E6h
E12h
PC2: 8.2% variance
PC1: 72.2% variance
b
infection
tumor
Opening
Closing
# of peak changes (1k)
N→6h→12h→24h
N→6h→12h→24h
c
N
E6h
E12h
E24h
T6h
T12h
T24h
2kb
N→E6h
DAC
5064 (15%)
Shared
DAC
22159 (64%)
N→T6h
DAC
7276 (21%)
d
Jund
Bach2
Bach1
Fos
Smarcc1
Jun
Fosl1
Junb
Nfe2l2
Batf
Irf2
Irf1
Stat2
Eomes
Mga
Irf7
Irf9
Irf4
Stat3
Stat1
Stat4
Stat5a
Stat5b
Zeb1
Tcf12
Rreb1
Tcf7
Lef1
Nfkb2
Nfkb1
Nr4a2
Relb
Hivep2
Hivep3
Rel
Rela
Ctcf
Ahctf1
Elf1
Etv6
Fli1
Ets1
Nfatc2
Nfatc3
Nfatc1
Zfp148
Zfp219
Hmg20b
Sp1
Mef2a
e
Pdcd1
-23 kb
N
E6h
E12h
E24h
T6h
T12h
T24h
Pdcd1 -23 kb
enhancer peak area
ns
ns
****
****
log2FC relative to N
E6h
E12h
T6h
T24h

Figure 3.2 T cells activated in infection and tumors undergo massive chromatin remodeling and begin to epigenetically diverge hours after activation *in vivo*. a, Principal component analysis (PCA) comparing peak accessibility of naive (N; grey), and TCR_{TAG} differentiating during acute infection (green) and in tumors (blue) at 6, 12, and 24h post-transfer by the top $25x10^3$ variable peaks. Each symbol represents a single biological replicate. **b**, Number of chromatin accessibility peak changes during each transition (opening peaks, red; closing peaks, blue; *FDR*<0.05). **c,** Chromatin accessibility heatmap. Each row represents one of 34,449 differentially accessible peaks (*FDR*<0.05, |Log2FC| >1.5) displayed over 2kb window centered on the peak summit. Scale units are reads per genomic content (RPGC) normalized to 1x sequencing depth for 20 bp bins with blue indicating closed chromatin and red open chromatin. Peaks are ordered by membership within each subset shown in the Venn diagram (right) and hierarchical-clustering within the subset. Venn diagram showing quantity of differentially accessible chromatin peaks (DAC) that are unique to T cells in infection, unique to T cells in tumors, or shared between T cells in infection and tumors. **d,** Heatmap of chromVAR computed deviations z-score for the top 50 most variable transcription factor (TF) motifs across TCR_{TAG} tumor and infection at 6, 12, and 24h. **e,** Chromatin accessibility profile across the *Pdcd1* locus with the exhaustion-associated -23kb enhancer boxed (left). Summary plot of Log_2FC chromatin accessibility at the -23kb enhancer peak for E6, E24, T6h, and T24h as compared to naive (N) (right) (ns; not significant; ****$P<1.5x10^{-5}$**)**

relatively minor changes occurring with additional 18h. In line with the onset of peak remodeling, principle component analysis (PCA) showed that most of the differences could be attributed to transition from T cell quiescent naive to activated states. Even by 6h some condition-specific differences could be detected with mild increases in separation occurring at 12h and 24h (**Figure 3.2a, b**). In line with these findings, heat map of global chromatin changes showed a large number of chromatin peaks that were conserved between the two activation conditions. There were, however, some peaks specific to the activation condition with 7,272 (21%) differentially accessible chromatin (DAC) peaks in tumor activated TCR_{TAG} (**Figure 3.2c)**. To understand potential drivers of condition-specific DAC across time we utilized TF motif analysis with ChromVAR. We found that TCR_{TAG} activated in tumors enriched for NFAT family motifs while infection activated TCR_{TAG} enriched for STAT family motifs. In line with surface and functional phenotypes, these data suggest an environment relatively devoid of inflammatory signaling and hyperactivation of NFAT signaling within tumors (**Figure 3.2d**). Interestingly, other components downstream of TCR signaling appeared relatively conserved with NFκB enriching comparably between tumor

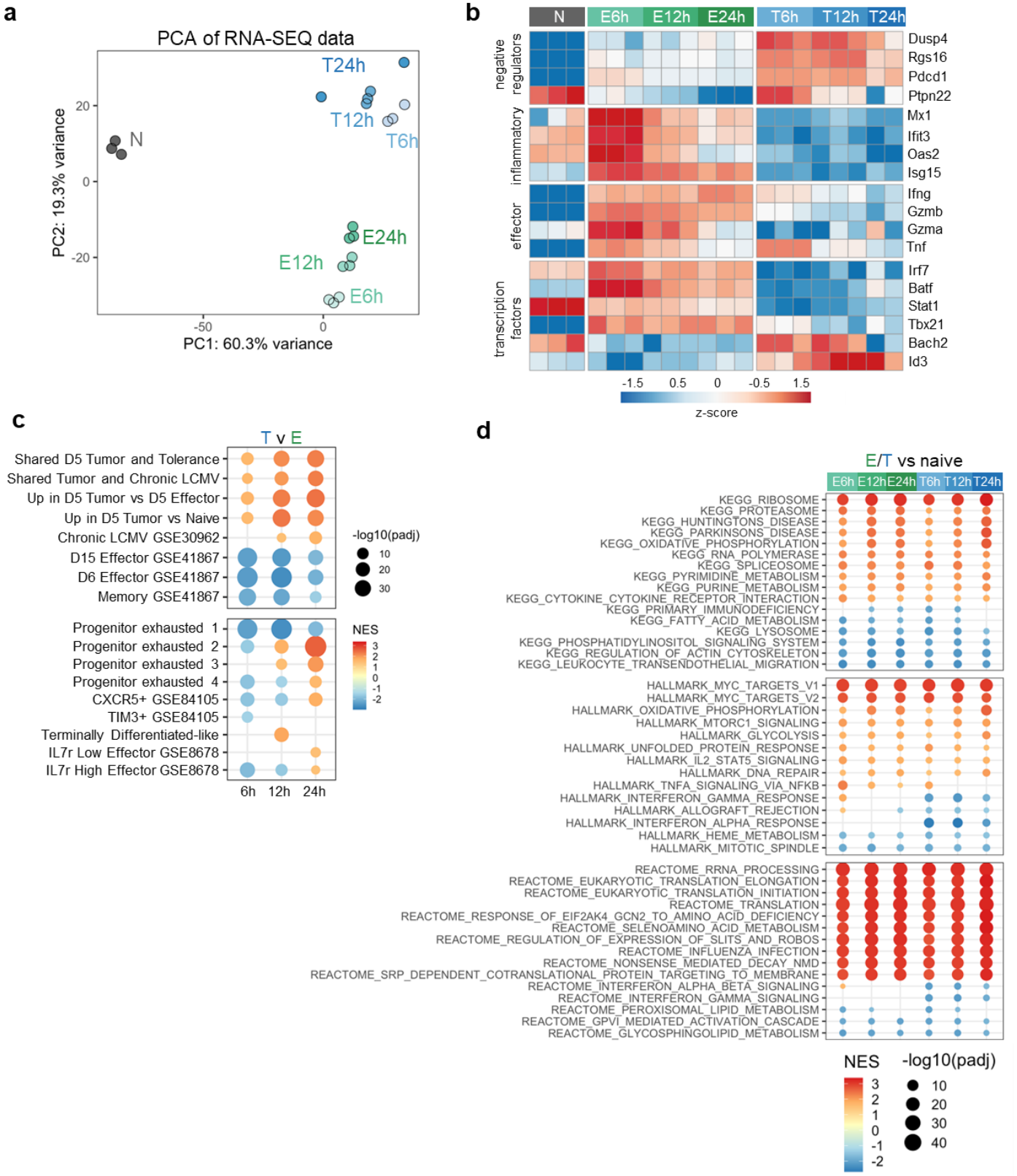
a
PCA of RNA-SEQ data
T24h
T12h
T6h
N
E24h
E12h
E6h
PC2: 19.3% variance
PC1: 60.3% variance
b
N
E6h
E12h
E24h
T6h
T12h
T24h
negative regulators
inflammatory
effector
transcription factors
Dusp4
Rgs16
Pdcd1
Ptpn22
Mx1
Ifit3
Oas2
Isg15
Ifng
Gzmb
Gzma
Tnf
Irf7
Batf
Stat1
Tbx21
Bach2
Id3
z-score
c
T v E
Shared D5 Tumor and Tolerance
Shared Tumor and Chronic LCMV
Up in D5 Tumor vs D5 Effector
Up in D5 Tumor vs Naive
Chronic LCMV GSE30962
D15 Effector GSE41867
D6 Effector GSE41867
Memory GSE41867
Progenitor exhausted 1
Progenitor exhausted 2
Progenitor exhausted 3
Progenitor exhausted 4
CXCR5+ GSE84105
TIM3+ GSE84105
Terminally Differentiated-like
IL7r Low Effector GSE8678
IL7r High Effector GSE8678
6h
12h
24h
-log10(padj)
NES
d
E/T vs naive
E6h
E12h
E24h
T6h
T12h
T24h
KEGG_RIBOSOME
KEGG_PROTEASOME
KEGG_HUNTINGTONS_DISEASE
KEGG_PARKINSONS_DISEASE
KEGG_OXIDATIVE_PHOSPHORYLATION
KEGG_RNA_POLYMERASE
KEGG_SPLICEOSOME
KEGG_PYRIMIDINE_METABOLISM
KEGG_PURINE_METABOLISM
KEGG_CYTOKINE_CYTOKINE_RECEPTOR_INTERACTION
KEGG_PRIMARY_IMMUNODEFICIENCY
KEGG_FATTY_ACID_METABOLISM
KEGG_LYSOSOME
KEGG_PHOSPHATIDYLINOSITOL_SIGNALING_SYSTEM
KEGG_REGULATION_OF_ACTIN_CYTOSKELETON
KEGG_LEUKOCYTE_TRANSENDOTHELIAL_MIGRATION
HALLMARK_MYC_TARGETS_V1
HALLMARK_MYC_TARGETS_V2
HALLMARK_OXIDATIVE_PHOSPHORYLATION
HALLMARK_MTORC1_SIGNALING
HALLMARK_GLYCOLYSIS
HALLMARK_UNFOLDED_PROTEIN_RESPONSE
HALLMARK_IL2_STAT5_SIGNALING
HALLMARK_DNA_REPAIR
HALLMARK_TNFA_SIGNALING_VIA_NFKB
HALLMARK_INTERFERON_GAMMA_RESPONSE
HALLMARK_ALLOGRAFT_REJECTION
HALLMARK_INTERFERON_ALPHA_RESPONSE
HALLMARK_HEME_METABOLISM
HALLMARK_MITOTIC_SPINDLE
REACTOME_RRNA_PROCESSING
REACTOME_EUKARYOTIC_TRANSLATION_ELONGATION
REACTOME_EUKARYOTIC_TRANSLATION_INITIATION
REACTOME_TRANSLATION
REACTOME_RESPONSE_OF_EIF2AK4_GCN2_TO_AMINO_ACID_DEFICIENCY
REACTOME_SELENOAMINO_ACID_METABOLISM
REACTOME_REGULATION_OF_EXPRESSION_OF_SLITS_AND_ROBOS
REACTOME_INFLUENZA_INFECTION
REACTOME_NONSENSE_MEDIATED_DECAY_NMD
REACTOME_SRP_DEPENDENT_COTRANSLATIONAL_PROTEIN_TARGETING_TO_MEMBRANE
REACTOME_INTERFERON_ALPHA_BETA_SIGNALING
REACTOME_INTERFERON_GAMMA_SIGNALING
REACTOME_PEROXISOMAL_LIPID_METABOLISM
REACTOME_GPVI_MEDIATED_ACTIVATION_CASCADE
REACTOME_GLYCOSPHINGOLIPID_METABOLISM
NES
-log10(padj)

Figure 3.3 T cells activated in infection and tumors exhibit unique transcriptional profiles hours after activation *in vivo*. a, Principal component analysis (PCA) of RNA-SEQ data comparing of naive (N; grey), and TCR_{TAG} differentiating during acute infection (green) and in tumors (blue) at 6, 12, and 24h post-transfer. Each symbol represents a single biological replicate. **b**, Heatmap showing differential gene expression between TCR_{TAG} in tumor versus infection versus naive at 6,12, and 24h from selected pathways (adjusted P <0.05, $|Log_2FC|$ >1), z-score normalization across rows. **c,** Gene set enrichment analysis (GSEA) of DEG up in tumor or effector for sets associated with later T cell differentiation (top), progenitor populations (middle), or inflammatory signaling (bottom). **d,** Gene set enrichment analysis (GSEA) of E versus N or T versus N at 6, 12, and 24h post transfer for top KEGG, HALLMARK, and REACTOME gene sets enriched at T6h. NES, normalized enrichment score.

and infection activated TCR_{TAG}. Furthermore, AP1 family TF (Jun, Fos, Bach) were enriched in both environments but with more rapid and transient kinetics in tumor activated T cells. As up to 21% of chromatin peaks were differentially accessible in tumors we sought to ask if hallmark epigenetic signatures associated with later T cell exhaustion can be detected early in dysfunctional T cell differentiation. Indeed, epigenetic tracks for the *Pdcd1* locus revealed that the -23 kb enhancer region exhibited DAC relative to quiescent naive levels. This was detected as early as 6h following TCR_{TAG} activation in tumors and was not detected during activation in effectors (**Figure 3.2e**). This coincides with the relative over induction of surface protein PD1 detected 6-12h following T cell activation in tumors. Taken together, T cells undergo impressive epigenetic remodeling incredibly rapidly, the degree and location of chromatin changes are similar between conditions, and environmental specific DAC can be detected early and include hallmarks of T cells previously observed at later stages of differentiation. These differences could be driven by unique TF patterns which would place NFAT induced dysfunction as beginning with antigen contact, not after prolonged TCR signaling.

Analysis of RNA-SEQ data revealed similar patterns of transcriptional divergence with significant amounts shared between activation conditions but with more variation between tumor and

infection activated T cells (**Figure 3.3a**). In line with observed protein expression, T-TCR_{TAG} induced greater expression of negative regulators of T cell function (*Rgs16*, *Pdcd1*, *Ptpn22*), and less expression of inflammatory associated genes (*Mx1*, *Isg15*), genes encoding cytokines/cytolytic mediators (*Ifng*, *Gzmb*, *Gzma*), and TF associated with functional differentiation (*Batf*, *Tbx21*)(Tsao, Kaminski et al. 2022) relative to E-TCR_{TAG}. T-TCR_{TAG} expressed more Bach2 and Id3, previously associated with memory phenotypes(Yang, Best et al. 2011) and restraint of effector differentiation (**Figure 3.3b**)(Roychoudhuri, Clever et al. 2016).

To compare transcriptional profiles more broadly between infection and tumor activated T cells, we turned to gene set enrichment analysis (GSEA) and compared gene sets enriched by differentially expressed genes (DEG) in each condition. Intriguingly, we found that we could detect some gene sets associated with day 5 or later dysfunction in both our tumor model (Philip, Fairchild et al. 2017) or models of chronic viral infection (Doering, Crawford et al. 2012). These findings indicate that transcriptional profiles of late dysfunctional T cells begin within hours of activation. Likewise, TCR_{TAG} activated in infection enriched for gene sets associated for late effector or memory (Doering, Crawford et al. 2012) (**Figure 3.3c**). As dysfunctional heterogeneity has been documented in tumors and chronic viral infection, we asked if we could detect signatures of progenitor exhausted T cells. While gene sets were enriched, they did not present a clear pattern for one condition or another indicating that little if any transcriptional profiles of progenitors from various studies (Joshi and Kaech 2008, Im, Hashimoto et al. 2016, Beltra, Manne et al. 2020) could be detected this early (**Figure 3.3c**). When compared to naive controls, both infection and tumor activated TCR_{TAG} exhibited very similar gene set enrichment in the KEGG, HALLMARK, and REACTOME gene set libraries. Many of these sets were related to anabolic

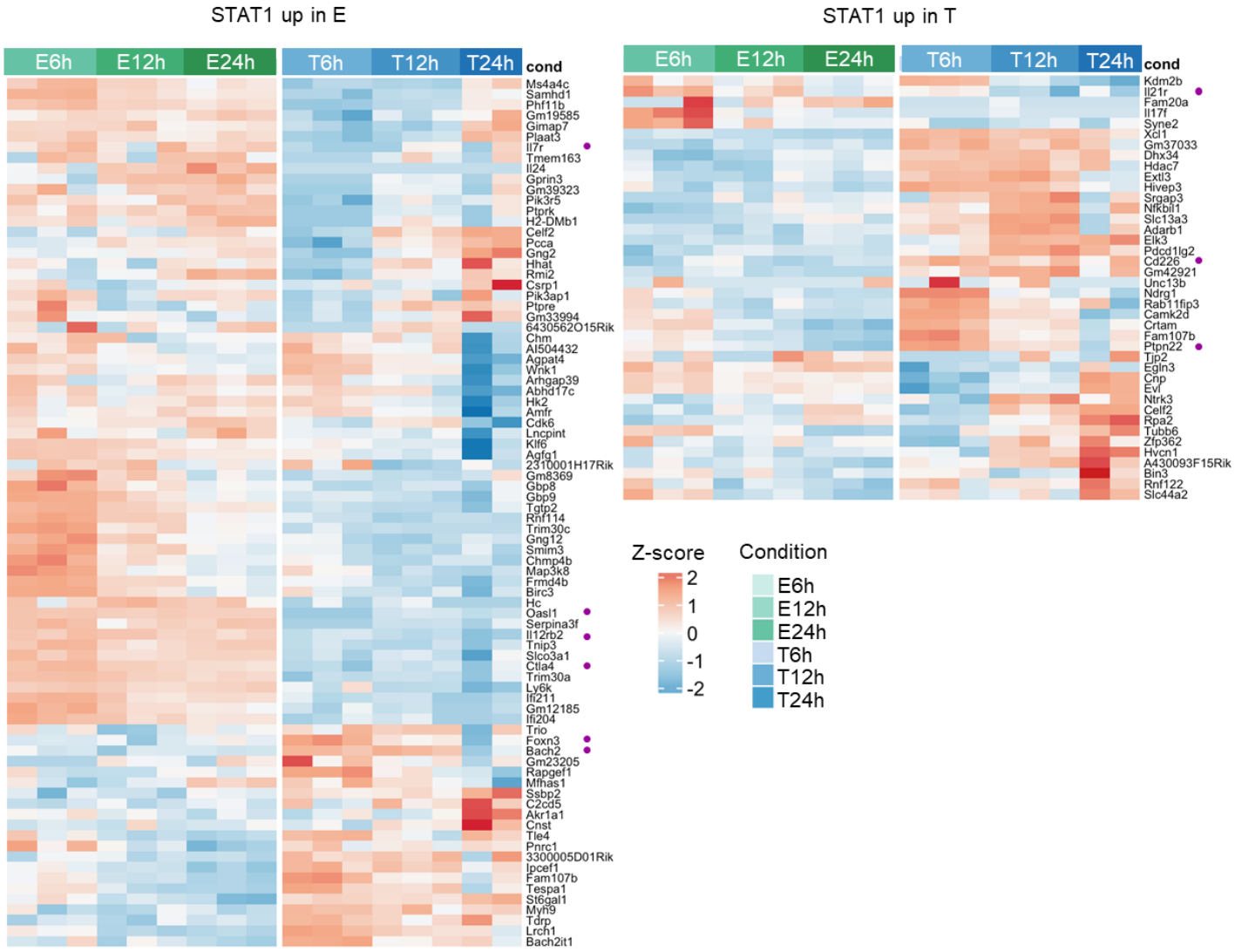

Figure 3.4 Differentially induced TF drive differential gene expression in early activated T cells. RNA expression of genes with enriched STAT1 binding motifs from effector (E) or tumor (T) conditions (cond) across timepoints. Heatmaps are Z-scores normalized across rows. Purple symbols denote genes of interest from each condition.

cellular processes such as MYC signaling, glycolysis, oxidative phosphorylation, nucleotide metabolism, transcription, and translation (**Figure 3.3d**). This was in contrast to naive T cells which were enriched for fatty acid oxidation pathways. Taken together with the comparable global chromatin remodeling and cell proliferation and expansion, this supports the notion that activation and differentiation is not impeded by nutrient availability or lack of resources in tumor

environments (Chisolm and Weinmann 2018).

In exploring how gene expression correlated with changes in chromatin accessibility, we looked at genes containing STAT1 motifs in DAC. There were more DEG with STAT1 motif-associated DAC in infection TCR_{TAG} compared to tumor activated TCR_{TAG}, and gene expression changes mainly correlated with the direction of the peak change (**Figure 3.4**). Genes induced by STAT1 included cytokine receptors such as *Il12rb* and inflammation-associated genes such as *Oasl1*. On the other hand, in tumor activated TCR_{TAG}, NFAT TF family motifs were enriched in DAC. NFAT has been previously described as a key driver of T cell dysfunction, thought to be induced by chronic/persistent antigen exposure (Martinez, Pereira et al. 2015, Philip, Fairchild et al. 2017); thus, our data suggests that NFAT hyperactivation occurs in tumors within a day of activation, even earlier than previously thought.

Pre-division tumor-induced chromatin remodeling is reinforced with time and tumor antigen exposure

We next asked whether pre-division dysfunction-associated chromatin accessibility changes are maintained or evolve as TCR_{TAG} undergo continued antigen exposure in progressing tumors. Therefore, we compared the 6-24h chromatin accessibility data with our previously published chromatin accessibility data from TCR_{TAG} isolated from pre-malignant and malignant liver tumors between 5-60d(Philip, Fairchild et al. 2017). In addition to pre-division time points, we sorted TCR_{TAG} at 5 days (T5d) and 10 days (T10d) after transfer into late tumor-bearing ASTxAlb-Cre mice and carried out ATAC-SEQ. PCA showed that TST clustered into three groups based on the time of tumor exposure: early (6-12h), intermediate (5-7d), and late (14-60+d) (**Figure 3.5a**).

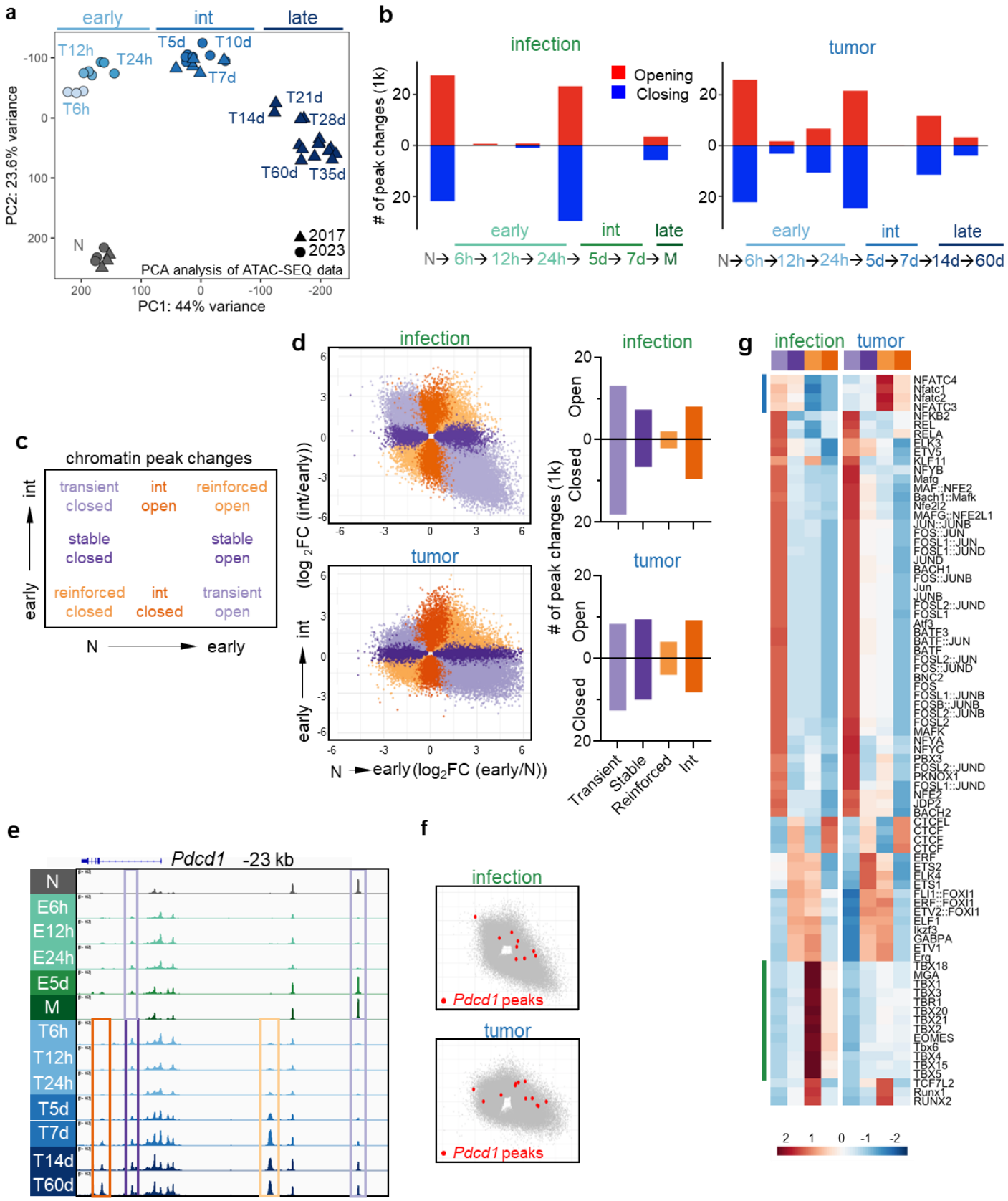
a
early
int
late
T12h
T24h
T5d
T10d
T7d
T6h
T21d
T14d
T28d
T60d
T35d
N
▲2017
●2023
PCA analysis of ATAC-SEQ data
PC2: 23.6% variance
PC1: 44% variance
b
infection
tumor
Opening
Closing
# of peak changes (1k)
early
int
late
N→ 6h→ 12h→ 24h→ 5d→ 7d→ M
N→6h→12h→24h→5d→7d→14d→60d
c
chromatin peak changes
transient closed
int open
reinforced open
stable closed
stable open
reinforced closed
int closed
transient open
int
early
N
early
d
infection
tumor
(log2FC (int/early))
N →early (log2FC (early/N))
# of peak changes (1k)
Open
Closed
Transient
Stable
Reinforced
Int
g
infection
tumor
NFATC4
Nfatc1
Nfatc2
NFATC3
NFKB2
REL
RELA
ELK3
ETV5
KLF11
NFYB
Mafg
MAF::NFE2
Bach1::Mafk
Nfe2l2
MAFG::NFE2L1
JUN::JUNB
FOS::JUN
FOSL1::JUN
FOSL1::JUND
JUND
BACH1
FOS::JUNB
Jun
JUNB
FOSL2::JUND
FOSL1
Atf3
BATF3
BATF::JUN
BATF
FOSL2::JUN
FOS::JUND
BNC2
FOS
FOSL1::JUNB
FOSB::JUNB
FOSL2::JUNB
FOSL2
MAFK
NFYA
NFYC
PBX3
FOSL2::JUND
PKNOX1
FOSL1::JUND
NFE2
JDP2
BACH2
CTCFL
CTCF
CTCF
CTCF
ERF
ETS2
ELK4
ETS1
FLI1::FOXI1
ERF::FOXI1
ETV2::FOXI1
ELF1
Ikzf3
GABPA
ETV1
Elf3
TBX18
MGA
TBX1
TBX3
TBR1
TBX20
TBX21
TBX2
EOMES
Tbx6
TBX4
TBX15
TBX5
TCF7L2
Runx1
RUNX2
2 1 0 -1 -2
e
Pdcd1 -23 kb
N
E6h
E12h
E24h
E5d
M
T6h
T12h
T24h
T5d
T7d
T14d
T60d
f
infection
Pdcd1 peaks
tumor
Pdcd1 peaks

Figure 3.5 Pre-division tumor-induced TST chromatin remodeling is reinforced with time and tumor antigen exposure. a, PCA of chromatin accessibility of naive TCR_{TAG} (N) and after 6, 12h (early), 5d, 7d (intermediate; int), 14d, 21d, 28d, 35d, and 60d+ (late) in liver tumors. Where circles represent current samples (predivisions-10d) and triangles represent previously published dataset (5d-60d)(Philip, Fairchild et al. 2017). **b**, Number of chromatin accessibility peak changes during CD8 T cell differentiation in tumors (upper) and infection (lower) across each transition (opening peaks, red; closing peaks, blue) *FDR*<0.05). **c**, Legend corresponding to part d identifying chromatin accessibility peak quadrants in scatterplots of early transition peak accessibility changes (x-axis) versus later transition peak changes (y-axis)**. d,** Upper panel shows chromatin peak accessibility changes during naive (N) → early (T6h) transition (log2FC T6h/N) versus early → int (T5d) transition (log2FC T5d/T12h). Lower panel shows chromatin peak accessibility changes during N→ early (E6h) transition (log2FC E6h/N) versus early → int (E5d) transition (log2FC E5d/E24h). Each point represents an individual DAC peak colored according to the legend in c. To the right are shown corresponding bar plots showing the number of chromatin peaks in each quadrant with opening peaks above the axis and closing peaks below the axis (includes DAC with adjusted *P*<0.05 for either comparison). **e**, Chromatin accessibility profile across the *Pdcd1* locus for TCR_{TAG} differentiating during infection and in liver tumors. Boxes highlight differentially accessible peaks in tumor and/or infection colored as in c. The exhaustion-associated -23kb enhancer peak in *Pdcd1* is highlighted in light orange denoting a chromatin peak whose opening is reinforced during tumor progression. Light purple boxes highlight transiently closed and open peaks found in TCR_{TAG} during infection, while for TCR_{TAG} in tumors, the dark purple box highlights a peak that opens and is maintained at later timepoints, and the dark orange boxes highlight peaks that open early and increase in accessibility at later timepoints. **f**, Scatterplot highlighting individual *Pdcd1* peaks (red) in TCR_{TAG} in tumors and infected mice relative to the overall pattern of chromatin peak changes (grey). **g,** Motif aNAlysis with Lisa (monaLisa) showing enriched transcription factor (TF) motifs represented in each peak classification for infection activated and tumor activated T cells between the early (N→6h) and intermediate (24h→5d) chromatin transition.

Newly generated T5d were similar in chromatin accessibility to T5d previously isolated from pre-malignant liver lesions, whereas T10d clustered within the intermediate samples (**Figure 3.5a**). Strikingly, in assessing TCR_{TAG} chromatin remodeling from 0h-60d, the largest number of changes occurred by 6h, with a second smaller round of peak changes between 24h-5d, and a third round between 7-14d, after which very few changes occurred (**Figure 3.5b, Figure 3.6a, b**). TCR_{TAG} in the setting of acute infection also had many early peak changes within 6h and a second round of peak changes between 24h and 5d. However, in contrast to TST in tumors that underwent a third wave of chromatin remodeling, likely driven by continued tumor antigen exposure, few peak changes occurred after E5d (**Figure 3.5b, Figure 3.6b**), demonstrating that the memory-associated chromatin state was largely established early upon pathogen/antigen clearance.

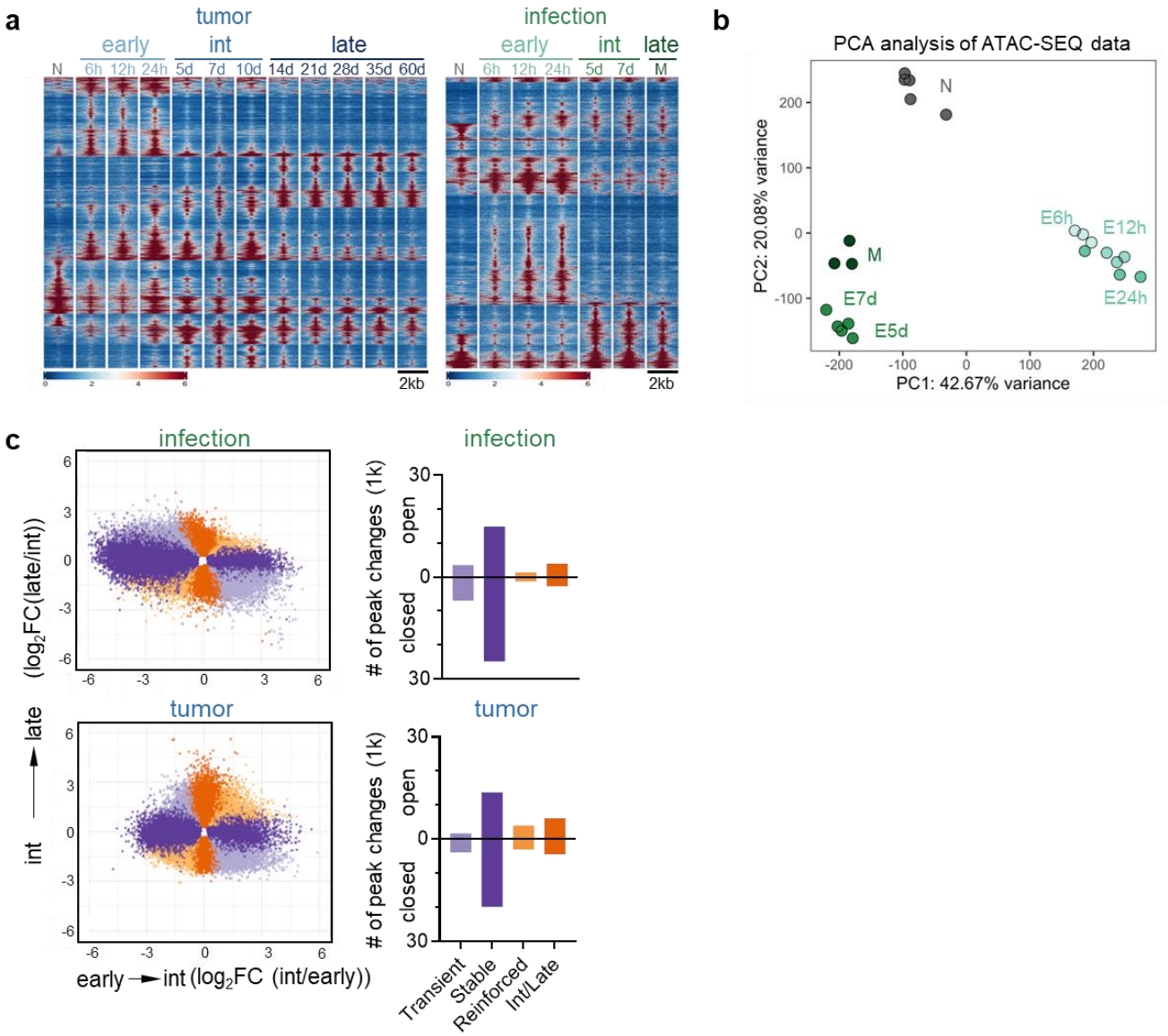

Figure 3.6 Chromatin remodeling is reinforced with time with relatively few changes occurring late. **a,** Chromatin accessibility heatmap showing naive (N) and TCR_{TAG} from 6h to 60+d in liver tumors of ASTxAlb-Cre mice (left) and 6h to 60+d memory (M) in LM_{TAG}-infected mice (right). Each row represents one of 39,225 (left) or 45,124 (right) differentially accessible peaks (DAC) (differentially accessible between at least one sequential timepoint comparison; adjusted P <0.05, $|Log_2FC|$ >1.5) displayed over 2kb window centered on the peak summit. Scale units are RPGC normalized to 1x sequencing depth for 20 bp bins with blue indicating closed chromatin and red open chromatin. Peaks are clustered by k-means (k=6). **b,** PCA comparing chromatin accessibility of TCR_{TAG} from 6h to M during infection. Each symbol represents a single biological replicate. **c,** Upper panel shows chromatin peak accessibility changes for early (T12h) → intermediate (T5d) transition (log2FC T5d/12h) versus int (T7d) → late (T14d) transition (log2FC T14d/T7d) (upper). Lower panel shows chromatin peak accessibility changes for early (E24h) → int (E5d) transition (log2FC E5d/E24h) versus int (E7d) → late (M) transition (log2FC M/E7d). Each point represents an individual DAC peak colored according to the scheme in Fig. 4c. To the right are shown corresponding bar plots showing the number of chromatin peaks in each sector with opening peaks above the axis and closing peaks below the axis (includes DAC with adjusted P<0.05 for either comparison).

We next compared how each individual chromatin peak changed over time by plotting the fold-change of each peak's accessibility during the early transition (naive (N) to 6h) versus fold-change during the intermediate (int) transition (24h to 5d) (**Figure 3.5c, d**). Thus, a peak in the "reinforced open" quadrant in the scheme in Fig. 6c had an increase in accessibility between N and 6h with a further increase in accessibility between 24h and 5d. In contrast, a peak in the "stable closed" quadrant had an early decrease in accessibility and remained "closed" during the later transition. This analysis revealed that 36% of pre-division remodeled chromatin peaks in TST remained stable (19% closed, 17% open) with continued tumor/antigen exposure, with additional peaks getting reinforced (13%) or opening at the intermediate transition (int, 16%) (**Figure 3.5c, d and Figure 3.6c lower)**. This was in marked contrast with differentiation during infection, in which many early chromatin accessibility changes were transient (51%) or newly occurring between 24h and 5d (int 19%) (**Figure 3.5c, d and Figure 3.6c upper**). The *Pdcd1* locus exemplifies these patterns, with peak changes maintained and reinforced with time in tumors and transient during acute infection-induced effector/memory differentiation (**Figure 3.5f**), consistent with its transient surface expression (Figure 1.2c). The dysfunction/exhausted-associated -23 kb *Pdcd1* enhancer peak opened early in tumors and had reinforced opening at later time points, while the peak at +4.5kb, transiently opened during infection, remained stably opened in tumors, and the peak at +10kb opened only at the intermediate time point (int open) in tumors (**Figure 3.5e, f**). To identify the TF that drove specific transitional peak changes during effector and TST differentiation, we carried out Motif aNAlysis with Lisa (monaLisa)(Machlab, Burger et al. 2022). While TF enrichment in the transiently opened peaks (light purple) was largely similar between E- and T-TCR_{TAG}, NFAT TF family motifs were particularly enriched in peaks with reinforced and later/intermediate opening in tumors while mainly in transient peaks during infection (**Figure**

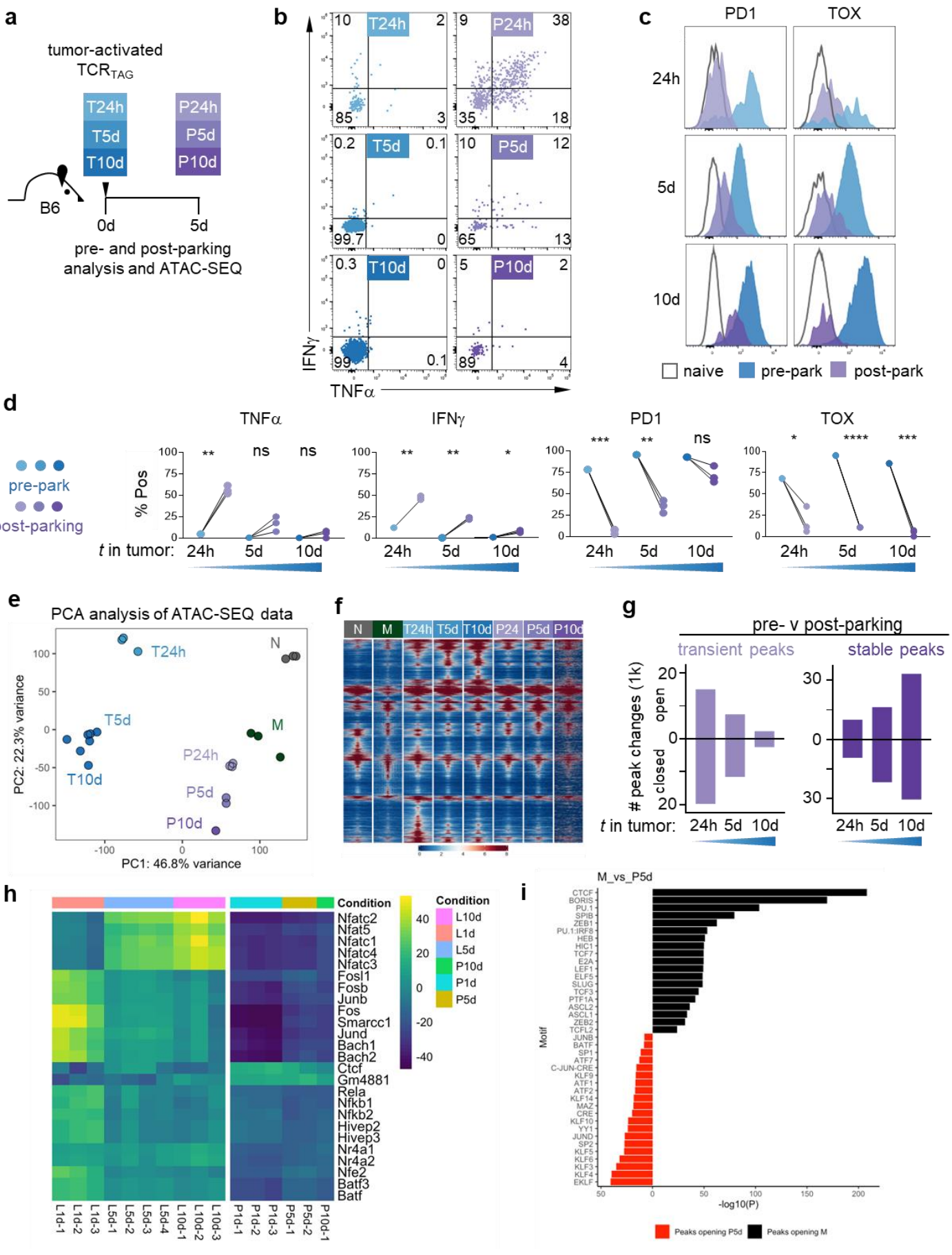
a
tumor-activated
TCR$_{TAG}$
T24h
T5d
T10d
P24h
P5d
P10d
B6
0d
5d
pre- and post-parking
analysis and ATAC-SEQ
b
T24h
P24h
T5d
P5d
T10d
P10d
IFNγ
TNFα
c
PD1
TOX
24h
5d
10d
naive
pre-park
post-park
d
pre-park
post-parking
TNFα
IFNγ
PD1
TOX
% Pos
t in tumor:
24h
5d
10d
e
PCA analysis of ATAC-SEQ data
PC2: 22.3% variance
PC1: 46.8% variance
N
M
f
g
pre- v post-parking
transient peaks
stable peaks
peak changes (1k)
open
closed
h
Condition
L10d
L1d
L5d
P10d
P1d
P5d
Nfatc2
Nfat5
Nfatc1
Nfatc4
Nfatc3
Fosl1
Fosb
Junb
Fos
Smarcc1
Jund
Bach1
Bach2
Ctcf
Gm4881
Rela
Nfkb1
Nfkb2
Hivep2
Hivep3
Nr4a1
Nr4a2
Nfe2
Batf3
Batf
L1d-1
L1d-2
L1d-3
L5d-1
L5d-2
L5d-3
L5d-4
L10d-1
L10d-2
L10d-3
P1d-1
P1d-2
P1d-3
P5d-1
P5d-2
P10d-1
i
M_vs_P5d
Motif
-log10(P)
Peaks opening P5d
Peaks opening M

Figure 3.7 Duration of tumor antigen exposure determines dysfunction stability and imprinting. a, Experimental scheme: TCR_{TAG} activated in tumors for 1, 5, or 10d were isolated from tumors, transferred to tumor-free B6 mice, parked for 5d, and then isolated from secondary hosts and analyzed. **b,** Live $CD8^+$ $Thy1.1^+$ TCR_{TAG} analyzed pre-park from tumors (upper) and after 5d parking (lower). TNFα and IFNγ production was measured following 4h *ex vivo* TAG peptide stim. Inset numbers represent percentage of population within each gate. Gates set based on no peptide stimulation controls. **c,** Histogram plots of pre-park tumor activated TCR_{TAG} (blue) and concatenated post-parking samples (purple), with naive (N; grey) for comparison. TCR_{TAG} activated in tumors for 24h (upper), 5d (middle), and 10d (lower). **d,** Summary plots show the percentage positive for TNFα, IFNγ, PD1, and TOX pre-park (for pooled donor TCR_{TAG} from 3-4 mice) and following 5d parking. **e,** Principal component analysis (PCA) comparing peak accessibility of naive (N; grey), memory, (M; green), TCR_{TAG} activated in tumor for 24h (T24h), 5d (T5d), 10d (T10d) pre parking (blue) and post parking (P24h, P5d, P10d) (purple) by the top $25x10^3$ variable peaks. Each symbol represents a single biological replicate. **f,** Chromatin accessibility heatmap showing naive (N) and TCR_{TAG} activated in tumors for 24h, 5d, and 10d pre- and post-parking. Each row represents one of 285,981 differentially accessible peaks (DAC) (differentially accessible between at least one sequential timepoint comparison; adjusted P <0.05, $|Log_2FC|$ >1.5) displayed over 2kb window centered on the peak summit. **g,** Number of chromatin peaks that are transient or stable post-parking relative to pre-parking. **h,** Heatmap of chromVAR computed deviations z-score for the top 25 most variable transcription factor (TF) motifs across TCR_{TAG} pre- and post-parking. **i,** Paired comparison of enriched TF motifs by HOMER between M and post-park 5d tumor activated (P5d) TCR_{TAG}. *P<0.05, **P<0.01, ***P<0.001, ****P<0.0001, ns=not significant, determined for change from baseline by one sample Student's t-test. Experiments were repeated twice with n=3-4 mice per group.

3.5g), consistent with TCR_{TAG} receiving persistent antigen exposure in tumors but only transient exposure in acute infection. In contrast, T-box TF family motifs, including those of TBET (TBX21) and EOMES, were more highly enriched in peaks that opened early and were predominantly reinforced during infection, but less so in tumors (**Figure 3.5g**), consistent with the role of these TF in facilitating functional effector formation during acute infection and functional memory populations following pathogen/antigen clearance(Pearce, Mullen et al. 2003, Sullivan, Juedes et al. 2003, Intlekofer, Takemoto et al. 2005, Intlekofer, Banerjee et al. 2008).

Duration of tumor antigen exposure determines dysfunction stability and imprinting

Given the observation that early chromatin accessibility changes in TCR_{TAG} were stabilized and/or reinforced with increased tumor/antigen exposure, we next asked to what extent TCR_{TAG} removed from tumors at different time points and transferred to tumor-free hosts would retain the functional, immunophenotypic, and epigenetic hallmarks of dysfunction. TCR_{TAG} were re-isolated from liver tumors after 1, 5, or 10 days (T24h, T5d, and T10d) and parked in tumor-free B6 mice (P24h, P5d, P10d) for 5 days prior to analysis (**Figure 3.7a**). In parallel with functional and immunophenotypic analysis, we carried out ATAC-SEQ on the pre- and post-parking samples. Prior to transfer, tumor-activated TCR_{TAG} failed to make cytokine (**Figure 3.7b**). After 5 days of parking, P24h had uniformly downregulated PD1 (**Figure 3.7c**), yet ~35-40% remained unable to produce TNFα or IFNγ (**Figure 3.7b, d**). With longer primary tumor exposure, more TCR_{TAG} had "imprinted" effector function loss, with nearly all P10d failing to make effector cytokine and also retaining PD1 expression (**Figure 3.7b, c**).

Heterogeneity has been described for dysfunctional/exhausted T cells, with more stem-like TCF1+ dysfunctional/exhausted T cells better able to regain the ability to regain function following immune checkpoint blockade(He, Xing et al. 2016, Im, Hashimoto et al. 2016, Utzschneider, Charmoy et al. 2016) (reviewed in (Philip and Schietinger 2021)). Therefore, we examined TCR_{TAG} expression of stem/progenitor vs terminal differentiation markers at early time points, intermediate, and late time points (**Figure 3.8a**). At 36h post-transfer into ASTxAlb-Cre mice, undivided and early division TCR_{TAG} in the spleens of ASTxAlb-Cre mice expressed TCF1 at the same or higher level as naive TCR_{TAG}, while TCR_{TAG} in the liver had slightly lower TCF1

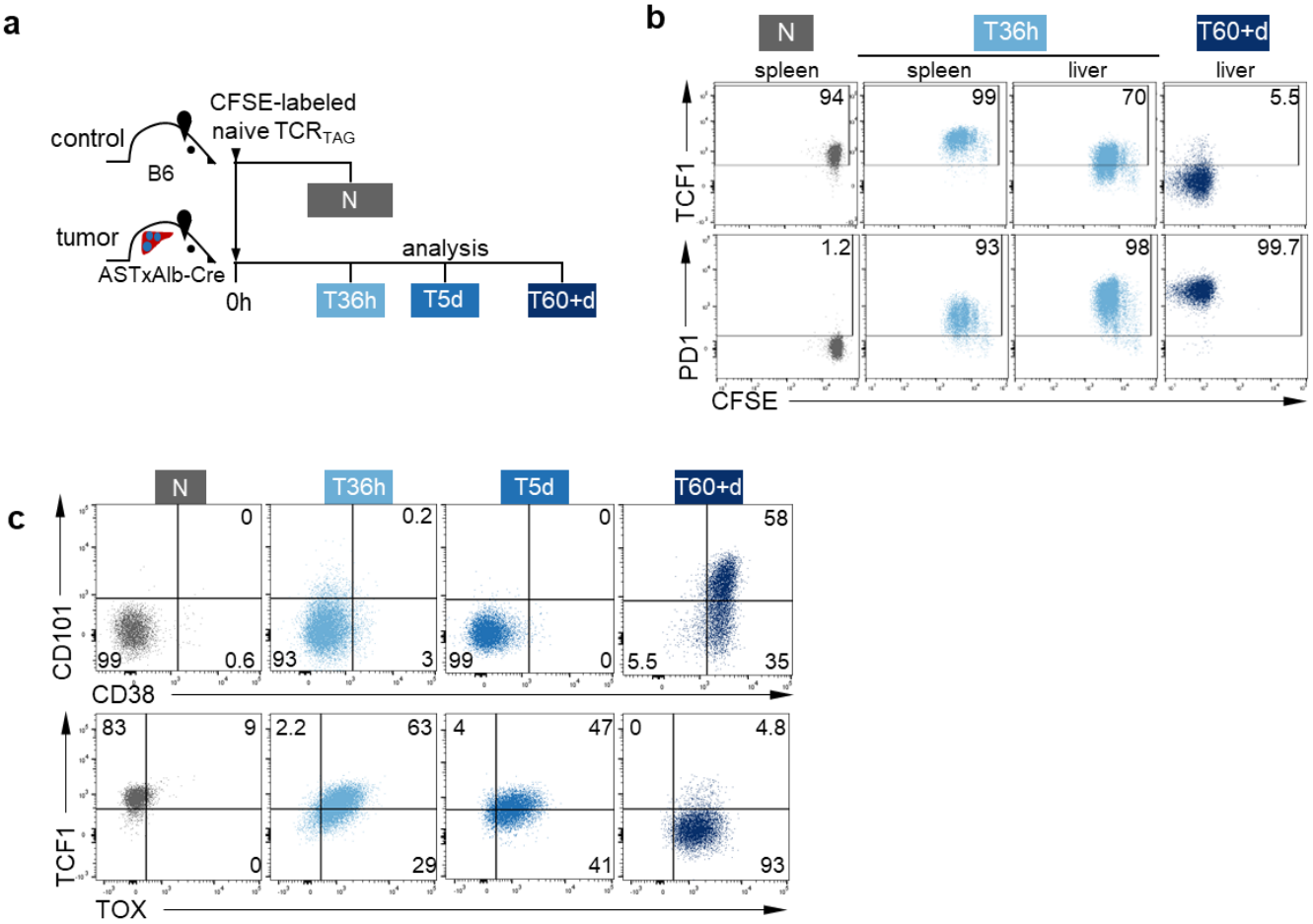

Figure 3.8 Tumor activated T cells do not exhibit progenitor subpopulations. a, Experimental scheme: CFSE-labeled naive TCR_{TAG} (Thy1.1) were adoptively transferred into B6 (Thy1.2) or ASTxAlb-Cre mice (Thy1.2) bearing late-stage liver tumors. TCR_{TAG} were re-isolated at 36 hours (h), 5 days, and and 60 days (d) from infected spleen or tumor livers for flow cytometric analysis (Naive *in vivo* (N; grey); Tumor (T; blue)). **b,** Dot plots of TCF1 and PD1 expression by CFSE dilution across timepoints. **c,** Dot plot comparing CD38 and CD101 (top) or TOX and TCF1 (bottom) across timepoints. Gates set based on N control with number representing percentage of population within each gate. Plots are concatenated from 3-4 samples. Experiments repeated twice.

expression than in the spleen, but still comparable to naive (**Figure 3.8b**). In contrast, T60+d TCR_{TAG} in the liver had markedly downregulated TCF1 (**Figure 3.8b**). To look for evidence of bimodal stem/progenitor or terminally-differentiated populations, we examined concurrent expression of CD38 and CD101, surface markers that predict whether TCR_{TAG} retain the ability to regain function upon removal from tumor and cytokine treatment (Philip, Fairchild et al. 2017).

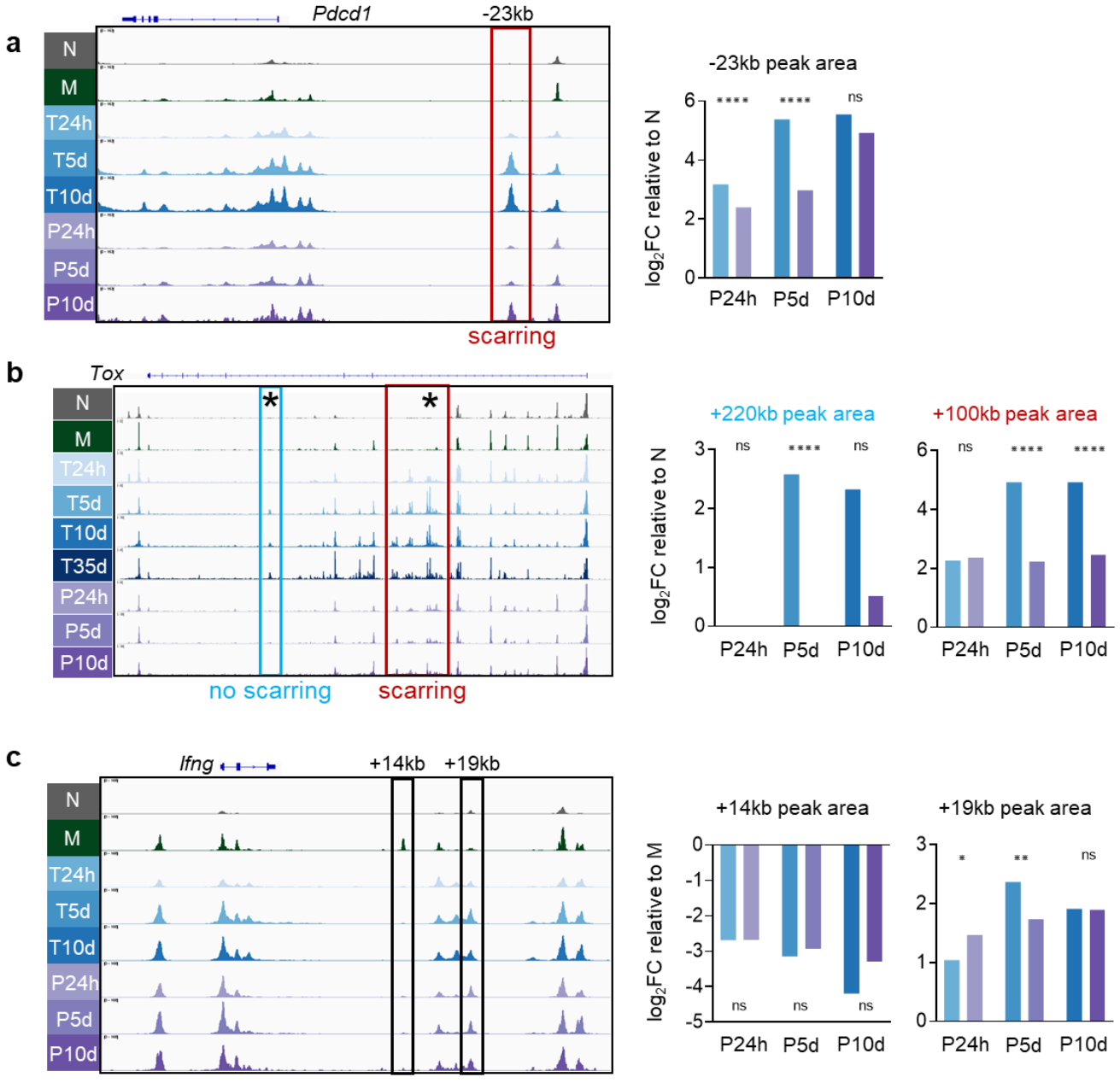

Figure 3.9 ATAC-SEQ tracks of genes of interest. a, Chromatin accessibility profiles across selected gene loci for TCR_{TAG} activated in tumor for 24h (T24h), 5d (T5d), 10d (T10d) pre-parking (blue) and post-parking (P24h, P5d, P10d) (purple) with naive (grey) and memory (green). **a,** *Pdcd1* gene locus with -23 kb enhancer region boxed in red. Summary plot (right) of -23 kb enhancer region peak area pre- (blue) and post-park (purple) relative to naive. **b,** *Tox* locus with blue box representing region of no epigenetic scarring and red box showing region demonstrating scarring. Star denotes representative +100 kb peak from scar region used for quantification on right. Summary plot (right) of +220kb and +100 kb peak area pre- (blue) and post-park (purple) relative to naïve. **c,** *Ifng* locus with black boxes denoting +14kb peak open in memory but not in pre- or post-parking samples, and +19kb open in both pre- and post-parking samples. Summary plot of +14kb and +19 kb peak area pre- (blue) and post-park (purple) relative to memory. *P<0.05, **P<0.01, ****P<0.0001, ns=not significant, determined between pre- and post-parking peak area by the Wald test.

TST remained low for both CD38 and CD101, in contrast to T60+d, which were CD38+ and heterogeneous for CD101 expression (**Figure 3.8c**). Early and intermediate T-TCR_{TAG} also showed homogeneous expression of TCF1 and TOX, becoming $TCF1^{low}$ and TOX^{high} at later time points (**Figure 3.8c**). Thus, the heterogeneity we observed in effector cytokine rescue observed in TST removed from tumors and parked in tumor-free hosts must result from factors other than expression of stem/progenitor markers/TF.

When we compared chromatin accessibility, we found that the post-parking samples had chromatin accessibility patterns intermediate between memory TCR_{TAG} and TCR_{TAG} in liver tumors (**Figure 3.7e, f**). We used a similar scatterplot analysis as in Fig. 6c to characterize peak changes pre- and post-parking, and while TCR_{TAG} only exposed for 24h to tumor had a large number of transient peak changes and a small number of stable peaks after parking, with increasing tumor exposure, the number of transient peaks decreased while the number of stable peaks increased (**Figure 3.7g**). Correspondingly, chromatin accessibility at the -23kb enhancer in post-parking TCR_{TAG} increased with longer initial tumor exposure (**Figure 3.9a**). In contrast, TOX expression was uniformly lost after TCR_{TAG} removal from tumor, even after 10d of initial tumor exposure (**Figure 3.9b**), suggesting that TOX expression is dependent on antigen/TCR stimulation or requires even longer tumor exposure to become imprinted. Recent studies have shown that later exhausted T cells (>30d exposure) from humans and murine models of chronic viral infection retain TOX expression together with exhaustion-associated chromatin peaks ("epigenetic scarring") after transfer to antigen-free hosts or viral cure with direct acting anti-viral therapy (Abdel-Hakeem, Manne et al. 2021, Hensel, Gu et al. 2021, Yates, Tonnerre et al. 2021). While we observed evidence of "epigenetic scarring" in some *Tox* locus peaks, other peaks, particularly peaks that appeared during

the intermediate and late time points, were not retained in post-parking TCR_{TAG} (**Figure 3.9b**). The *Ifng* locus also exhibited DAC on chromatin tracks. For example, a +14 kb peak uniquely gained in memory populations was absent pre- and post-parking tumor groups. This peak has shown putative binding to TBET and could further highlight the long-term detriment of lack of inflammation in the tumor environment. Conversely, a +19 kb peak is over induced in pre-parking and maintained in post-parking tumor activated TCR_{TAG} and could represent an example of a negative regulator peak (**Figure 3.9c**).

Given the progressive imprinting of dysfunctional hallmarks with increasing tumor exposure, we asked how TF activity changed in pre- and post-parking samples. Open chromatin peaks in post-parking TCR_{TAG} showed enrichment for binding motifs for the transcription factory CTCF, which is thought to regulate the folding of genomic DNA into loops. This finding is intriguing in light of recent studies showing that CTCF-mediated genome reorganization promotes CD8 T effector differentiation (Liu, Zhu et al. 2023). NFAT TF family enrichment, which increased in intermediate TCR_{TAG}, was lost upon removal from tumors (**Figure 2.7h**), suggesting that NFAT-mediated DAC requires continued TCR signaling. We hypothesize that antigen withdrawal and a resultant quiescent state was in part responsible for the increased similarity between post-parking and memory TCR_{TAG}. However, though memory TCR_{TAG} produce high levels of TNFα and IFNγ upon antigen restimulation (Schietinger, Philip et al. 2016, Philip, Fairchild et al. 2017)), the post-parking TCR_{TAG} largely failed to do so (**Figure 2.8b**). We found that KLF family motifs were predominant in accessible chromatin peaks in non-functional post-parking TCR_{TAG} (**Figure 2.7i**), consistent with previously described roles in T cell quiescence and functional restraint (Yamada, Park et al. 2009, Cao, Sun et al. 2010). In contrast, accessible chromatin peaks in functional

memory enriched for memory-associated TCF1 and ZEB family (Omilusik, Best et al. 2015, Guan, Dominguez et al. 2018, Scott and Omilusik 2019) members (**Figure 2.7i).** Taken together, these data suggest that while removing T cells from the tumor at early and intermediate time points can reverse TCR-driven inhibitory signals, T cells activated in tumors failed to receive the necessary signaling to induce functional/memory-defining TF.

Discussion

Here we show that *in vivo* activated T cells in both functional and dysfunctional environments begin large scale chromatin remodeling pre cell division, which is in line with rapid onset first observed with *in vitro* antibody stimulation methods (Yukawa, Jagannathan et al. 2020). This counters the notion that cell division is required to begin epigenetic remodeling in CD8 T cells. Globally, this also suggests that CD8 T cells initiate differentiation in general immediately following contact with cognate antigen, integrating TCR and environmental signals. Intriguingly, epigenetic remodeling that occurred prior to cell division was not incrementally increased with time but exhibited the most changes just hours after receiving TCR signaling.

Significant portions of epigenetic remodeling were stable or reinforced with time, nearly 50% in total, with continued T cell differentiation in tumors. Unsurprisingly, additional TCR signaling with antigen contact facilitates more chromatin remodeling relative to acute infection where antigen is cleared. However, these data suggest that significant portions of epigenetic signatures originate from pioneer chromatin remodeling that occurred prior to cell division, with large quantities of pioneer remodeling shared between functional and dysfunctional differentiation. Thus, “dysfunctional” or “exhausted” epigenetic signatures, similar to PD1(Ahn, Araki et al. 2018)

and TOX expression (Scott, Dundar et al. 2019, Soerens, Kunzli et al. 2023), are likely present in functional T cell differentiation and are aberrantly induced to prevent immunopathology or to facilitate long term persistence.

While the differentiation to the functional or dysfunctional state was initiated rapidly prior to cell division, continuous TCR signaling stabilized and reinforced initial dysfunctional epigenetic programs. These findings together with our previous work (Philip, Fairchild et al. 2017, Scott, Dundar et al. 2019) demonstrate that the T cell dysfunctional state is composed of different modules (loss of effector function, upregulation of inhibitory receptors, proliferative capacity), which are regulated independently. This was borne out when we tested the degree to which early TST dysfunction was "imprinted"—that is retained upon removal from the tumor and transfer into tumor-free hosts. Loss of effector function is imprinted in a significant fraction of dysfunctional TST after only brief tumor exposure, while PD1 expression requires more prolonged tumor exposure and epigenetic reinforcement to become fixed. These imprinted dysfunctional phenotypes coincided with increased stability global dysfunctional chromatin signature. Functional heterogeneity following brief exposure of TST to tumors, could not be explained by presence of progenitor or terminal exhausted populations observed in early timepoints of chronic LCMV infections (Utzschneider, Gabriel et al. 2020) as expression of surface markers or TF, such as TCF1 were uniform in our system. It is possible that the relative lack of inflammation in tumors with higher antigen burden produces unique differentiation patterns relative to those in models of chronic viral infection.

While our findings mirror functional and epigenetic findings of T cells days after differentiating

in chronic versus acute LCMV (Utzschneider, Gabriel et al. 2020), the degree and acuity of dysfunctional differentiation is much more severe in tumors. In fact, TST exposed to tumors for 5-10 days exhibit similar stability in cytokine dysfunction, and PD1 expression as later exhausted T cells (>30d exposure) from humans and murine models of chronic viral infection (Abdel-Hakeem, Manne et al. 2021, Hensel, Gu et al. 2021, Yates, Tonnerre et al. 2021). Dysfunctional TST from our studies and later exhausted T cells from chronic viral models failed to regain cytokine function and maintained exhaustion-associated chromatin peaks after transfer to antigen-free hosts or viral cure with direct acting anti-viral therapy (Abdel-Hakeem, Manne et al. 2021, Hensel, Gu et al. 2021, Yates, Tonnerre et al. 2021). Interestingly, expression of TOX, a key dysfunction-associated TF found to be stabilized in later exhausted T cells during chronic viral infection, was not imprinted even after 10d of tumor exposure, suggesting that TOX expression is dependent on antigen/TCR stimulation or requires even longer tumor exposure to become imprinted. Taken together, tumor induced dysfunctional differentiation is a dynamic process that begins hours after antigen encounter in tumors.

CHAPTER 4: TARGETING EARLY SIGNALING PATHWAYS TO PRESERVE T CELL FUNCTION IN TUMORS

Introduction

In chapter 3 we found that NFAT enrichment is present in tumor activated T cells at the onset of T cell activation, not requiring time to accumulate over days to weeks. Continuous TCR signaling in the context of low or absent inflammation has been implicated in driving dysfunction in tumor models and the imbalance of NFAT and AP1 has been implicated in dysfunction in both tumors and chronic viral infections (Macian, Lopez-Rodriguez et al. 2001, Martinez, Pereira et al. 2015, Mognol, Spreafico et al. 2017). Furthermore, STAT signaling remains a target of interest for reinvigorating dysfunctional T cells (Codarri Deak, Nicolini et al. 2022, Tichet, Wullschleger et al. 2023) and preserving T cell function for adoptive cell therapies (Lin, Rayman et al. 2019) in patients with cancer. As we identified NFAT hyperactivation and lack of STAT signaling in tumor activated T cells, we sought to preserve function of effectors following transfer into tumor bearing mice by targeting these pathways.

Modulating NFAT hyperactivation and inflammation to preserve CD8 T cell function in tumors

To attempt downregulation of NFAT signaling in tumor activated T cells we utilized the calcineurin inhibitor, FK506, to mitigate NFAT dephosphorylation and translocation to the nucleus. We performed FK506 treatments prior to and after adoptive transfer of TCR_{TAG} T cells into tumor bearing hosts (**Figure 4.1a**). E5d TCR_{TAG} were generated as described in chapter 2 and adoptively transferred into normal saline (NS) or FK506 treated animals and harvested 2 days later

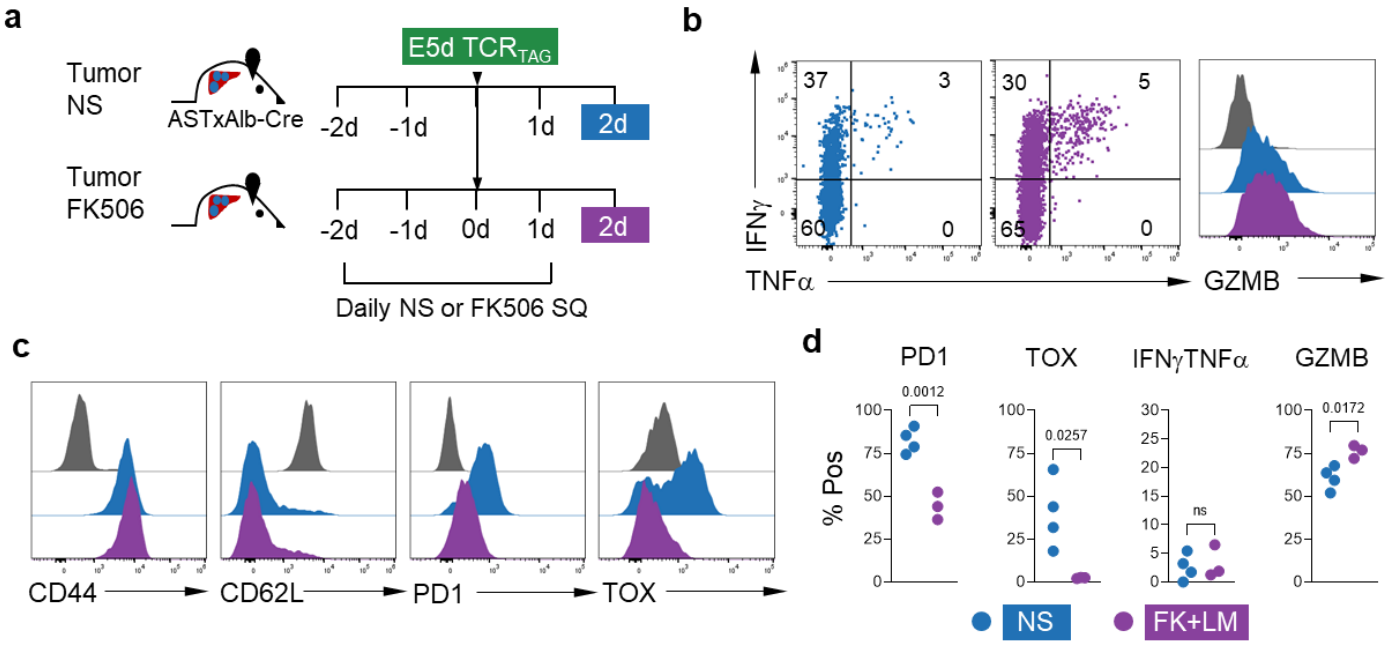

Figure 4.1 FK506 treatment of effector T cells preserves cytolytic function but not cytokines. **a,** Experimental scheme: LM_{TAG} generated day 5 effector TCR_{TAG} (Thy1.1) were adoptively transferred into ASTxAlb-Cre mice (Thy1.2) bearing late-stage liver tumors treated daily SQ with NS or treated with 10 mg/kg FK506. Donor mice were treated FK506 or NS for 2d prior to transfer. Lymphocytes were re-isolated at day 2 from tumor livers for analysis by flow cytometry. **b,** TCR_{TAG} T cells stained for surface CD44, CD62L, PD1, and intracellular TOX. **c,** TCR_{TAG} intracellular IFNγ and TNFα after 4-hour *ex vivo* TAG peptide stimulation or intracellular GZMB expression *ex vivo*. **d,** Summary plots show percentage of PD1, TOX, IFNγTNFα double positive, and GZMB positive. Each symbol represents an individual mouse. Histograms and dot plots are concatenations from 3-4 biologic replicates. Experiments were repeated twice with n=3-4 per group. Statistical significance calculated using unpaired two-tailed t-test.

(**Figure 4.1a**). We found that FK506 treatment did not produce a measurable increase in cytokine production with both the NS and FK506 treated groups mostly dysfunctional at this timepoint. Intriguingly, while FK506 treated groups trended toward a slightly higher double positive cytokine profile, they exhibited less IFNγ single positive and more cytokine double negative populations than NS treated controls (**Figure 4.1b, d**). Furthermore, FK506 treated groups did exhibit mild but significant gains in GZMB in both expression and percentage of population indicating different

functional readouts are differentially regulated (**Figure 4.1b, d**). The general surface immunophenotype as judged by CD44 and CD62L was comparable between the two groups however the FK506 treated group exhibited significantly less PD1 expression and percentage positive of the population (**Figure 4.1c, d**). Furthermore, TF analysis revealed that TOX expression was drastically reduced to naive levels (**Figure 4.1c, d**). These data are in line with the established role of NFAT signaling in driving both PD1 (Ahn, Araki et al. 2018) and TOX (Khan, Giles et al. 2019) in early activation. However, these data also underscore that despite rescue of these markers, functional readouts are only mildly rescued if at all.

As we also observed homogeneous enrichment of STAT signaling and aberrant AP1 enrichment patterns we asked if function could be preserved by providing inflammation to tumor bearing mice. To induce inflammation, we leveraged an empty *Listeria* strain (LM) that would elicit inflammatory responses without providing additional TAG antigen to the model. Tumor bearing ASTxAlb-Cre mice were either untreated, inoculated with 5 million colony-forming units (CFU; standard dose), or 20 million CFU (high dose). E5d were transferred into all groups and harvested 36h later for analysis (**Figure 4.2a**). As seen previously, tumor bearing mice not inoculated with LM lost double positive cytokine populations rapidly. Mice inoculated with LM exhibited incremental gains of IFNγ production in a dose dependent manner with highest dose exhibiting similar expression levels and percent positive to effector controls (**Figure 4.2b, c**). Granzyme B exhibited even gain in expression with increasing LM dose than IFNγ with virtually 100 percent of T cells GZMB positive and mean expression levels 10-fold higher than that of untreated controls (**Figure 4.2b, c**). TNFα however exhibited very minor gains in expression

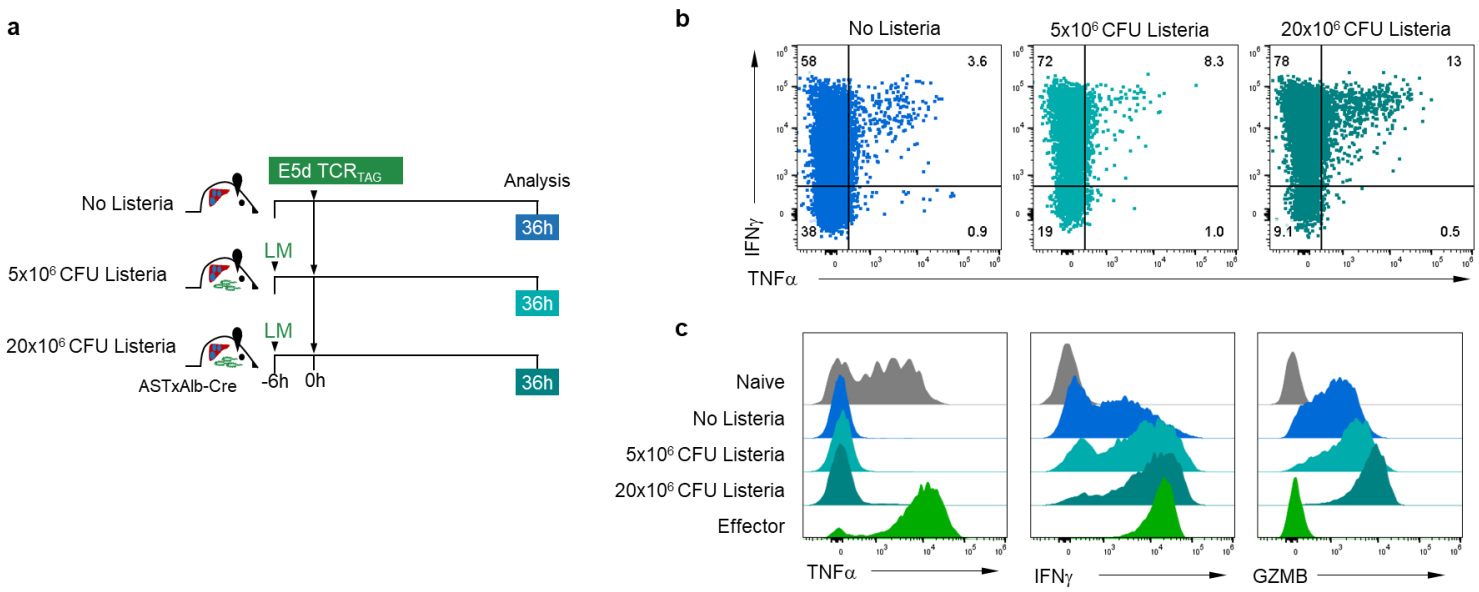

Figure 4.2 Increasing inflammation incrementally preserves cytokines and granzyme B. a, Experimental scheme: Effector TCR_{TAG} (Thy1.1) were adoptively transferred into ASTxAlb-Cre mice (Thy1.2) bearing late-stage liver tumors alone, inoculated with 5 million CFU LM, or inoculated with 20 million CFU LM and treated. Lymphocytes were re-isolated at 36 hours from tumor livers for analysis by flow cytometry. **b,** TCR_{TAG} intracellular IFNγ and TNFα production after 4 hour *ex vivo* TAG peptide stimulation or intracellular GZMB expression *ex vivo*. **c,** TCR_{TAG} intracellular IFNγ and TNFα production after 4 hour *ex vivo* TAG peptide stimulation or intracellular GZMB expression *ex vivo*. Histograms and dot plots are of a representative sample from each group.

despite large doses of LM. This again underscores differential regulation of functional readouts and suggests targeting negative regulators as well as providing supporting cytokines and costimulation will be required to rescue all aspects of T cell function.

To assess a combination approach of targeting NFAT and inflammation in tumors, we leveraged both FK506 treatment and presence or absence of inflammation using LM. TCR_{TAG} were transferred into tumor bearing hosts receiving no treatment, LM alone, or LM and FK506 treatment

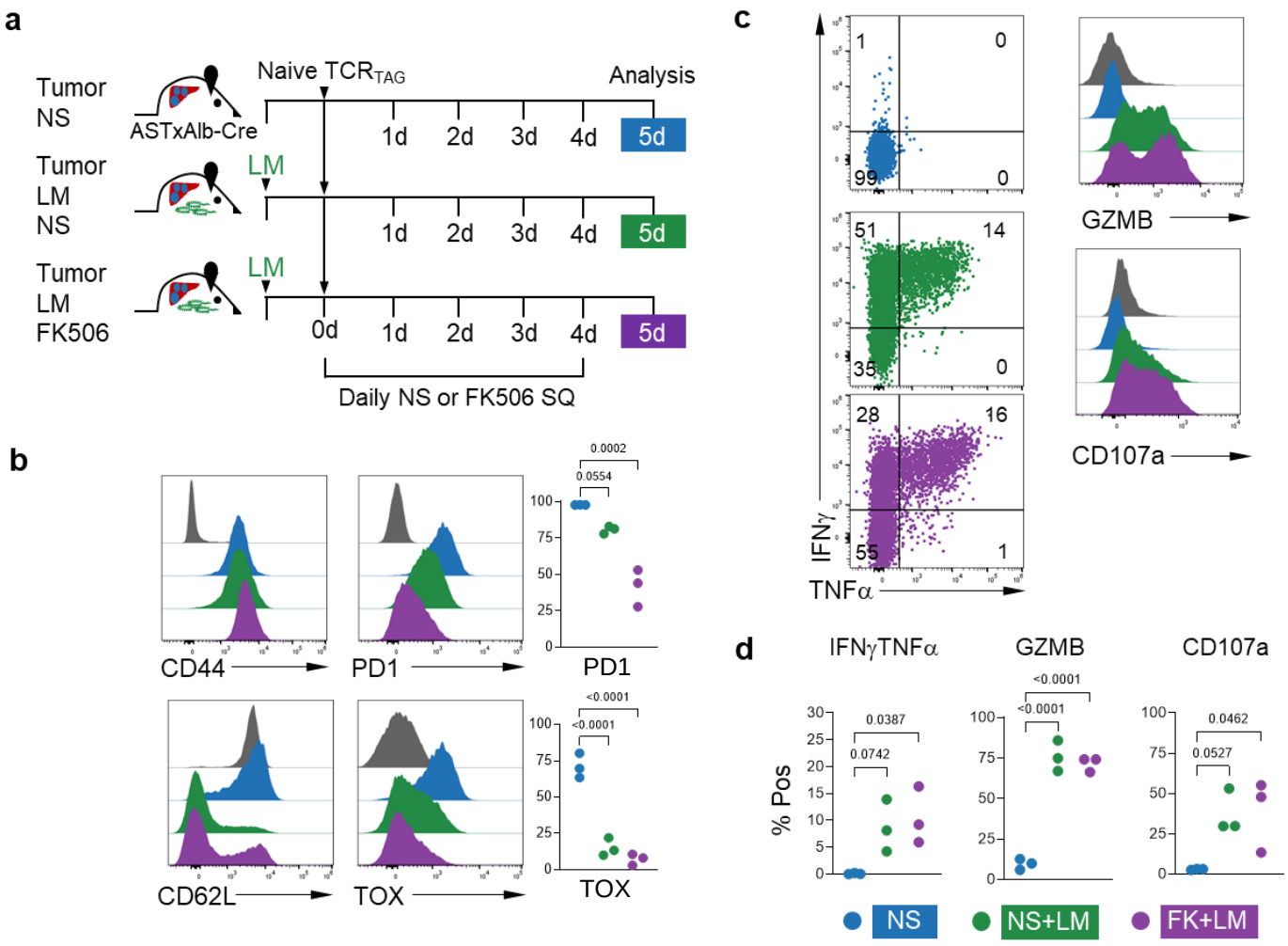

Figure 4.3 Combination of FK506 and inflammation provides rescue of functional outputs. a, Experimental scheme: naïve TCR_{TAG} (Thy1.1) were adoptively transferred into ASTxAlb-Cre mice (Thy1.2) bearing late-stage liver tumors alone, inoculated with LM, or inoculated with LM and treated with 5 mg/kg FK506. FK506 or normal saline (NS) sham injections performed daily subcutaneously (SQ). Lymphocytes were re-isolated at day 5 from tumor livers for analysis by flow cytometry. **b**, Live CD8+ Thy1.1+ TCR_{TAG} T cells stained for surface CD44, CD62L, PD1, and intracellular TOX with PD1 and TOX summary plots shown. Each symbol represents a single mouse. **c**, TCR_{TAG} intracellular IFNγ and TNFα production and surface CD107a induction after 4-hour *ex vivo* TAG peptide stimulation or intracellular GZMB expression *ex vivo*. **d**, Summary plots show percentage of IFNγTNFα double positive, CD107a, and GZMB positive. Each symbol represents an individual mouse. Histograms and dot plots are of a representative sample from each group. Histograms and dot plots are concatenations from 3-4 biologic replicates. Experiments were repeated twice with n=3-4 per group. Statistical significance calculated using one way ANOVA and posthoc Dunnett's multiple comparison test.

(**Figure 4.3a**). As observed in Figure 3.1, CD44 and CD62L were comparable between groups (**Figure 4.3b**). PD1 and TOX were also rescued with treatment, most significantly in the combination treatment group. PD1 down trended with inflammation in line with observations that PD1 is negatively regulated by inflammation induced TBET (Kao, Oestreich et al. 2011). Interestingly, TOX was significantly rescued by inflammation alone suggesting that inflammation induced changes in TCR signaling or TF may down tune TOX expression. From a functional perspective, FK506+LM combination provided additional rescue of the TNFα and IFNγ double positive population (**Figure 4.3c, d**). While GZMB was more dependent on inflammation, combination treatment appeared to boost both the percent positive and degree of degranulation as evident by CD107a translocation (**Figure 4.3c, d**).

Modulating TCR signaling with Cas9 mediated deletion of CD8 coreceptor

To use a genetic approach of TCR downtuning, we turned to a CRISPRCas9 to delete CD8 from the surface of T cells. Coreceptor deletion produces a lower affinity TCR interaction that decreases degree of NFAT driven differentiation (Shakiba, Zumbo et al. 2022). We transferred Cas9 expressing TCR_{TAG} transduced with empty vector or *Cd8* targeting gRNA (**Figure 4.4a**). Transduced T cells activated identically as evidenced by CD44 expression but only *Cd8* gRNA transduced T cells produced a majority CD8 KO for downstream studies (**Figure 4.4b**). As seen in FK506 experiments, CD8 KO populations exhibited partially rescued PD1 and TOX relative to control populations. Again, despite rescue of PD1 and TOX, CD8 deleted cells did not exhibit any functional benefit from a cytokine or degranulation capacity (**Figure 4.4c-e**).

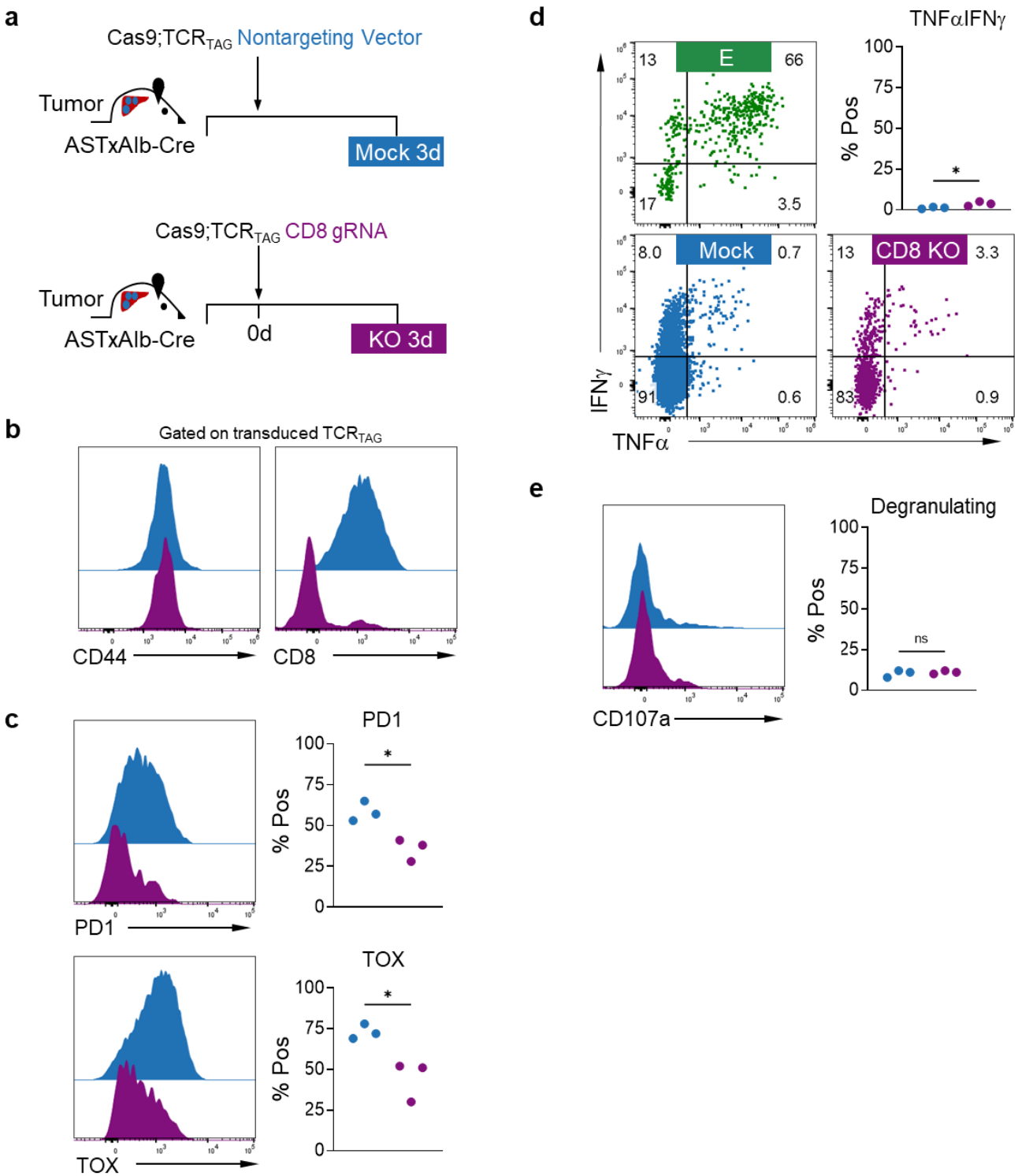
a
Cas9;TCR$_{TAG}$ Nontargeting Vector
Tumor
ASTxAlb-Cre
Mock 3d
Cas9;TCR$_{TAG}$ CD8 gRNA
Tumor
ASTxAlb-Cre
0d
KO 3d
b
Gated on transduced TCR$_{TAG}$
CD44
CD8
c
PD1
% Pos
PD1
TOX
% Pos
TOX
d
TNFαIFNγ
E
13
66
17
3.5
% Pos
Mock
8.0
0.7
91
0.6
CD8 KO
13
3.3
83
0.9
IFNγ
TNFα
e
Degranulating
% Pos
ns
CD107a

Figure 4.4 CD8 KO rescues PD1 and TOX but not cytokine or cytolytic function. a, Experimental scheme: Cas9 expressing TCR_{TAG} T cells were transduced with empty vector (blue) or *Cd8* targeting gRNA (purple). Transduced TCR_{TAG} E5d (Thy1.1) were adoptively transferred into ASTxAlb-Cre mice (Thy1.2) bearing late-stage liver tumors Lymphocytes were re-isolated at day 3 from tumor livers for analysis by flow cytometry. **b,** TCR_{TAG} T cells stained for surface CD44 and CD8 gated on transduced cell population. **c,** Histograms of TCR_{TAG} T cells stained for PD1 and TOX. Summary plots show percentage of PD1 and TOX (left). Each symbol represents an individual mouse. or intracellular GZMB expression *ex vivo.* **d,** Intracellular IFNγ and TNFα after 4-hour *ex vivo* TAG peptide stimulation. **e,** Degranulation histogram and summary plot. Each symbol represents an individual mouse. Histograms and dot plots are concatenations from 3-4 biologic replicates. Experiments were done once with n=3-4 per group. Statistical significance calculated using unpaired two-tailed t-test. ns= not significant, $*P<0.05$.

Assessing the role of PD1 in early T cell dysfunction with Cas9 mediated deletion

Finally, we sought to evaluate the role of early PD1 expression in tumor activated T cells in conferring dysfunctional phenotypes. We again leveraged our Cas9 expressing TCR_{TAG} cells transduced with either nontargeting vector or *Pdcd1* targeting gRNA. We transferred transduced T cells into tumor bearing mice and harvested 3 days later (**Figure 3.5a**). Both transduced populations activated and induced CD44 expression but only the *Pdcd1* targeted group exhibited deletion of PD1 surface protein (**Figure 3.5b**). Despite negative PD1 surface expression, tumor activated TCR_{TAG} exhibited no benefit in cytokine function (**Figure 3.5c**). PD1 deletion also failed to produce any benefit in degranulation capacity of TCR_{TAG} activated in tumors (**Figure 3.5d**). PD1 knockout did however produce slight functional gain in secondary lymphoid tissue and an overall numbers benefit relative to untreated controls consistent with studies from checkpoint blockade (data not shown).

Discussion

Taken together, these data support a two-component model of rapid dysfunction. There is a lack

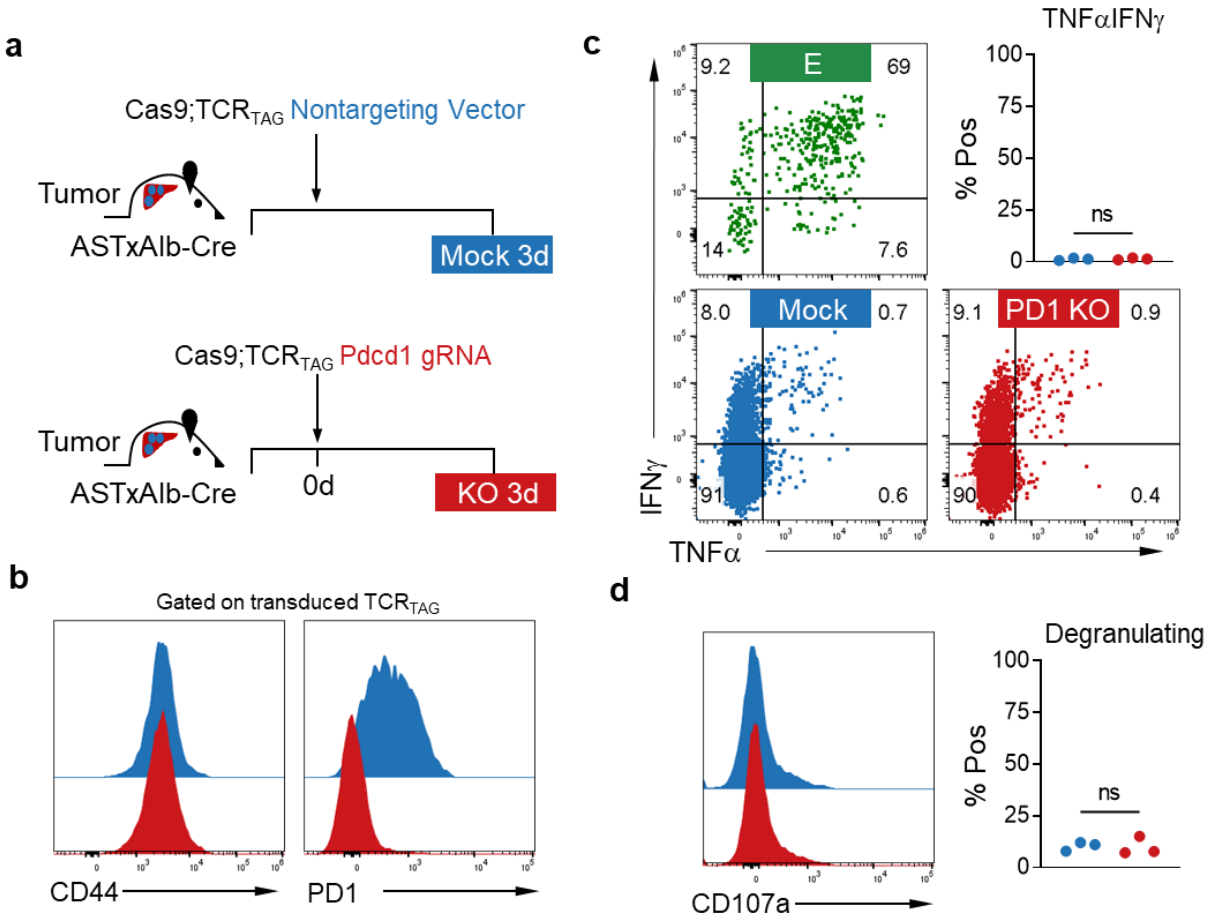

Figure 3.5 PD1 does not drive early functional loss in tumor activated T cells. a, Experimental scheme: Cas9 expressing TCR$_{TAG}$ T cells were transduced with empty vector (blue) or *Pdcd1* targeting gRNA (red). Transduced TCR$_{TAG}$ E5d (Thy1.1) were adoptively transferred into ASTxAlb-Cre mice (Thy1.2) bearing late-stage liver tumors Lymphocytes were re-isolated at day 3 from tumor livers for analysis by flow cytometry. **b,** TCR$_{TAG}$ T cells stained for surface CD44 and PD1 gated on transduced cell population. **c,** Intracellular IFNγ and TNFα after 4-hour *ex vivo* TAG peptide stimulation. **d,** Degranulation histogram and summary plot. Each symbol represents an individual mouse. Histograms and dot plots are concatenations from 3-4 biologic replicates. Experiments were done once with n=3-4 per group. Statistical significance calculated using unpaired two-tailed t-test. ns= not significant, **P*<0.05.

of supporting signals, likely through STAT and costimulation, but also a negative signal that is actively specifically provided by the tumor, such as TCR hyperactivation. In line with these findings, providing LM, which induces inflammation including IL-12 and type I IFN signaling

(Sinnathamby, Lauer et al. 2009) induced several components of function. First, IFNγ and GZMB was preserved in a dose dependent fashion but not TNFα. Secondly, PD1 and TOX were also decreased by added inflammation. As TBET has been implicated in downregulation of surface PD1 (Kao, Oestreich et al. 2011) it is likely that TOX is also positively and negatively regulated depending on the relative expression and combinations of TF. Blocking NFAT with FK506 potentiated these findings which is in line with the known role NFAT1 and NFAT2 have in inducing TOX and PD1 expression (Ahn, Araki et al. 2018, Khan, Giles et al. 2019). Combination of NFAT blockade and inflammation did increase some functional aspects in tumor activated T cells. The failure of CD8 deletion alone to rescue function is counter to favorable responses observed in subcutaneous tumor models (Shakiba, Zumbo et al. 2022). Differences in innate levels of inflammation could provide a possible rationale for this as diminished NFAT signaling may only be beneficial if a T cell can enter or maintain a functional state in an IL-12 or type I IFN dependent manner (Agarwal, Raghavan et al. 2009, Lin, Rayman et al. 2019). In line with these findings is recent work showing an essential role of IL-2 signaling in reinvigorating dysfunctional T cells in the context of checkpoint blockade (Codarri Deak, Nicolini et al. 2022). However, numerous studies and clinical trials using cytokine have shown that toxicity limits efficacy in mice and humans (Lasek, Zagozdzon et al. 2014).

Marginal benefits with FK506 support the notion that NFAT hyperactivation plays a role in driving early tumor induced T cell dysfunction. However, benefit with FK506 was small at best. Similar studies modulating signaling strength have leveraged more general TCR signaling pharmacologic inhibition (dasatanib) or removable TCR/CAR-T constructs (Weber, Parker et al. 2021) to produce more extensive rescue but in relatively lower tumor burdens. Nevertheless, it is possible that a

more complete NFAT down tuning or removal may be a way to prolong effector T cell responses therapeutically. Targeting TCR signaling strength and NFAT has also been shown to diminish transcriptional and epigenetic signatures associated with dysfunction which may also delay the stabilization of dysfunction over time (Weber, Parker et al. 2021, Shakiba, Zumbo et al. 2022). However, there is also evidence suggesting that relatively high affinity T cells are most likely to outcompete and persist in tumor environments and provide therapeutic benefit for checkpoint blockade (Burger, Cruz et al. 2021).

These data also illustrate the decoupling of functional readouts such as cytokine and cytotoxicity to surface and TF markers associated with dysfunction such as PD1 and TOX. Previous work by our group has shown that deletion of TOX and subsequently, PD1, had no impact on functional outcomes of tumor activated T cells but did negatively affect cellular persistence at later timepoints (Scott, Dundar et al. 2019). Here we show that through pharmacologic or immune environment modulation, we can significantly or completely rescue these markers and show that this provides no benefit to early T cell dysfunction in tumors. We show that PD1 does not drive early dysfunction as deletion in tumor specific T cells again does not rescue function in tumors. This is in line with observations at later timepoints and observations that T cell functional rescue is predominantly derived from tumor specific T cells in secondary or tertiary lymphoid tissue that are more stemlike or exhibit precursor dysfunctional states (Jansen, Prokhnevska et al. 2019, Dammeijer, van Gulijk et al. 2020), providing a burst of fresh T cells that can infiltrate tumors and continue anti-tumor immunity (Im, Hashimoto et al. 2016).

CHAPTER 5: OVERALL DISCUSSION AND FUTURE DIRECTIONS

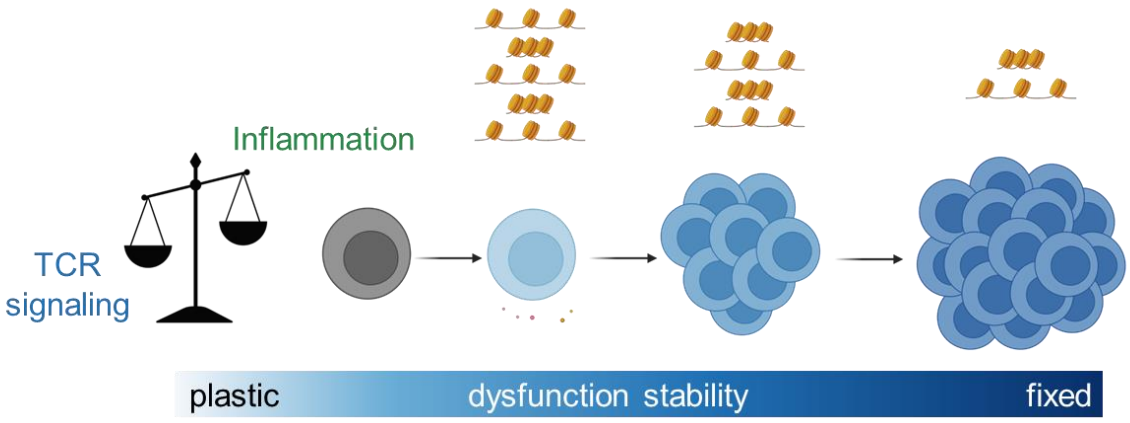

Here, we describe for the first time the functional, immunophenotypic, epigenetic, and transcriptional features of CD8 tumor specific T cells (TST) differentiating cell division by cell division within the hours following tumor antigen encounter *in vivo*. Though TST were activated and proliferated rapidly and identically to CD8 T cells during acute infection, TST in tumor-bearing hosts lost/failed to gain both effector cytokine and cytolytic function. Remarkably, this dysfunction was evident even prior to cell division. Rapid loss of effector function *in vivo* coincided with extensive chromatin remodeling and transcriptional alterations in TST, including chromatin peak accessibility changes previously characterized as "exhaustion-associated" (**Figure 5.1)**. These findings upend the previous paradigm that tumor-induced T cell dysfunction occurs through chronic antigen stimulation over days to weeks and instead show that CD8 T cells integrate multiple signaling inputs (TCR, co-stimulatory/inhibitory, and cytokine) immediately following activation in different contexts, which dictate their differentiation to the functional effector fate (infection) or the dysfunction fate (tumors).

Proliferation and differentiation are intimately connected throughout development (Zhu and

Skoultchi 2001), and previous studies showed that proliferation was required for the epigenetic remodeling associated with differentiation for thymocytes and other adaptive immune lineages (Bird, Brown et al. 1998, Tangye and Hodgkin 2004, Kreslavsky, Gleimer et al. 2012, Scharer, Barwick et al. 2018). However, we find that CD8 T cells execute large scale chromatin remodeling and differentiation prior to undergoing cell division. As our study is the first to examine adaptive immune cell differentiation and chromatin remodeling during the first hours following activation *in vivo* prior to cell division, it remains to be seen whether other immune cells similarly undergo early rapid differentiation to the functional or dysfunctional state. Nevertheless, despite dramatic effector function loss, dysfunctional TST proliferated as rapidly and robustly as T cells during acute infection; thus, the regulation of proliferation and functional effector differentiation is uncoupled. This finding, in line with previous studies *in vitro* or in self-tolerance models (Otten and Germain 1991, Hernandez, Aung et al. 2002, Curtsinger, Lins et al. 2003) has important implications for cancer immunotherapy, as efforts aimed at boosting TST proliferation by gene targeting may not be sufficient to reverse effector function loss (Belk, Yao et al. 2022, Guo, Huang et al. 2022, Legut, Gajic et al. 2022).

There are additional studies that would further supplement our understanding of early differentiation in general. First, assessing generalizability of early differentiation across other immune cell types. It is possible that CD8 T cells represent a unique example of early differentiation relative to other classes of immune cells such as B cells. As the functional decisions of CD8 T cells are somewhat binary (they either initiate cytotoxic programs or not), they may be capable of more rapid epigenetic and functional differentiation relative to CD4 T cells, which can differentiate into several fates depending on contextual signals. Nevertheless, early differentiation

studies on other cell types would advance our understanding of how lymphocytes respond to activation conditions. While the work outlined here focused on characterization of early dysfunction in the context of tumors, this begs the question as to the importance of the early gain of cytotoxic function during acute infection. T cells undergoing functional differentiation exhibited rapid pre-division gain of cytokine and cytolytic function in response to infection. This suggests that T cells can effectively respond to invading microbes much earlier than canonical thinking implies. This also raises questions for contact duration of T cells and dendritic cells and how antigen presenting cells avoid CD8 mediated killing as they activate T cells, which may be best studied with *in vivo* imaging approaches.

While dysfunctional hallmarks, including impaired effector function, inhibitory receptor expression, and dysfunction/exhaustion-associated chromatin accessibility changes, were manifested in TST with different kinetics prior to cell division, with continued tumor/antigen stimulation and proliferation, TST underwent additional chromatin remodeling that stabilized and reinforced initial dysfunction epigenetic programs. These findings together with our previous work (Philip, Fairchild et al. 2017, Scott, Dundar et al. 2019) demonstrate that the T cell dysfunctional state is composed of different modules (loss of effector function, upregulation of inhibitory receptors, proliferative capacity), which are regulated independently. This was borne out when we tested the degree to which early TST dysfunction was "imprinted"—that is retained upon removal from the tumor and transfer into tumor-free hosts. Effector function impairment was not reversed upon tumor removal in a significant fraction of TST exposed to tumor for 24h, in contrast to PD1 expression, which was nearly absent in P24h and did not become fixed until after 5+ days of tumor exposure, with epigenetic reinforcement. Interestingly, expression of TOX, a key dysfunction-

associated TF, was not imprinted even after 10d of tumor exposure, suggesting that TOX expression is dependent on antigen/TCR stimulation or requires even longer tumor exposure to become imprinted. Indeed, recent studies showed that later exhausted T cells (>30d exposure) from humans and murine models of chronic viral infection retained TOX expression and exhaustion-associated chromatin peaks after transfer to antigen-free hosts or viral cure with direct acting anti-viral therapy (Abdel-Hakeem, Manne et al. 2021, Hensel, Gu et al. 2021, Yates, Tonnerre et al. 2021).

The heterogeneity observed in effector function recovery upon early TST removal to tumor-free hosts raised the question as to whether there was bifurcation in early/intermediate time point populations towards stem/progenitor or terminally-differentiated dysfunctional/exhausted states. However, in contrast to studies in chronic LCMV infection models (Utzschneider, Gabriel et al. 2020), we found that early/intermediate TST had homogeneous expression of TCF1 and did not express late/terminal exhaustion/dysfunction markers. While TST dysfunction shares many features with the chronic viral infection-induced exhaustion, there are important biological differences between hosts with late-stage tumors and hosts with chronic infection that may be particularly relevant during the initial hours and days immediately following activation. Early time point TST did not show induction of inflammation-associated TF or downstream inflammation-associated genes, and this lack of innate/inflammatory cytokine stimulation may lead to the failure of TST to induce functional/memory-associated gene programs, even upon removal from the tumor. In contrast, chronic viral infection does induce innate signaling, and indeed, CD8 T cells activated during acute and chronic viral infection have comparable effector function, with loss of cytokine and cytolytic function occurring over days to weeks (Wherry, Ha et al. 2007).

Taken together, our studies suggest that there are two major contributing factors to TST dysfunction in hosts with late-stage tumors. First, TST activated in tumors or secondary lymphoid organs may receive strong TCR signaling due to a surfeit of tumor antigen, leading to robust proliferation, however the lack of innate inflammatory signals and defective priming on non-activated APC or tumor cells does not induce TF needed to induce functional effector differentiation. Second, persistent tumor antigen/TCR stimulation and/or other negative regulatory signals in tumor-bearing hosts leads to NFAT overactivation, or partnerless NFAT activation, further impairing effector function, inducing TOX expression and the hierarchical progression of dysfunction/exhaustion hallmarks. Furthermore, chronic tumor antigen/TCR stimulation reinforces epigenetic changes encoding dysfunctional hallmarks, eventually leading to fixed dysfunctional TST.

In the future, we hope to further dissect the underlying mechanism executing rapid dysfunction in tumors, and an outstanding question is how NFAT or other downstream TCR pathways could be playing a role. Given how quickly functional changes occur, it is possible that posttranscriptional regulation is critical in rapidly quenching cytokine or cytolytic expression. The fact that RNA expression of some critical effector genes (*Tnf, Ifng*) does not match corresponding protein expression supports this notion. RNA binding proteins have been well documented in regulating cytokine expression across immune cell types, commonly through AU rich elements in the 3' untranslated region (Salerno, Engels et al. 2018, Petkau, Mitchell et al. 2022). As discussed previously this includes metabolic proteins such as GAPDH (Chang, Curtis et al. 2013), and while GSEA analysis did not suggest global metabolism deficits, protein level changes could still be

evaluated for therapeutic development. ZFP36 family proteins are among the most common post transcriptional regulators and indeed, ZFP36L1 was found to be transcriptionally induced in tumors relative to infection, which could impose a translational block on effector gene mRNA (Salerno, Engels et al. 2018, Makita, Takatori et al. 2021). Genetic deletion approaches using Cas9;TCR_{TAG} system could be implemented to assess contribution of these RNA-binding proteins in driving dysfunction. As global changes in splicing and RNA binding can occur with different T cell activation conditions (Karginov, Menoret et al. 2022), a more global approach could be taken to compare and contrast isoform differences in transcriptional data using Whippet supplemented with analysis of RNA interactions with RNA binding proteins using CLIP-SEQ (Stork and Zheng 2016). This could identify tumor specific isoform and RNA binding protein patterns to inform therapeutic intervention.

The rapid onset of cytokine and cytolytic impairment in committed effector CD8 T cells upon transfer into mice with late-stage liver and pulmonary melanoma metastases was particularly striking, demonstrating that negative regulatory factors in hosts with late-stage tumors can overwrite functional epigenetic programs in CD8 T cells. Thus, even T cells that have been properly primed in tumor-bearing hosts (e.g. through immunization or due to seeing antigen on activated antigen presenting cells in draining lymph nodes), may succumb to tumor-induced dysfunction upon entry into tumors. These findings have important implications for immunotherapies such as adoptive T cell therapies and immune checkpoint blockade. Despite presence of stem-like populations (Jansen, Prokhnevska et al. 2019, Connolly, Kuchroo et al. 2021) or successful activation and mobilization of progenitor dysfunctional T cells to the tumor (Im, Hashimoto et al. 2016, Dammeijer, van Gulijk et al. 2020), fleeting functional states may be

insufficient to effectively mediate antitumor immunity.

What approaches would best preserve T cell function in tumors? Based on our TF analysis and rescue experiments, a combination approach appears to be required to prolong antitumor immunity even in previously committed effector T cells. While global TCR and inflammatory manipulation with FK506 may be limited by toxicity (Lasek, Zagozdzon et al. 2014), targeting these pathways through manipulation of T cells may provide benefit. Inducible TCR like those used in CAR-T approaches could be used to prevent break up of NFAT signaling and prevent dysfunctional programming from building. STAT signaling is also of interest for cellular therapies and could be used to support function while also downregulating genes such as *Pdcd1* and *Tox*. Overexpression of STAT1 or STAT4 may increase sensitivity in tumor activated T cells without producing systemic toxicity. This has gained traction for STAT5 in the context of checkpoint blockade in chronic viral infection (Codarri Deak, Nicolini et al. 2022, Tichet, Wullschleger et al. 2023). Approaches applied for CAR-T rescue of inducible cytokine receptors or constitutively active cytokine receptors may also be employed here and our model could be used to determine the optimal combinations to produce the most durable T cell function (Engelowski, Schneider et al. 2018, Bell and Gottschalk 2021). As effector T cells exhibit heterogeneity in how they undergo hierarchical cytokine loss and loss of cytolytic function, an alternative approach would be to leverage single cell sequencing to map progression of epigenetic and transcriptional remodeling. Effector TST could be transferred into tumor bearing mice or tumor bearing mice immunized with LM and submitted for scATAC-SEQ and scRNA-SEQ in parallel to provide a granular understanding of pathways and progression of early tumor differentiation. As our initial hypothesis that few epigenetic and transcriptional changes would occur pre-division was incorrect, comparing

previously activated effector populations may allow for efficient identification of functional or dysfunctional specific programs over shared differentiation programming.

Given how rapidly CD8 T cells differentiate to the dysfunctional state in tumor-bearing hosts, with early epigenetic remodeling further reinforced over time/tumor progression, in order to improve T cell-based cancer immunotherapy, we need to target both early dysfunction induction as well as dysfunction reinforcement. Further studies are needed to understand how CD8 T cells rapidly integrate TCR and context-dependent inputs to make fate choices. Only by deciphering the complex network of signaling and gene regulatory networks that lie between TCR and context-dependent inputs and fate choice outputs, can we design strategies to alter or redirect T cells into functional cancer killers.

CHAPTER 6: METHODS

Mice

TCR_{TAG} transgenic mice (B6.Cg-Tg(TcraY1,TcrbY1)416Tev/J)(Staveley-O'Carroll, Schell et al. 2003), TCR-OT1 (C57BL/6-Tg(TcraTcrb)1100Mjb/J), Ly5.1 (B6.SJL-Ptprca Pepcb/BoyJ), Alb-Cre (B6.Cg-Tg(Alb-cre)21Mgn/J), Cas9 (B6J.129(Cg)-Gt(ROSA)26Sortm1.1(CAG-cas9*,-EGFP)Fezh/J) and C57BL/6J Thy1.1 mice were purchased from The Jackson Laboratory. TCR_{TAG};Thy1.1 double transgenic mice were generated by crossing Thy1.1 mice to TCR_{TAG} mice. TCR_{OVA};Ly5.1 double transgenic mice were generated by crossing the TCR-OTI mice with Ly5.1 mice. Cas9;TCR_{TAG};Thy1.12 triple transgenic mice were generated by crossing Cas9 mice to TCR_{TAG};Thy1.1 mice. ASTxAlb-Cre (Schietinger, Philip et al. 2016) double transgenic mice were generated by crossing AST (Albumin-floxStop-SV40 large T antigen (TAG)) (Stahl, Sacher et al. 2009) with Alb-Cre mice. Both female and male mice were used for studies. T cell donor mice were between 6-10 weeks of age and sex-matched to recipient male and female C57BL/6 and ASTxAlb-Cre recipients. All mice were bred and housed in the animal facility at Vanderbilt University Medical Center (VUMC). All animal experiments were performed in compliance with VUMC Institutional Animal Care and Use Committee (IACUC) regulations.

Adoptive T cell transfer in acute infection and tumor models

C57BL/6 mice were inoculated i.v. with $5x10^6$ or $10x10^6$ CFU *Listeria monocytogenes* (LM) Δ*actA* Δ*inlB* strain (Brockstedt, Giedlin et al. 2004) expressing the TAG-I epitope (SAINNYAQKL, SV40 large T antigen 206–215) (Aduro Biotech) or the OVA epitope (SIINFEKL), respectively, 6-12h prior to T cell adoptive transfer for generation of effectors. Spleens from naive TCR_{TAG};Thy1.1 mice were mechanically disrupted with the back of 3 mL

syringe and filtered through a 70 μm strainer into ammonium chloride potassium (ACK) buffer to lyse erythrocytes. Cells were washed twice with cold serum-free RPMI 1640 media and $2.5x10^6$ TCR_{TAG};Thy1.1 $CD8^+$ T cells were adoptively transferred into C57BL/6 (Thy1.2) mice inoculated with LM_{TAG} or ASTxAlb-Cre tumor bearing mice. For OTI experiments $2.5x10^6$ TCR_{OVA};Ly5.1 splenocytes were prepared in the same manner from OTI;Ly5.1 mice and adoptively transferred into mice inoculated with LM_{OVA} or mice bearing B16-OVA lung tumors. For CFSE labeling studies, splenocytes were resuspended after first wash in 2.5 mL of plain, serum-free RPMI 1640, rapidly mixed with equal volumes of 2x CFSE [10 μM] solution, incubated for 5 min at 37°C at a final CFSE [5 μM], quenched by mixing CFSE/cell solution with equal volume of pure FBS, washed twice with serum-free RPMI, and resuspended in serum-free RPMI for transfer.

B16-OVA production and lung metastasis

B16-F10 mouse melanoma cell line was obtained from ATCC (CRL-6475). B16-OVA expressing cell line was produced by transduction with pMFG-OVAx2-EGFP overexpression vector. Briefly, pMFG-EGFP was linearized with NcoI and ligated with OVAx2 (SIINFEKL-AAY-SIINFEKL) containing oligonucleotide (IDT). Cloned constructs were sequence verified. Phoenix-AMPHO (ATCC, CRL-3213) packaging cells were transfected with pMFG-OVAx2-EGFP in calcium phosphate and B16-F10 was transduced with viral supernatant. B16-OVA cells were sorted by EGFP expression for freeze downs and culturing. B16-OVA were cultured in Dulbecco's Modified Eagle's Medium (DMEM) supplemented with 10% FBS and L-Glutamine (cDMEM) at 37°C in a 5% CO_2 humidified incubator. For inoculation of lung metastasis, B16-OVA was harvested at 60-80% confluency. Media was replaced with fresh cDMEM the day prior to harvest. Cells were washed twice with ice cold serum free RPMI and $2\text{-}4x10^5$ cells were injected by tail vein into B6

mice. Tumors were allowed to grow for 3 weeks prior to T cell transfer experiments.

Cas9 primary T cell knockout

The following targeting gRNA oligos were cloned into pMIUR expression vector (Shakiba, Zumbo et al. 2022): *Pdcd1*; 5' CACCGCAGCTTGTCCAACTGGTCGG 3' (Chen, Arai et al. 2021), *Cd8a* 1; 5' CACCGTGGGTGAGTCGATTATCC TG 3', and *Cd8a* 2; 5' CACCG ATCCCACAACAAGATAACGT 3' (Shakiba, Zumbo et al. 2022). Targeting or empty pMIUR vectors were lipid transfected into Platinum-E packaging line (Cell Biolabs, Cat# RV-101) using the TransIT-LT1 Transfection Kit (Mirus, Cat#Mir2300). For *Cd8a* targeting, equal concentrations quantities of both *Cd8a* gRNA were used in transfection. Splenocytes of Cas9;TCR_{TAG};Thy1.12 mice were harvested and processed as described above and activated with anti-murine CD3e (Clone 145-2C11 BioLegend 100331) and anti-murine CD28 (Clone 37.51 Tonbo 400281-U500). Splenocytes were transduced with retroviral supernatant via spinfection at 1 and 2 days post activation. Transduced T cells were maintained in culture with RPMI 1640 containing 2 μM glutamine, 100 U/mL penicillin/streptomycin, and 10% FBS (cRPMI) supplemented with 50 U/mL IL-2 and 50 μM 2Mercaptoethanol at $1x10^6$ T cells/mL until 5 days post activation where they were transferred into tumor bearing hosts for downstream analysis.

FK506 treatment workflow

FK506 (Tacrolimus, Prograf) was diluted in normal saline (NS). Recipient mice were weighed and administered 10 mg/kg subcutaneously (SQ) as indicated. For effector adoptive transfer experiments, donor mice were administered 10 mg/kg (SQ) for 2 days prior to transfer. Mice in no treatment group received NS injections as indicated.

Cell isolation for subsequent analyses

Spleens from experimental mice were mechanically disrupted with the back of 3 mL syringe and filtered through a 70 μm strainer into ACK buffer. Cells were washed once and resuspended in cold cRPMI. Liver tissue was mechanically disrupted using a 150 μm metal mesh and glass pestle in ice-cold 2% FBS/PBS and passed through a 70 μm strainer. Liver homogenate was centrifuged at 400g for 5 min at 4℃ and supernatant discarded. Liver pellet was resuspended in 20 mL of 2% FBS/PBS buffer containing 500 U heparin, mixed with 13 mL of Percoll (GE) by inversion, and centrifuged at 500g for 10 min at 4°C. Supernatant was discarded and pellet was RBC lysed in ACK buffer and resuspended in cRPMI for downstream applications. Periportal and celiac lymph nodes were collected and pooled for tumor draining lymph node analysis. Lymph nodes were mechanically dissociated into single cell solutions using the textured surface of two frosted microscope slides into ice-cold cRPMI. Prior to cell sorting workflows, target populations were enriched from spleens or malignant livers with CD8 negative selection kit (Stem Cell, Catalog # 19853) per manufacturer's instructions.

Intracellular cytokine and transcription factor staining

Intracellular cytokine staining was performed with the Foxp3/Transcription Factor Staining Buffer Kit (Tonbo) per manufacturer's instructions. Briefly, T cells were mixed with $2x10^6$ C57BL/6 splenocytes and stimulated with 0.5 μg/mL of TAG epitope I peptide in cRPMI for 4 hours at 37°C in the presence of brefeldin A (BioLegend). Where indicated, stim media contained anti-CD107a antibody. Following peptide stimulation, cells were stained with for surface markers, fixed, permeabilized, and stained for IFNγ, TNFα, perforin, and granzyme B. Intracellular transcription

factor staining was performed with the Foxp3/Transcription Factor Staining Buffer Kit (Tonbo) per manufacturer's instructions.

Flow cytometry and flow sorting

All flow analysis was performed on the Attune NXT Acoustic Focusing Cytometer (ThermoFisher Scientific). Data was analyzed using FlowJo v.10.8.1 (Tree Star Inc.). Cell sorting was performed using the BD FACS Aria III (BD Biosciences) at the VUMC Flow Cytometry Shared Resource Core with BD FACSDiva Software.

RNA sequencing (RNA-SEQ)

ACK lysed single cell suspensions from livers and spleens were processed as described above using sterile technique and stained with antibodies against CD8, CD90.1, and CD69 and (4',6-diamidino-2-phenylindole) DAPI for dead cell exclusion. 5,000 cells were sorted directly into Trizol LS and frozen. Total RNA was extracted from sorted cells using the Rneasy Micro kit (Qiagen) and amplified using the SMART-Seq v4 UltraLow Input RNA Kit (Clontech). The cDNA was quantified and analyzed on the BioAnalyzer. Libraries were prepared using 7.7-300 ng of cDNA and the NEB DNA Ultra II kit. Each library was quantitated post PCR and run on the Caliper GX to assess each library profile. A final quality control assay consisting of qPCR was completed for each sample. The libraries were sequenced using the NovaSeq 6000 with 150 bp paired end reads targeting 50M reads per sample. RTA (version 2.4.11; Illumina) was used for base calling and analysis was completed using MultiQC v1.7.5.

ATAC sequencing (ATAC-SEQ)

Profiling of chromatin was performed by ATAC-seq as previously described(Staveley-O'Carroll, Schell et al. 2003). ACK lysed single cell suspensions from livers and spleens were processed as described above using sterile technique and stained with antibodies against CD8, CD90.1, and CD69 and (4',6-diamidino-2-phenylindole) DAPI for dead cell exclusion. 15-20,000 cells were sorted into cold FCS, DMSO added to 10%, and cells frozen. Frozen T cells were then thawed and washed in cold PBS and lysed. The transposition reaction was incubated at 42°C for 45 min. The DNA was cleaned with the MinElute PCR Purification Kit (Qiagen), and material was amplified for five cycles. After evaluation by real-time PCR, 7–13 additional PCR cycles were done. The final product was cleaned by AMPure XP beads (Beckman Coulter) at a 1× ratio, and size selection was performed at a 0.5× ratio. Libraries were sequenced on a HiSeq 2500 or HiSeq 4000 in a 50-bp/50-bp paired-end run using the TruSeq SBS Kit v4, HiSeq Rapid SBS Kit v2, or HiSeq 3000/4000 SBS Kit (Illumina).

Statistical analyses

Statistical analyses on flow cytometric data were performed as described in the figure legends using Prism 9.0 software (GraphPad Software).

Bioinformatics methods

The quality of the sequenced reads was assessed with FastQC (Andrews 2010) and QoRTs (Hartley and Mullikin 2015) (for RNA-seq samples). Unless otherwise stated, plots involving high-throughput sequencing data were created using R v4.1.0 (R Core Team 2017) and ggplot2 (Wickham, Chang et al. 2016). Code has been deposited in GitHub: https://github.com/abcwcm/Rudloff2022.

RNA-SEQ data analysis

Adaptors were trimmed from raw sequencing reads with TrimGalore v0.5.0 (http://www.bioinformatics.babraham.ac.uk/projects/trim_galore/) and Cutadapt v2.8 (Martin 2011). Trimmed reads were mapped with STAR v2.7.6a (Dobin, Davis et al. 2013) to the mouse reference genome (GRCm38.p6). Fragments per gene were counted with featureCounts v2.0.7 (Liao, Smyth et al. 2014) with respect to Gencode vM25 comprehensive gene annotations. Differentially expressed genes were identified by Wald tests using DESeq2 v1.32.0 (Love, Huber et al. 2014), and only Benjamini–Hochberg corrected *P* values < 0.05 were considered statistically significant.

Principial component analysis and expression heatmaps were created using variance-stabilizing transformed counts generated by the DESeq2 package. Heatmaps are centered and scaled by row.

ATAC-SEQ data analysis

Alignment and identification of open chromatin regions

Reads were aligned to the mouse reference genome (GRCm38) with BWA-backtrack (Li and Durbin 2009). Post alignment filtering was done with samtools v1.8 (Li, Handsaker et al. 2009) and Broad Institute's Picard tools (http://broadinstitute.github.io/picard/) to remove unmapped reads, improperly paired reads, nonunique reads, and duplicates. To identify regions of open chromatin, peak calling was performed with MACS2 v2.2.7.1 (Liu 2014). Only peaks with adjusted *P* values smaller than 0.01 were retained.

ATAC-SEQ peak atlas creation

Consensus peak sets were generated for tumor and infection at each transition if a peak was found in at least two replicates. Reproducible peaks at each transition were merged with DiffBind v3.2.1(Stark and Brown 2011) to create an atlas of accessible peaks, which was used for downstream analyses. The peak atlas was annotated using the ChIPseeker v1.30.0 (Yu, Wang et al. 2015) and TxDb.Mmusculus.UCSC.mm10.knownGene (BioconductorCoreTeam and BioconductorPackageMaintainer 2019).

Differentially accessible regions

Regions where the chromatin accessibility changed between different conditions were identified with DESeq2 v1.32.0, and only Benjamini–Hochberg corrected *P* values < 0.05 were considered statistically significant. A $\log_2$fold change cutoff of 1 was used in some analyses as indicated. When comparing earlier time points against previously published chromatin accessibility data at later time points, hidden batch effects were estimated using the svaseq function from sva v3.40.0 (Leek, Johnson et al. 2022), and the top 3 surrogate variables were accounted for in DESeq2.

Motif analysis

Peaks were analyzed for transcription factor (TF) motif enrichment using chromVAR v1.14.0 (Schep, Wu et al. 2017). Motifs from the CIS-BP database (Weirauch, Yang et al. 2014) ('mouse_pwms_v2' from chromVARmotifs v0.2.0) were used as input, after removing TFs that were lowly expressed based on the RNA-SEQ data (average count-per-million < 10). TF accessibility deviation scores and variability were calculated by chromVAR, and z-scores of deviations of the top 25 most variable TFs were visualized in a heatmap.

Peak heatmaps and genome coverage plots

Genome coverage files per replicate were normalized for differences in sequencing depth (RPGC normalization) with bamCoverage from deepTools v3.1.0 (Ramirez, Ryan et al. 2016). Blacklisted regions were excluded (https://sites.google.com/site/anshulkundaje/projects/blacklists). Replicates were averaged together using UCSC-tools bigWigMerge and by dividing by the number of samples. ATAC-SEQ heatmaps were created using profileplyr v1.8.0 (Carroll and Barrows 2022) and ComplexHeatmap v2.8.0 (Gu, Eils et al. 2016), by binning the region +/− 1kb around the peak summits in 20bp bins. To improve visibility, bins with read counts greater than the 75th percentile + 1.5*IQR were capped at that value.

REFERENCES

Abdel-Hakeem, M. S., S. Manne, J. C. Beltra, E. Stelekati, Z. Chen, K. Nzingha, M. A. Ali, J. L. Johnson, J. R. Giles, D. Mathew, A. R. Greenplate, G. Vahedi and E. J. Wherry (2021). "Epigenetic scarring of exhausted T cells hinders memory differentiation upon eliminating chronic antigenic stimulation." Nat Immunol **22**(8): 1008-1019.

Agarwal, P., A. Raghavan, S. L. Nandiwada, J. M. Curtsinger, P. R. Bohjanen, D. L. Mueller and M. F. Mescher (2009). "Gene regulation and chromatin remodeling by IL-12 and type I IFN in programming for CD8 T cell effector function and memory." J Immunol **183**(3): 1695-1704.

Agnellini, P., P. Wolint, M. Rehr, J. Cahenzli, U. Karrer and A. Oxenius (2007). "Impaired NFAT nuclear translocation results in split exhaustion of virus-specific CD8+ T cell functions during chronic viral infection." Proc Natl Acad Sci U S A **104**(11): 4565-4570.

Ahn, E., K. Araki, M. Hashimoto, W. Li, J. L. Riley, J. Cheung, A. H. Sharpe, G. J. Freeman, B. A. Irving and R. Ahmed (2018). "Role of PD-1 during effector CD8 T cell differentiation." Proc Natl Acad Sci U S A **115**(18): 4749-4754.

Ahn, E., B. Youngblood, J. Lee, J. Lee, S. Sarkar and R. Ahmed (2016). "Demethylation of the PD-1 Promoter Is Imprinted during the Effector Phase of CD8 T Cell Exhaustion." J Virol **90**(19): 8934-8946.

Ahuja, D., M. T. Saenz-Robles and J. M. Pipas (2005). "SV40 large T antigen targets multiple cellular pathways to elicit cellular transformation." Oncogene **24**(52): 7729-7745.

Andrews, S. (2010). "FastQC: a quality control tool for high throughput sequence data.".

Asrir, A., C. Tardiveau, J. Coudert, R. Laffont, L. Blanchard, E. Bellard, K. Veerman, S. Bettini, F. Lafouresse, E. Vina, D. Tarroux, S. Roy, I. Girault, I. Molinaro, F. Martins, J. Y. Scoazec, N. Ortega, C. Robert and J. P. Girard (2022). "Tumor-associated high endothelial venules mediate lymphocyte entry into tumors and predict response to PD-1 plus CTLA-4 combination immunotherapy." Cancer Cell **40**(3): 318-334 e319.

Atsaves, V., V. Leventaki, G. Z. Rassidakis and F. X. Claret (2019). "AP-1 Transcription Factors as Regulators of Immune Responses in Cancer." Cancers (Basel) **11**(7).

Auphan-Anezin, N., G. Verdeil and A. M. Schmitt-Verhulst (2003). "Distinct thresholds for CD8 T cell activation lead to functional heterogeneity: CD8 T cell priming can occur independently of cell division." J Immunol **170**(5): 2442-2448.

Badovinac, V. P., S. E. Hamilton and J. T. Harty (2003). "Viral infection results in massive CD8+ T cell expansion and mortality in vaccinated perforin-deficient mice." Immunity **18**(4): 463-474.

Badovinac, V. P., J. S. Haring and J. T. Harty (2007). "Initial T cell receptor transgenic cell precursor frequency dictates critical aspects of the CD8(+) T cell response to infection." Immunity **26**(6): 827-841.

Bartholdy, C., J. P. Christensen, D. Wodarz and A. R. Thomsen (2000). "Persistent virus infection despite chronic cytotoxic T-lymphocyte activation in gamma interferon-deficient mice infected with lymphocytic choriomeningitis virus." J Virol **74**(22): 10304-10311.

Belk, J. A., W. Yao, N. Ly, K. A. Freitas, Y. T. Chen, Q. Shi, A. M. Valencia, E. Shifrut, N. Kale, K. E. Yost, C. V. Duffy, B. Daniel, M. A. Hwee, Z. Miao, A. Ashworth, C. L. Mackall, A. Marson, J. Carnevale, S. A. Vardhana and A. T. Satpathy (2022). "Genome-wide CRISPR screens of T cell exhaustion identify chromatin remodeling factors that limit T cell persistence." Cancer Cell **40**(7): 768-786 e767.

Bell, M. and S. Gottschalk (2021). "Engineered Cytokine Signaling to Improve CAR T Cell Effector Function." Front Immunol **12**: 684642.

Beltra, J. C., S. Manne, M. S. Abdel-Hakeem, M. Kurachi, J. R. Giles, Z. Chen, V. Casella, S. F. Ngiow, O. Khan, Y. J. Huang, P. Yan, K. Nzingha, W. Xu, R. K. Amaravadi, X. Xu, G. C. Karakousis, T. C. Mitchell, L. M. Schuchter, A. C. Huang and E. J. Wherry (2020). "Developmental Relationships of Four Exhausted CD8(+) T Cell Subsets Reveals Underlying Transcriptional and Epigenetic Landscape Control Mechanisms." Immunity **52**(5): 825-841 e828.

Betts, M. R., M. C. Nason, S. M. West, S. C. De Rosa, S. A. Migueles, J. Abraham, M. M. Lederman, J. M. Benito, P. A. Goepfert, M. Connors, M. Roederer and R. A. Koup (2006). "HIV nonprogressors preferentially maintain highly functional HIV-specific CD8+ T cells." Blood **107**(12): 4781-4789.

BioconductorCoreTeam and BioconductorPackageMaintainer (2019). "TxDb.Mmusculus.UCSC.mm10.knownGene: Annotation package for TxDb object(s)." R package version 3.4.7.

Bird, J. J., D. R. Brown, A. C. Mullen, N. H. Moskowitz, M. A. Mahowald, J. R. Sider, T. F. Gajewski, C. R. Wang and S. L. Reiner (1998). "Helper T cell differentiation is controlled by the cell cycle." Immunity **9**(2): 229-237.

Blattman, J. N., R. Antia, D. J. Sourdive, X. Wang, S. M. Kaech, K. Murali-Krishna, J. D. Altman and R. Ahmed (2002). "Estimating the precursor frequency of naive antigen-specific CD8 T cells." J Exp Med **195**(5): 657-664.

Bowen, D. G. and C. M. Walker (2005). "Adaptive immune responses in acute and chronic hepatitis C virus infection." Nature **436**(7053): 946-952.

Brockstedt, D. G., M. A. Giedlin, M. L. Leong, K. S. Bahjat, Y. Gao, W. Luckett, W. Liu, D. N. Cook, D. A. Portnoy and T. W. Dubensky, Jr. (2004). "Listeria-based cancer vaccines that segregate immunogenicity from toxicity." Proc Natl Acad Sci U S A **101**(38): 13832-13837.

Bucks, C. M., J. A. Norton, A. C. Boesteanu, Y. M. Mueller and P. D. Katsikis (2009). "Chronic antigen stimulation alone is sufficient to drive CD8+ T cell exhaustion." J Immunol **182**(11): 6697-6708.

Buenrostro, J. D., P. G. Giresi, L. C. Zaba, H. Y. Chang and W. J. Greenleaf (2013). "Transposition of native chromatin for fast and sensitive epigenomic profiling of open chromatin, DNA-binding proteins and nucleosome position." Nat Methods **10**(12): 1213-1218.

Burger, M. L., A. M. Cruz, G. E. Crossland, G. Gaglia, C. C. Ritch, S. E. Blatt, A. Bhutkar, D. Canner, T. Kienka, S. Z. Tavana, A. L. Barandiaran, A. Garmilla, J. M. Schenkel, M. Hillman, I. de Los Rios Kobara, A. Li, A. M. Jaeger, W. L. Hwang, P. M. K. Westcott, M. P. Manos, M. M. Holovatska, F. S. Hodi, A. Regev, S. Santagata and T. Jacks (2021). "Antigen dominance hierarchies shape TCF1(+) progenitor CD8 T cell phenotypes in tumors." Cell **184**(19): 4996-5014 e4926.

Cao, Z., X. Sun, B. Icli, A. K. Wara and M. W. Feinberg (2010). "Role of Kruppel-like factors in leukocyte development, function, and disease." Blood **116**(22): 4404-4414.

Carroll, T. and D. Barrows (2022). "profileplyr: Visualization and annotation of read signal over genomic ranges with profileplyr." R package version 1.12.0.

Castellino, F., A. Y. Huang, G. Altan-Bonnet, S. Stoll, C. Scheinecker and R. N. Germain (2006). "Chemokines enhance immunity by guiding naive CD8+ T cells to sites of CD4+ T cell-dendritic cell interaction." Nature **440**(7086): 890-895.

Chang, C. H., J. D. Curtis, L. B. Maggi, Jr., B. Faubert, A. V. Villarino, D. O'Sullivan, S. C. Huang, G. J. van der Windt, J. Blagih, J. Qiu, J. D. Weber, E. J. Pearce, R. G. Jones and E. L. Pearce (2013). "Posttranscriptional control of T cell effector function by aerobic glycolysis." Cell **153**(6): 1239-1251.

Chauveau, A., G. Pirgova, H. W. Cheng, A. De Martin, F. Y. Zhou, S. Wideman, J. Rittscher, B. Ludewig and T. I. Arnon (2020). "Visualization of T Cell Migration in the Spleen Reveals a Network of Perivascular Pathways that Guide Entry into T Zones." Immunity **52**(5): 794-807 e797.

Chen, L. and D. B. Flies (2013). "Molecular mechanisms of T cell co-stimulation and co-inhibition." Nat Rev Immunol **13**(4): 227-242.

Chen, Z., E. Arai, O. Khan, Z. Zhang, S. F. Ngiow, Y. He, H. Huang, S. Manne, Z. Cao, A. E. Baxter, Z. Cai, E. Freilich, M. A. Ali, J. R. Giles, J. E. Wu, A. R. Greenplate, M. A. Hakeem, Q. Chen, M. Kurachi, K. Nzingha, V. Ekshyyan, D. Mathew, Z. Wen, N. A. Speck, A. Battle, S. L. Berger, E. J. Wherry and J. Shi (2021). "In vivo CD8(+) T cell CRISPR screening reveals control by Fli1 in infection and cancer." Cell **184**(5): 1262-1280 e1222.

Chisolm, D. A. and A. S. Weinmann (2018). "Connections Between Metabolism and Epigenetics in

Programming Cellular Differentiation." Annu Rev Immunol **36**: 221-246.
Codarri Deak, L., V. Nicolini, M. Hashimoto, M. Karagianni, P. C. Schwalie, L. Lauener, E. M. Varypataki, M. Richard, E. Bommer, J. Sam, S. Joller, M. Perro, F. Cremasco, L. Kunz, E. Yanguez, T. Husser, R. Schlenker, M. Mariani, V. Tosevski, S. Herter, M. Bacac, I. Waldhauer, S. Colombetti, X. Gueripel, S. Wullschleger, M. Tichet, D. Hanahan, H. T. Kissick, S. Leclair, A. Freimoser-Grundschober, S. Seeber, V. Teichgraber, R. Ahmed, C. Klein and P. Umana (2022). "PD-1-cis IL-2R agonism yields better effectors from stem-like CD8(+) T cells." Nature **610**(7930): 161-172.
Conley, J. M., M. P. Gallagher and L. J. Berg (2016). "T Cells and Gene Regulation: The Switching On and Turning Up of Genes after T Cell Receptor Stimulation in CD8 T Cells." Front Immunol **7**: 76.
Connolly, K. A., M. Kuchroo, A. Venkat, A. Khatun, J. Wang, I. William, N. I. Hornick, B. L. Fitzgerald, M. Damo, M. Y. Kasmani, C. Cui, E. Fagerberg, I. Monroy, A. Hutchins, J. F. Cheung, G. G. Foster, D. L. Mariuzza, M. Nader, H. Zhao, W. Cui, S. Krishnaswamy and N. S. Joshi (2021). "A reservoir of stem-like CD8(+) T cells in the tumor-draining lymph node preserves the ongoing antitumor immune response." Sci Immunol **6**(64): eabg7836.
Crispe, I. N., T. Dao, K. Klugewitz, W. Z. Mehal and D. P. Metz (2000). "The liver as a site of T-cell apoptosis: graveyard, or killing field?" Immunol Rev **174**: 47-62.
Cruz-Guilloty, F., M. E. Pipkin, I. M. Djuretic, D. Levanon, J. Lotem, M. G. Lichtenheld, Y. Groner and A. Rao (2009). "Runx3 and T-box proteins cooperate to establish the transcriptional program of effector CTLs." J Exp Med **206**(1): 51-59.
Curtsinger, J. M., D. C. Lins and M. F. Mescher (2003). "Signal 3 determines tolerance versus full activation of naive CD8 T cells: dissociating proliferation and development of effector function." J Exp Med **197**(9): 1141-1151.
Dall'Olio, F. G., A. Marabelle, C. Caramella, C. Garcia, M. Aldea, N. Chaput, C. Robert and B. Besse (2022). "Tumour burden and efficacy of immune-checkpoint inhibitors." Nat Rev Clin Oncol **19**(2): 75-90.
Dammeijer, F., M. van Gulijk, E. E. Mulder, M. Lukkes, L. Klaase, T. van den Bosch, M. van Nimwegen, S. P. Lau, K. Latupeirissa, S. Schetters, Y. van Kooyk, L. Boon, A. Moyaart, Y. M. Mueller, P. D. Katsikis, A. M. Eggermont, H. Vroman, R. Stadhouders, R. W. Hendriks, J. V. Thusen, D. J. Grunhagen, C. Verhoef, T. van Hall and J. G. Aerts (2020). "The PD-1/PD-L1-Checkpoint Restrains T cell Immunity in Tumor-Draining Lymph Nodes." Cancer Cell.
Danilo, M., V. Chennupati, J. G. Silva, S. Siegert and W. Held (2018). "Suppression of Tcf1 by Inflammatory Cytokines Facilitates Effector CD8 T Cell Differentiation." Cell Rep **22**(8): 2107-2117.
Di Pilato, M., R. Kfuri-Rubens, J. N. Pruessmann, A. J. Ozga, M. Messemaker, B. L. Cadilha, R. Sivakumar, C. Cianciaruso, R. D. Warner, F. Marangoni, E. Carrizosa, S. Lesch, J. Billingsley, D. Perez-Ramos, F. Zavala, E. Rheinbay, A. D. Luster, M. Y. Gerner, S. Kobold, M. J. Pittet and T. R. Mempel (2021). "CXCR6 positions cytotoxic T cells to receive critical survival signals in the tumor microenvironment." Cell **184**(17): 4512-4530 e4522.
Dobin, A., C. A. Davis, F. Schlesinger, J. Drenkow, C. Zaleski, S. Jha, P. Batut, M. Chaisson and T. R. Gingeras (2013). "STAR: ultrafast universal RNA-seq aligner." Bioinformatics **29**(1): 15-21.
Doering, T. A., A. Crawford, J. M. Angelosanto, M. A. Paley, C. G. Ziegler and E. J. Wherry (2012). "Network analysis reveals centrally connected genes and pathways involved in CD8+ T cell exhaustion versus memory." Immunity **37**(6): 1130-1144.
Doherty, D. G. (2016). "Immunity, tolerance and autoimmunity in the liver: A comprehensive review." J Autoimmun **66**: 60-75.
Dolmetsch, R. E., R. S. Lewis, C. C. Goodnow and J. I. Healy (1997). "Differential activation of transcription factors induced by Ca2+ response amplitude and duration." Nature **386**(6627): 855-858.
Engelowski, E., A. Schneider, M. Franke, H. Xu, R. Clemen, A. Lang, P. Baran, C. Binsch, B. Knebel,

H. Al-Hasani, J. M. Moll, D. M. Floss, P. A. Lang and J. Scheller (2018). "Synthetic cytokine receptors transmit biological signals using artificial ligands." Nat Commun **9**(1): 2034.

Forster, R., A. C. Davalos-Misslitz and A. Rot (2008). "CCR7 and its ligands: balancing immunity and tolerance." Nat Rev Immunol **8**(5): 362-371.

Fuller, M. J., A. Khanolkar, A. E. Tebo and A. J. Zajac (2004). "Maintenance, loss, and resurgence of T cell responses during acute, protracted, and chronic viral infections." J Immunol **172**(7): 4204-4214.

Fuller, M. J. and A. J. Zajac (2003). "Ablation of CD8 and CD4 T cell responses by high viral loads." J Immunol **170**(1): 477-486.

Girard, J. P., C. Moussion and R. Forster (2012). "HEVs, lymphatics and homeostatic immune cell trafficking in lymph nodes." Nat Rev Immunol **12**(11): 762-773.

Gounari, F. and K. Khazaie (2022). "TCF-1: a maverick in T cell development and function." Nat Immunol **23**(5): 671-678.

Gray, S. M., S. M. Kaech and M. M. Staron (2014). "The interface between transcriptional and epigenetic control of effector and memory CD8(+) T-cell differentiation." Immunol Rev **261**(1): 157-168.

Groom, J. R. and A. D. Luster (2011). "CXCR3 ligands: redundant, collaborative and antagonistic functions." Immunol Cell Biol **89**(2): 207-215.

Grusdat, M., D. R. McIlwain, H. C. Xu, V. I. Pozdeev, J. Knievel, S. Q. Crome, C. Robert-Tissot, R. J. Dress, A. A. Pandyra, D. E. Speiser, E. Lang, S. K. Maney, A. R. Elford, S. R. Hamilton, S. Scheu, K. Pfeffer, J. Bode, H. W. Mittrucker, M. Lohoff, M. Huber, D. Haussinger, P. S. Ohashi, T. W. Mak, K. S. Lang and P. A. Lang (2014). "IRF4 and BATF are critical for CD8(+) T-cell function following infection with LCMV." Cell Death Differ **21**(7): 1050-1060.

Gu, Z., R. Eils and M. Schlesner (2016). "Complex heatmaps reveal patterns and correlations in multidimensional genomic data." Bioinformatics **32**(18): 2847-2849.

Guan, T., C. X. Dominguez, R. A. Amezquita, B. J. Laidlaw, J. Cheng, J. Henao-Mejia, A. Williams, R. A. Flavell, J. Lu and S. M. Kaech (2018). "ZEB1, ZEB2, and the miR-200 family form a counterregulatory network to regulate CD8(+) T cell fates." J Exp Med **215**(4): 1153-1168.

Guidotti, L. G., D. Inverso, L. Sironi, P. Di Lucia, J. Fioravanti, L. Ganzer, A. Fiocchi, M. Vacca, R. Aiolfi, S. Sammicheli, M. Mainetti, T. Cataudella, A. Raimondi, G. Gonzalez-Aseguinolaza, U. Protzer, Z. M. Ruggeri, F. V. Chisari, M. Isogawa, G. Sitia and M. Iannacone (2015). "Immunosurveillance of the liver by intravascular effector CD8(+) T cells." Cell **161**(3): 486-500.

Guo, A., H. Huang, Z. Zhu, M. J. Chen, H. Shi, S. Yuan, P. Sharma, J. P. Connelly, S. Liedmann, Y. Dhungana, Z. Li, D. Haydar, M. Yang, H. Beere, J. T. Yustein, C. DeRenzo, S. M. Pruett-Miller, J. C. Crawford, G. Krenciute, C. W. M. Roberts, H. Chi and D. R. Green (2022). "cBAF complex components and MYC cooperate early in CD8(+) T cell fate." Nature **607**(7917): 135-141.

Guy, C., D. M. Mitrea, P. C. Chou, J. Temirov, K. M. Vignali, X. Liu, H. Zhang, R. Kriwacki, M. P. Bruchez, S. C. Watkins, C. J. Workman and D. A. A. Vignali (2022). "LAG3 associates with TCR-CD3 complexes and suppresses signaling by driving co-receptor-Lck dissociation." Nat Immunol **23**(5): 757-767.

Han, J., M. Wan, Z. Ma and P. He (2022). "The TOX subfamily: all-round players in the immune system." Clin Exp Immunol **208**(3): 268-280.

Hartley, S. W. and J. C. Mullikin (2015). "QoRTs: a comprehensive toolset for quality control and data processing of RNA-Seq experiments." BMC Bioinformatics **16**: 224.

Haslam, A. and V. Prasad (2019). "Estimation of the Percentage of US Patients With Cancer Who Are Eligible for and Respond to Checkpoint Inhibitor Immunotherapy Drugs." JAMA Netw Open **2**(5): e192535.

He, B., S. Xing, C. Chen, P. Gao, L. Teng, Q. Shan, J. A. Gullicksrud, M. D. Martin, S. Yu, J. T. Harty, V. P. Badovinac, K. Tan and H. H. Xue (2016). "CD8(+) T Cells Utilize Highly Dynamic Enhancer Repertoires and Regulatory Circuitry in Response to Infections." Immunity **45**(6): 1341-1354.

Hellstrom, I., K. E. Hellstrom, G. E. Pierce and J. P. Yang (1968). "Cellular and humoral immunity to different types of human neoplasms." Nature **220**(5174): 1352-1354.

Hensel, N., Z. Gu, Sagar, D. Wieland, K. Jechow, J. Kemming, S. Llewellyn-Lacey, E. Gostick, O. Sogukpinar, F. Emmerich, D. A. Price, B. Bengsch, T. Boettler, C. Neumann-Haefelin, R. Eils, C. Conrad, R. Bartenschlager, D. Grun, N. Ishaque, R. Thimme and M. Hofmann (2021). "Memory-like HCV-specific CD8(+) T cells retain a molecular scar after cure of chronic HCV infection." Nat Immunol **22**(2): 229-239.

Hernandez, J., S. Aung, K. Marquardt and L. A. Sherman (2002). "Uncoupling of proliferative potential and gain of effector function by CD8(+) T cells responding to self-antigens." J Exp Med **196**(3): 323-333.

Hodi, F. S., S. J. O'Day, D. F. McDermott, R. W. Weber, J. A. Sosman, J. B. Haanen, R. Gonzalez, C. Robert, D. Schadendorf, J. C. Hassel, W. Akerley, A. J. van den Eertwegh, J. Lutzky, P. Lorigan, J. M. Vaubel, G. P. Linette, D. Hogg, C. H. Ottensmeier, C. Lebbe, C. Peschel, I. Quirt, J. I. Clark, J. D. Wolchok, J. S. Weber, J. Tian, M. J. Yellin, G. M. Nichol, A. Hoos and W. J. Urba (2010). "Improved survival with ipilimumab in patients with metastatic melanoma." N Engl J Med **363**(8): 711-723.

Hu, X., J. Li, M. Fu, X. Zhao and W. Wang (2021). "The JAK/STAT signaling pathway: from bench to clinic." Signal Transduct Target Ther **6**(1): 402.

Huang, A. C., M. A. Postow, R. J. Orlowski, R. Mick, B. Bengsch, S. Manne, W. Xu, S. Harmon, J. R. Giles, B. Wenz, M. Adamow, D. Kuk, K. S. Panageas, C. Carrera, P. Wong, F. Quagliarello, B. Wubbenhorst, K. D'Andrea, K. E. Pauken, R. S. Herati, R. P. Staupe, J. M. Schenkel, S. McGettigan, S. Kothari, S. M. George, R. H. Vonderheide, R. K. Amaravadi, G. C. Karakousis, L. M. Schuchter, X. Xu, K. L. Nathanson, J. D. Wolchok, T. C. Gangadhar and E. J. Wherry (2017). "T-cell invigoration to tumour burden ratio associated with anti-PD-1 response." Nature **545**(7652): 60-65.

Hui, E., J. Cheung, J. Zhu, X. Su, M. J. Taylor, H. A. Wallweber, D. K. Sasmal, J. Huang, J. M. Kim, I. Mellman and R. D. Vale (2017). "T cell costimulatory receptor CD28 is a primary target for PD-1-mediated inhibition." Science **355**(6332): 1428-1433.

Im, S. J., M. Hashimoto, M. Y. Gerner, J. Lee, H. T. Kissick, M. C. Burger, Q. Shan, J. S. Hale, J. Lee, T. H. Nasti, A. H. Sharpe, G. J. Freeman, R. N. Germain, H. I. Nakaya, H. H. Xue and R. Ahmed (2016). "Defining CD8+ T cells that provide the proliferative burst after PD-1 therapy." Nature **537**(7620): 417-421.

Intlekofer, A. M., A. Banerjee, N. Takemoto, S. M. Gordon, C. S. Dejong, H. Shin, C. A. Hunter, E. J. Wherry, T. Lindsten and S. L. Reiner (2008). "Anomalous type 17 response to viral infection by CD8+ T cells lacking T-bet and eomesodermin." Science **321**(5887): 408-411.

Intlekofer, A. M., N. Takemoto, E. J. Wherry, S. A. Longworth, J. T. Northrup, V. R. Palanivel, A. C. Mullen, C. R. Gasink, S. M. Kaech, J. D. Miller, L. Gapin, K. Ryan, A. P. Russ, T. Lindsten, J. S. Orange, A. W. Goldrath, R. Ahmed and S. L. Reiner (2005). "Effector and memory CD8+ T cell fate coupled by T-bet and eomesodermin." Nat Immunol **6**(12): 1236-1244.

Jansen, C. S., N. Prokhnevska, V. A. Master, M. G. Sanda, J. W. Carlisle, M. A. Bilen, M. Cardenas, S. Wilkinson, R. Lake, A. G. Sowalsky, R. M. Valanparambil, W. H. Hudson, D. McGuire, K. Melnick, A. I. Khan, K. Kim, Y. M. Chang, A. Kim, C. P. Filson, M. Alemozaffar, A. O. Osunkoya, P. Mullane, C. Ellis, R. Akondy, S. J. Im, A. O. Kamphorst, A. Reyes, Y. Liu and H. Kissick (2019). "An intra-tumoral niche maintains and differentiates stem-like CD8 T cells." Nature **576**(7787): 465-470.

Joshi, N. S., W. Cui, A. Chandele, H. K. Lee, D. R. Urso, J. Hagman, L. Gapin and S. M. Kaech (2007). "Inflammation directs memory precursor and short-lived effector CD8(+) T cell fates via the graded expression of T-bet transcription factor." Immunity **27**(2): 281-295.

Joshi, N. S. and S. M. Kaech (2008). "Effector CD8 T cell development: a balancing act between memory cell potential and terminal differentiation." J Immunol **180**(3): 1309-1315.

Kaech, S. M. and R. Ahmed (2001). "Memory CD8+ T cell differentiation: initial antigen encounter

triggers a developmental program in naive cells." Nat Immunol **2**(5): 415-422.
Kaech, S. M. and W. Cui (2012). "Transcriptional control of effector and memory CD8+ T cell differentiation." Nat Rev Immunol **12**(11): 749-761.
Kao, C., K. J. Oestreich, M. A. Paley, A. Crawford, J. M. Angelosanto, M. A. Ali, A. M. Intlekofer, J. M. Boss, S. L. Reiner, A. S. Weinmann and E. J. Wherry (2011). "Transcription factor T-bet represses expression of the inhibitory receptor PD-1 and sustains virus-specific CD8+ T cell responses during chronic infection." Nat Immunol **12**(7): 663-671.
Karginov, T. A., A. Menoret and A. T. Vella (2022). "Optimal CD8(+) T cell effector function requires costimulation-induced RNA-binding proteins that reprogram the transcript isoform landscape." Nat Commun **13**(1): 3540.
Khan, O., J. R. Giles, S. McDonald, S. Manne, S. F. Ngiow, K. P. Patel, M. T. Werner, A. C. Huang, K. A. Alexander, J. E. Wu, J. Attanasio, P. Yan, S. M. George, B. Bengsch, R. P. Staupe, G. Donahue, W. Xu, R. K. Amaravadi, X. Xu, G. C. Karakousis, T. C. Mitchell, L. M. Schuchter, J. Kaye, S. L. Berger and E. J. Wherry (2019). "TOX transcriptionally and epigenetically programs CD8(+) T cell exhaustion." Nature **571**(7764): 211-218.
Kim, K., S. Park, S. Y. Park, G. Kim, S. M. Park, J. W. Cho, D. H. Kim, Y. M. Park, Y. W. Koh, H. R. Kim, S. J. Ha and I. Lee (2020). "Single-cell transcriptome analysis reveals TOX as a promoting factor for T cell exhaustion and a predictor for anti-PD-1 responses in human cancer." Genome Med **12**(1): 22.
Kim, S. I., C. R. Cassella and K. T. Byrne (2020). "Tumor Burden and Immunotherapy: Impact on Immune Infiltration and Therapeutic Outcomes." Front Immunol **11**: 629722.
Kreslavsky, T., M. Gleimer, M. Miyazaki, Y. Choi, E. Gagnon, C. Murre, P. Sicinski and H. von Boehmer (2012). "beta-Selection-Induced Proliferation Is Required for alphabeta T Cell Differentiation." Immunity **37**(5): 840-853.
Krummel, M. F. and J. P. Allison (1995). "CD28 and CTLA-4 have opposing effects on the response of T cells to stimulation." J Exp Med **182**(2): 459-465.
Kurachi, M., R. A. Barnitz, N. Yosef, P. M. Odorizzi, M. A. DiIorio, M. E. Lemieux, K. Yates, J. Godec, M. G. Klatt, A. Regev, E. J. Wherry and W. N. Haining (2014). "The transcription factor BATF operates as an essential differentiation checkpoint in early effector CD8+ T cells." Nat Immunol **15**(4): 373-383.
Lasek, W., R. Zagozdzon and M. Jakobisiak (2014). "Interleukin 12: still a promising candidate for tumor immunotherapy?" Cancer Immunol Immunother **63**(5): 419-435.
Lechner, F., D. K. Wong, P. R. Dunbar, R. Chapman, R. T. Chung, P. Dohrenwend, G. Robbins, R. Phillips, P. Klenerman and B. D. Walker (2000). "Analysis of successful immune responses in persons infected with hepatitis C virus." J Exp Med **191**(9): 1499-1512.
Leek, J. T., W. E. Johnson, H. S. Parker, E. J. Fertig, A. E. Jaffe, Y. Zhang, J. D. Storey and L. C. Torres (2022). "sva: Surrogate Variable Analysis." R package version 3.44.0.
Legut, M., Z. Gajic, M. Guarino, Z. Daniloski, J. A. Rahman, X. Xue, C. Lu, L. Lu, E. P. Mimitou, S. Hao, T. Davoli, C. Diefenbach, P. Smibert and N. E. Sanjana (2022). "A genome-scale screen for synthetic drivers of T cell proliferation." Nature **603**(7902): 728-735.
Li, F. and Z. Tian (2013). "The liver works as a school to educate regulatory immune cells." Cell Mol Immunol **10**(4): 292-302.
Li, H. and R. Durbin (2009). "Fast and accurate short read alignment with Burrows-Wheeler transform." Bioinformatics **25**(14): 1754-1760.
Li, H., B. Handsaker, A. Wysoker, T. Fennell, J. Ruan, N. Homer, G. Marth, G. Abecasis, R. Durbin and S. Genome Project Data Processing (2009). "The Sequence Alignment/Map format and SAMtools." Bioinformatics **25**(16): 2078-2079.
Li, Z., Z. K. Tuong, I. Dean, C. Willis, F. Gaspal, R. Fiancette, S. Idris, B. Kennedy, J. R. Ferdinand, A. Penalver, M. Cabantous, S. Murtuza Baker, J. W. Fry, G. Carlesso, S. A. Hammond, S. J. Dovedi, M. R. Hepworth, M. R. Clatworthy and D. R. Withers (2022). "In vivo labeling reveals continuous trafficking of TCF-1+ T cells between tumor and lymphoid tissue." J Exp Med **219**(6).

Liao, Y., G. K. Smyth and W. Shi (2014). "featureCounts: an efficient general purpose program for assigning sequence reads to genomic features." Bioinformatics **30**(7): 923-930.
Lin, L., P. Rayman, P. G. Pavicic, Jr., C. Tannenbaum, T. Hamilton, A. Montero, J. Ko, B. Gastman, J. Finke, M. Ernstoff and C. M. Diaz-Montero (2019). "Ex vivo conditioning with IL-12 protects tumor-infiltrating CD8(+) T cells from negative regulation by local IFN-gamma." Cancer Immunol Immunother **68**(3): 395-405.
Link, M. A., K. Lucke, J. Schmid, V. Schumacher, T. Eden, S. Rose-John and H. W. Mittrucker (2017). "The role of ADAM17 in the T-cell response against bacterial pathogens." PLoS One **12**(9): e0184320.
Liu, J., S. Zhu, W. Hu, X. Zhao, Q. Shan, W. Peng and H. H. Xue (2023). "CTCF mediates CD8+ effector differentiation through dynamic redistribution and genomic reorganization." J Exp Med **220**(4).
Liu, T. (2014). "Use model-based Analysis of ChIP-Seq (MACS) to analyze short reads generated by sequencing protein-DNA interactions in embryonic stem cells." Methods Mol Biol **1150**: 81-95.
Love, M. I., W. Huber and S. Anders (2014). "Moderated estimation of fold change and dispersion for RNA-seq data with DESeq2." Genome Biol **15**(12): 550.
Lynn, R. C., E. W. Weber, E. Sotillo, D. Gennert, P. Xu, Z. Good, H. Anbunathan, J. Lattin, R. Jones, V. Tieu, S. Nagaraja, J. Granja, C. F. A. de Bourcy, R. Majzner, A. T. Satpathy, S. R. Quake, M. Monje, H. Y. Chang and C. L. Mackall (2019). "c-Jun overexpression in CAR T cells induces exhaustion resistance." Nature **576**(7786): 293-300.
Machlab, D., L. Burger, C. Soneson, F. M. Rijli, D. Schubeler and M. B. Stadler (2022). "monaLisa: an R/Bioconductor package for identifying regulatory motifs." Bioinformatics **38**(9): 2624-2625.
Macian, F. (2005). "NFAT proteins: key regulators of T-cell development and function." Nat Rev Immunol **5**(6): 472-484.
Macian, F., C. Lopez-Rodriguez and A. Rao (2001). "Partners in transcription: NFAT and AP-1." Oncogene **20**(19): 2476-2489.
Makita, S., H. Takatori and H. Nakajima (2021). "Post-Transcriptional Regulation of Immune Responses and Inflammatory Diseases by RNA-Binding ZFP36 Family Proteins." Front Immunol **12**: 711633.
Mansurov, A., J. Ishihara, P. Hosseinchi, L. Potin, T. M. Marchell, A. Ishihara, J. M. Williford, A. T. Alpar, M. M. Raczy, L. T. Gray, M. A. Swartz and J. A. Hubbell (2020). "Collagen-binding IL-12 enhances tumour inflammation and drives the complete remission of established immunologically cold mouse tumours." Nat Biomed Eng **4**(5): 531-543.
Marangoni, F., T. T. Murooka, T. Manzo, E. Y. Kim, E. Carrizosa, N. M. Elpek and T. R. Mempel (2013). "The transcription factor NFAT exhibits signal memory during serial T cell interactions with antigen-presenting cells." Immunity **38**(2): 237-249.
Martin, M. (2011). "Cutadapt removes adapter sequences from high-throughput sequencing reads." EMBnet.journal **17**: 10-12.
Martinez, G. J., R. M. Pereira, T. Aijo, E. Y. Kim, F. Marangoni, M. E. Pipkin, S. Togher, V. Heissmeyer, Y. C. Zhang, S. Crotty, E. D. Lamperti, K. M. Ansel, T. R. Mempel, H. Lahdesmaki, P. G. Hogan and A. Rao (2015). "The transcription factor NFAT promotes exhaustion of activated CD8(+) T cells." Immunity **42**(2): 265-278.
Matoba, T., K. Minohara, D. Kawakita, G. Takano, K. Oguri, A. Murashima, K. Nakai, S. Iwaki, H. Tsuge, N. Tanaka, S. Imaizumi, W. Hojo, A. Matsumura, K. Tsukamoto, S. Esaki and S. Iwasaki (2022). "Impact of tumor burden on survival in patients with recurrent or metastatic head and neck cancer treated with immune checkpoint inhibitors." Sci Rep **12**(1): 14319.
McKinney, E. F., J. C. Lee, D. R. Jayne, P. A. Lyons and K. G. Smith (2015). "T-cell exhaustion, co-stimulation and clinical outcome in autoimmunity and infection." Nature **523**(7562): 612-616.
McLane, L. M., M. S. Abdel-Hakeem and E. J. Wherry (2019). "CD8 T Cell Exhaustion During Chronic Viral Infection and Cancer." Annu Rev Immunol.
Mescher, M. F., J. M. Curtsinger, P. Agarwal, K. A. Casey, M. Gerner, C. D. Hammerbeck, F. Popescu and Z. Xiao (2006). "Signals required for programming effector and memory development by

CD8+ T cells." Immunol Rev **211**: 81-92.
Michalek, R. D. and J. C. Rathmell (2010). "The metabolic life and times of a T-cell." Immunol Rev **236**: 190-202.
Migueles, S. A., K. A. Weeks, E. Nou, A. M. Berkley, J. E. Rood, C. M. Osborne, C. W. Hallahan, N. A. Cogliano-Shutta, J. A. Metcalf, M. McLaughlin, R. Kwan, J. M. Mican, R. T. Davey, Jr. and M. Connors (2009). "Defective human immunodeficiency virus-specific CD8+ T-cell polyfunctionality, proliferation, and cytotoxicity are not restored by antiretroviral therapy." J Virol **83**(22): 11876-11889.
Miller, B. C., D. R. Sen, R. Al Abosy, K. Bi, Y. V. Virkud, M. W. LaFleur, K. B. Yates, A. Lako, K. Felt, G. S. Naik, M. Manos, E. Gjini, J. R. Kuchroo, J. J. Ishizuka, J. L. Collier, G. K. Griffin, S. Maleri, D. E. Comstock, S. A. Weiss, F. D. Brown, A. Panda, M. D. Zimmer, R. T. Manguso, F. S. Hodi, S. J. Rodig, A. H. Sharpe and W. N. Haining (2019). "Subsets of exhausted CD8(+) T cells differentially mediate tumor control and respond to checkpoint blockade." Nat Immunol **20**(3): 326-336.
Mognol, G. P., R. Spreafico, V. Wong, J. P. Scott-Browne, S. Togher, A. Hoffmann, P. G. Hogan, A. Rao and S. Trifari (2017). "Exhaustion-associated regulatory regions in CD8(+) tumor-infiltrating T cells." Proc Natl Acad Sci U S A **114**(13): E2776-E2785.
Nagy, J. A., S. H. Chang, A. M. Dvorak and H. F. Dvorak (2009). "Why are tumour blood vessels abnormal and why is it important to know?" Br J Cancer **100**(6): 865-869.
Nah, J. and R. H. Seong (2022). "Kruppel-like factor 4 regulates the cytolytic effector function of exhausted CD8 T cells." Sci Adv **8**(47): eadc9346.
Nguyen, L. T. and P. S. Ohashi (2015). "Clinical blockade of PD1 and LAG3--potential mechanisms of action." Nat Rev Immunol **15**(1): 45-56.
Obst, R. (2015). "The Timing of T Cell Priming and Cycling." Front Immunol **6**: 563.
Omilusik, K. D., J. A. Best, B. Yu, S. Goossens, A. Weidemann, J. V. Nguyen, E. Seuntjens, A. Stryjewska, C. Zweier, R. Roychoudhuri, L. Gattinoni, L. M. Bird, Y. Higashi, H. Kondoh, D. Huylebroeck, J. Haigh and A. W. Goldrath (2015). "Transcriptional repressor ZEB2 promotes terminal differentiation of CD8+ effector and memory T cell populations during infection." J Exp Med **212**(12): 2027-2039.
Otten, G. R. and R. N. Germain (1991). "Split anergy in a CD8+ T cell: receptor-dependent cytolysis in the absence of interleukin-2 production." Science **251**(4998): 1228-1231.
Oxenius, A., R. M. Zinkernagel and H. Hengartner (1998). "Comparison of activation versus induction of unresponsiveness of virus-specific CD4+ and CD8+ T cells upon acute versus persistent viral infection." Immunity **9**(4): 449-457.
Paley, M. A., D. C. Kroy, P. M. Odorizzi, J. B. Johnnidis, D. V. Dolfi, B. E. Barnett, E. K. Bikoff, E. J. Robertson, G. M. Lauer, S. L. Reiner and E. J. Wherry (2012). "Progenitor and terminal subsets of CD8+ T cells cooperate to contain chronic viral infection." Science **338**(6111): 1220-1225.
Pearce, E. L., A. C. Mullen, G. A. Martins, C. M. Krawczyk, A. S. Hutchins, V. P. Zediak, M. Banica, C. B. DiCioccio, D. A. Gross, C. A. Mao, H. Shen, N. Cereb, S. Y. Yang, T. Lindsten, J. Rossant, C. A. Hunter and S. L. Reiner (2003). "Control of effector CD8+ T cell function by the transcription factor Eomesodermin." Science **302**(5647): 1041-1043.
Petkau, G., T. J. Mitchell, K. Chakraborty, S. E. Bell, D. A. V, L. Matheson, D. J. Turner, A. Saveliev, O. Gizlenci, F. Salerno, P. D. Katsikis and M. Turner (2022). "The timing of differentiation and potency of CD8 effector function is set by RNA binding proteins." Nat Commun **13**(1): 2274.
Philip, M., L. Fairchild, L. Sun, E. L. Horste, S. Camara, M. Shakiba, A. C. Scott, A. Viale, P. Lauer, T. Merghoub, M. D. Hellmann, J. D. Wolchok, C. S. Leslie and A. Schietinger (2017). "Chromatin states define tumour-specific T cell dysfunction and reprogramming." Nature **545**(7655): 452-456.
Philip, M. and A. Schietinger (2021). "CD8(+) T cell differentiation and dysfunction in cancer." Nat Rev Immunol.
Prinzing, B., C. C. Zebley, C. T. Petersen, Y. Fan, A. A. Anido, Z. Yi, P. Nguyen, H. Houke, M. Bell, D.

Haydar, C. Brown, S. K. Boi, S. Alli, J. C. Crawford, J. M. Riberdy, J. J. Park, S. Zhou, M. P. Velasquez, C. DeRenzo, C. R. Lazzarotto, S. Q. Tsai, P. Vogel, S. M. Pruett-Miller, D. M. Langfitt, S. Gottschalk, B. Youngblood and G. Krenciute (2021). "Deleting DNMT3A in CAR T cells prevents exhaustion and enhances antitumor activity." Sci Transl Med **13**(620): eabh0272.

Quah, B. J., H. S. Warren and C. R. Parish (2007). "Monitoring lymphocyte proliferation in vitro and in vivo with the intracellular fluorescent dye carboxyfluorescein diacetate succinimidyl ester." Nat Protoc **2**(9): 2049-2056.

Quigley, M., F. Pereyra, B. Nilsson, F. Porichis, C. Fonseca, Q. Eichbaum, B. Julg, J. L. Jesneck, K. Brosnahan, S. Imam, K. Russell, I. Toth, A. Piechocka-Trocha, D. Dolfi, J. Angelosanto, A. Crawford, H. Shin, D. S. Kwon, J. Zupkosky, L. Francisco, G. J. Freeman, E. J. Wherry, D. E. Kaufmann, B. D. Walker, B. Ebert and W. N. Haining (2010). "Transcriptional analysis of HIV-specific CD8+ T cells shows that PD-1 inhibits T cell function by upregulating BATF." Nat Med **16**(10): 1147-1151.

Quinn, W. J., 3rd, J. Jiao, T. TeSlaa, J. Stadanlick, Z. Wang, L. Wang, T. Akimova, A. Angelin, P. M. Schafer, M. D. Cully, C. Perry, P. K. Kopinski, L. Guo, I. A. Blair, L. R. Ghanem, M. S. Leibowitz, W. W. Hancock, E. K. Moon, M. H. Levine, E. B. Eruslanov, D. C. Wallace, J. A. Baur and U. H. Beier (2020). "Lactate Limits T Cell Proliferation via the NAD(H) Redox State." Cell Rep **33**(11): 108500.

R Core Team (2017). "R: A Language and Environment for Statistical Computing." R Foundation for Statistical Computing.

Ramirez, F., D. P. Ryan, B. Gruning, V. Bhardwaj, F. Kilpert, A. S. Richter, S. Heyne, F. Dundar and T. Manke (2016). "deepTools2: a next generation web server for deep-sequencing data analysis." Nucleic Acids Res **44**(W1): W160-165.

Rao, A., C. Luo and P. G. Hogan (1997). "Transcription factors of the NFAT family: regulation and function." Annu Rev Immunol **15**: 707-747.

Rao, R. R., Q. Li, K. Odunsi and P. A. Shrikant (2010). "The mTOR kinase determines effector versus memory CD8+ T cell fate by regulating the expression of transcription factors T-bet and Eomesodermin." Immunity **32**(1): 67-78.

Reina-Campos, M., N. E. Scharping and A. W. Goldrath (2021). "CD8(+) T cell metabolism in infection and cancer." Nat Rev Immunol **21**(11): 718-738.

Rosenberg, E. S., M. Altfeld, S. H. Poon, M. N. Phillips, B. M. Wilkes, R. L. Eldridge, G. K. Robbins, R. T. D'Aquila, P. J. Goulder and B. D. Walker (2000). "Immune control of HIV-1 after early treatment of acute infection." Nature **407**(6803): 523-526.

Ross, S. H. and D. A. Cantrell (2018). "Signaling and Function of Interleukin-2 in T Lymphocytes." Annu Rev Immunol **36**: 411-433.

Roychoudhuri, R., D. Clever, P. Li, Y. Wakabayashi, K. M. Quinn, C. A. Klebanoff, Y. Ji, M. Sukumar, R. L. Eil, Z. Yu, R. Spolski, D. C. Palmer, J. H. Pan, S. J. Patel, D. C. Macallan, G. Fabozzi, H. Y. Shih, Y. Kanno, A. Muto, J. Zhu, L. Gattinoni, J. J. O'Shea, K. Okkenhaug, K. Igarashi, W. J. Leonard and N. P. Restifo (2016). "BACH2 regulates CD8(+) T cell differentiation by controlling access of AP-1 factors to enhancers." Nat Immunol **17**(7): 851-860.

Salerno, F., S. Engels, M. van den Biggelaar, F. P. J. van Alphen, A. Guislain, W. Zhao, D. L. Hodge, S. E. Bell, J. P. Medema, M. von Lindern, M. Turner, H. A. Young and M. C. Wolkers (2018). "Translational repression of pre-formed cytokine-encoding mRNA prevents chronic activation of memory T cells." Nat Immunol **19**(8): 828-837.

Scharer, C. D., B. G. Barwick, M. Guo, A. P. R. Bally and J. M. Boss (2018). "Plasma cell differentiation is controlled by multiple cell division-coupled epigenetic programs." Nat Commun **9**(1): 1698.

Schep, A. N., B. Wu, J. D. Buenrostro and W. J. Greenleaf (2017). "chromVAR: inferring transcription-factor-associated accessibility from single-cell epigenomic data." Nat Methods **14**(10): 975-978.

Schietinger, A., M. Philip, V. E. Krisnawan, E. Y. Chiu, J. J. Delrow, R. S. Basom, P. Lauer, D. G. Brockstedt, S. E. Knoblaugh, G. J. Hammerling, T. D. Schell, N. Garbi and P. D. Greenberg (2016). "Tumor-Specific T Cell Dysfunction Is a Dynamic Antigen-Driven Differentiation

Program Initiated Early during Tumorigenesis." Immunity **45**(2): 389-401.
Scott-Browne, J. P., I. F. Lopez-Moyado, S. Trifari, V. Wong, L. Chavez, A. Rao and R. M. Pereira (2016). "Dynamic Changes in Chromatin Accessibility Occur in CD8(+) T Cells Responding to Viral Infection." Immunity **45**(6): 1327-1340.
Scott, A. C., F. Dundar, P. Zumbo, S. S. Chandran, C. A. Klebanoff, M. Shakiba, P. Trivedi, L. Menocal, H. Appleby, S. Camara, D. Zamarin, T. Walther, A. Snyder, M. R. Femia, E. A. Comen, H. Y. Wen, M. D. Hellmann, N. Anandasabapathy, Y. Liu, N. K. Altorki, P. Lauer, O. Levy, M. S. Glickman, J. Kaye, D. Betel, M. Philip and A. Schietinger (2019). "TOX is a critical regulator of tumour-specific T cell differentiation." Nature **571**(7764): 270-274.
Scott, C. L. and K. D. Omilusik (2019). "ZEBs: Novel Players in Immune Cell Development and Function." Trends Immunol **40**(5): 431-446.
Sekine, T., A. Perez-Potti, S. Nguyen, J. B. Gorin, V. H. Wu, E. Gostick, S. Llewellyn-Lacey, Q. Hammer, S. Falck-Jones, S. Vangeti, M. Yu, A. Smed-Sorensen, A. Gaballa, M. Uhlin, J. K. Sandberg, C. Brander, P. Nowak, P. A. Goepfert, D. A. Price, M. R. Betts and M. Buggert (2020). "TOX is expressed by exhausted and polyfunctional human effector memory CD8(+) T cells." Sci Immunol **5**(49).
Sen, D. R., J. Kaminski, R. A. Barnitz, M. Kurachi, U. Gerdemann, K. B. Yates, H. W. Tsao, J. Godec, M. W. LaFleur, F. D. Brown, P. Tonnerre, R. T. Chung, D. C. Tully, T. M. Allen, N. Frahm, G. M. Lauer, E. J. Wherry, N. Yosef and W. N. Haining (2016). "The epigenetic landscape of T cell exhaustion." Science **354**(6316): 1165-1169.
Seo, H., J. Chen, E. Gonzalez-Avalos, D. Samaniego-Castruita, A. Das, Y. H. Wang, I. F. Lopez-Moyado, R. O. Georges, W. Zhang, A. Onodera, C. J. Wu, L. F. Lu, P. G. Hogan, A. Bhandoola and A. Rao (2019). "TOX and TOX2 transcription factors cooperate with NR4A transcription factors to impose CD8(+) T cell exhaustion." Proc Natl Acad Sci U S A **116**(25): 12410-12415.
Shakiba, M., P. Zumbo, G. Espinosa-Carrasco, L. Menocal, F. Dundar, S. E. Carson, E. M. Bruno, F. J. Sanchez-Rivera, S. W. Lowe, S. Camara, R. P. Koche, V. P. Reuter, N. D. Socci, B. Whitlock, F. Tamzalit, M. Huse, M. D. Hellmann, D. K. Wells, N. A. Defranoux, D. Betel, M. Philip and A. Schietinger (2022). "TCR signal strength defines distinct mechanisms of T cell dysfunction and cancer evasion." J Exp Med **219**(2).
Sinclair, L. V., A. J. Howden, A. Brenes, L. Spinelli, J. L. Hukelmann, A. N. Macintyre, X. Liu, S. Thomson, P. M. Taylor, J. C. Rathmell, J. W. Locasale, A. I. Lamond and D. A. Cantrell (2019). "Antigen receptor control of methionine metabolism in T cells." Elife **8**.
Sinnathamby, G., P. Lauer, J. Zerfass, B. Hanson, A. Karabudak, J. Krakover, A. A. Secord, T. M. Clay, M. A. Morse, T. W. Dubensky, Jr., D. G. Brockstedt, R. Philip and M. Giedlin (2009). "Priming and activation of human ovarian and breast cancer-specific CD8+ T cells by polyvalent Listeria monocytogenes-based vaccines." J Immunother **32**(8): 856-869.
Slaney, C. Y., M. H. Kershaw and P. K. Darcy (2014). "Trafficking of T cells into tumors." Cancer Res **74**(24): 7168-7174.
Soerens, A. G., M. Kunzli, C. F. Quarnstrom, M. C. Scott, L. Swanson, J. J. Locquiao, H. E. Ghoneim, D. Zehn, B. Youngblood, V. Vezys and D. Masopust (2023). "Functional T cells are capable of supernumerary cell division and longevity." Nature **614**(7949): 762-766.
Stahl, S., T. Sacher, A. Bechtold, U. Protzer, R. Ganss, G. J. Hammerling, B. Arnold and N. Garbi (2009). "Tumor agonist peptides break tolerance and elicit effective CTL responses in an inducible mouse model of hepatocellular carcinoma." Immunol Lett **123**(1): 31-37.
Stark, R. and G. Brown (2011). "DiffBind: differential binding analysis of ChIP-Seq peak data."
Staveley-O'Carroll, K., T. D. Schell, M. Jimenez, L. M. Mylin, M. J. Tevethia, S. P. Schoenberger and S. S. Tevethia (2003). "In vivo ligation of CD40 enhances priming against the endogenous tumor antigen and promotes CD8+ T cell effector function in SV40 T antigen transgenic mice." J Immunol **171**(2): 697-707.
Stelekati, E., H. Shin, T. A. Doering, D. V. Dolfi, C. G. Ziegler, D. P. Beiting, L. Dawson, J. Liboon, D. Wolski, M. A. Ali, P. D. Katsikis, H. Shen, D. S. Roos, W. N. Haining, G. M. Lauer and E. J.

Wherry (2014). "Bystander chronic infection negatively impacts development of CD8(+) T cell memory." Immunity **40**(5): 801-813.
Stork, C. and S. Zheng (2016). "Genome-Wide Profiling of RNA-Protein Interactions Using CLIP-Seq." Methods Mol Biol **1421**: 137-151.
Sullivan, B. M., A. Juedes, S. J. Szabo, M. von Herrath and L. H. Glimcher (2003). "Antigen-driven effector CD8 T cell function regulated by T-bet." Proc Natl Acad Sci U S A **100**(26): 15818-15823.
Tangye, S. G. and P. D. Hodgkin (2004). "Divide and conquer: the importance of cell division in regulating B-cell responses." Immunology **112**(4): 509-520.
Thompson, E. D., H. L. Enriquez, Y. X. Fu and V. H. Engelhard (2010). "Tumor masses support naive T cell infiltration, activation, and differentiation into effectors." J Exp Med **207**(8): 1791-1804.
Tichet, M., S. Wullschleger, A. Chryplewicz, N. Fournier, R. Marcone, A. Kauzlaric, K. Homicsko, L. C. Deak, P. Umana, C. Klein and D. Hanahan (2023). "Bispecific PD1-IL2v and anti-PD-L1 break tumor immunity resistance by enhancing stem-like tumor-reactive CD8(+) T cells and reprogramming macrophages." Immunity **56**(1): 162-179 e166.
Tsao, H. W., J. Kaminski, M. Kurachi, R. A. Barnitz, M. A. DiIorio, M. W. LaFleur, W. Ise, T. Kurosaki, E. J. Wherry, W. N. Haining and N. Yosef (2022). "Batf-mediated epigenetic control of effector CD8(+) T cell differentiation." Sci Immunol **7**(68): eabi4919.
Utzschneider, D. T., M. Charmoy, V. Chennupati, L. Pousse, D. P. Ferreira, S. Calderon-Copete, M. Danilo, F. Alfei, M. Hofmann, D. Wieland, S. Pradervand, R. Thimme, D. Zehn and W. Held (2016). "T Cell Factor 1-Expressing Memory-like CD8(+) T Cells Sustain the Immune Response to Chronic Viral Infections." Immunity **45**(2): 415-427.
Utzschneider, D. T., S. S. Gabriel, D. Chisanga, R. Gloury, P. M. Gubser, A. Vasanthakumar, W. Shi and A. Kallies (2020). "Early precursor T cells establish and propagate T cell exhaustion in chronic infection." Nat Immunol.
van Stipdonk, M. J., E. E. Lemmens and S. P. Schoenberger (2001). "Naive CTLs require a single brief period of antigenic stimulation for clonal expansion and differentiation." Nat Immunol **2**(5): 423-429.
Virgin, H. W., E. J. Wherry and R. Ahmed (2009). "Redefining chronic viral infection." Cell **138**(1): 30-50.
Walsh, C. M., M. Matloubian, C. C. Liu, R. Ueda, C. G. Kurahara, J. L. Christensen, M. T. Huang, J. D. Young, R. Ahmed and W. R. Clark (1994). "Immune function in mice lacking the perforin gene." Proc Natl Acad Sci U S A **91**(23): 10854-10858.
Watson, M. J., P. D. A. Vignali, S. J. Mullett, A. E. Overacre-Delgoffe, R. M. Peralta, S. Grebinoski, A. V. Menk, N. L. Rittenhouse, K. DePeaux, R. D. Whetstone, D. A. A. Vignali, T. W. Hand, A. C. Poholek, B. M. Morrison, J. D. Rothstein, S. G. Wendell and G. M. Delgoffe (2021). "Metabolic support of tumour-infiltrating regulatory T cells by lactic acid." Nature **591**(7851): 645-651.
Weber, E. W., K. R. Parker, E. Sotillo, R. C. Lynn, H. Anbunathan, J. Lattin, Z. Good, J. A. Belk, B. Daniel, D. Klysz, M. Malipatlolla, P. Xu, M. Bashti, S. Heitzeneder, L. Labanieh, P. Vandris, R. G. Majzner, Y. Qi, K. Sandor, L. C. Chen, S. Prabhu, A. J. Gentles, T. J. Wandless, A. T. Satpathy, H. Y. Chang and C. L. Mackall (2021). "Transient rest restores functionality in exhausted CAR-T cells through epigenetic remodeling." Science **372**(6537).
Weirauch, M. T., A. Yang, M. Albu, A. G. Cote, A. Montenegro-Montero, P. Drewe, H. S. Najafabadi, S. A. Lambert, I. Mann, K. Cook, H. Zheng, A. Goity, H. van Bakel, J. C. Lozano, M. Galli, M. G. Lewsey, E. Huang, T. Mukherjee, X. Chen, J. S. Reece-Hoyes, S. Govindarajan, G. Shaulsky, A. J. M. Walhout, F. Y. Bouget, G. Ratsch, L. F. Larrondo, J. R. Ecker and T. R. Hughes (2014). "Determination and inference of eukaryotic transcription factor sequence specificity." Cell **158**(6): 1431-1443.
Wherry, E. J. (2011). "T cell exhaustion." Nat Immunol **12**(6): 492-499.
Wherry, E. J. and R. Ahmed (2004). "Memory CD8 T-cell differentiation during viral infection." J Virol **78**(11): 5535-5545.

Wherry, E. J., D. L. Barber, S. M. Kaech, J. N. Blattman and R. Ahmed (2004). "Antigen-independent memory CD8 T cells do not develop during chronic viral infection." Proc Natl Acad Sci U S A **101**(45): 16004-16009.

Wherry, E. J., J. N. Blattman, K. Murali-Krishna, R. van der Most and R. Ahmed (2003). "Viral persistence alters CD8 T-cell immunodominance and tissue distribution and results in distinct stages of functional impairment." J Virol **77**(8): 4911-4927.

Wherry, E. J., S. J. Ha, S. M. Kaech, W. N. Haining, S. Sarkar, V. Kalia, S. Subramaniam, J. N. Blattman, D. L. Barber and R. Ahmed (2007). "Molecular signature of CD8+ T cell exhaustion during chronic viral infection." Immunity **27**(4): 670-684.

Wickham, H., W. Chang, L. Henry, T. L. Pedersen, K. Takahashi, C. Wilke, K. Woo, H. Yutani and D. Dunnington (2016). "ggplot2: Elegant Graphics for Data Analysis.".

Williams, M. A. and M. J. Bevan (2004). "Shortening the infectious period does not alter expansion of CD8 T cells but diminishes their capacity to differentiate into memory cells." J Immunol **173**(11): 6694-6702.

Wolint, P., M. R. Betts, R. A. Koup and A. Oxenius (2004). "Immediate cytotoxicity but not degranulation distinguishes effector and memory subsets of CD8+ T cells." J Exp Med **199**(7): 925-936.

Yamada, T., C. S. Park, M. Mamonkin and H. D. Lacorazza (2009). "Transcription factor ELF4 controls the proliferation and homing of CD8+ T cells via the Kruppel-like factors KLF4 and KLF2." Nat Immunol **10**(6): 618-626.

Yang, C. Y., J. A. Best, J. Knell, E. Yang, A. D. Sheridan, A. K. Jesionek, H. S. Li, R. R. Rivera, K. C. Lind, L. M. D'Cruz, S. S. Watowich, C. Murre and A. W. Goldrath (2011). "The transcriptional regulators Id2 and Id3 control the formation of distinct memory CD8+ T cell subsets." Nat Immunol **12**(12): 1221-1229.

Yates, K. B., P. Tonnerre, G. E. Martin, U. Gerdemann, R. Al Abosy, D. E. Comstock, S. A. Weiss, D. Wolski, D. C. Tully, R. T. Chung, T. M. Allen, A. Y. Kim, S. Fidler, J. Fox, J. Frater, G. M. Lauer, W. N. Haining and D. R. Sen (2021). "Epigenetic scars of CD8(+) T cell exhaustion persist after cure of chronic infection in humans." Nat Immunol **22**(8): 1020-1029.

Yoon, H., T. S. Kim and T. J. Braciale (2010). "The cell cycle time of CD8+ T cells responding in vivo is controlled by the type of antigenic stimulus." PLoS One **5**(11): e15423.

Yu, G., L. G. Wang and Q. Y. He (2015). "ChIPseeker: an R/Bioconductor package for ChIP peak annotation, comparison and visualization." Bioinformatics **31**(14): 2382-2383.

Yu, P., Y. Lee, W. Liu, R. K. Chin, J. Wang, Y. Wang, A. Schietinger, M. Philip, H. Schreiber and Y. X. Fu (2004). "Priming of naive T cells inside tumors leads to eradication of established tumors." Nat Immunol **5**(2): 141-149.

Yukawa, M., S. Jagannathan, S. Vallabh, A. V. Kartashov, X. Chen, M. T. Weirauch and A. Barski (2020). "AP-1 activity induced by co-stimulation is required for chromatin opening during T cell activation." J Exp Med **217**(1).

Zajac, A. J., J. N. Blattman, K. Murali-Krishna, D. J. Sourdive, M. Suresh, J. D. Altman and R. Ahmed (1998). "Viral immune evasion due to persistence of activated T cells without effector function." J Exp Med **188**(12): 2205-2213.

Zhang, N. and M. J. Bevan (2011). "CD8(+) T cells: foot soldiers of the immune system." Immunity **35**(2): 161-168.

Zhu, L. and A. I. Skoultchi (2001). "Coordinating cell proliferation and differentiation." Curr Opin Genet Dev **11**(1): 91-97.